Mathematical Modelling of Cancer Cell Population Dynamics

Liene Daukšte

A thesis submitted in partial fulfilment
of the requirements for the degree of
Doctor of Philosophy

Department of Mathematics and Statistics
University of Canterbury

2012

To Elza and Jazeps

Abstract

Mathematical models, that depict the dynamics of a cancer cell population growing out of the human body (*in vitro*) in unconstrained microenvironment conditions, are considered in this thesis. Cancer cells *in vitro* grow and divide much faster than cancer cells in the human body, therefore, the effects of various cancer treatments applied to them can be identified much faster. These cell populations, when not exposed to any cancer treatment, exhibit exponential growth that we refer to as the balanced exponential growth (BEG) state. This observation has led to several effective methods of estimating parameters that thereafter are not required to be determined experimentally.

We present derivation of the age-structured model and its theoretical analysis of the existence of the solution. Furthermore, we have obtained the condition for BEG existence using the Perron-Frobenius theorem. A mathematical description of the cell-cycle control is shown for one-compartment and two-compartment populations, where a compartment refers to a cell population consisting of cells that exhibit similar kinetic properties. We have incorporated into our mathematical model the required growing/aging times in each phase of the cell cycle for the biological viability. Moreover, we have derived analytical formulae for vital parameters in cancer research, such as population doubling time, the average cell-cycle age, and the average removal age from all phases, which we argue is the average cell-cycle time of the population. An estimate of the average cell-cycle time is of a particular interest for biologists and clinicians, and for patient survival prognoses as it is considered that short cell-cycle times correlate with poor survival prognoses for patients.

Applications of our mathematical model to experimental data have been shown. First, we have derived algebraic expressions to determine the population doubling time from single experimental observation as an alternative to empirically constructed growth curve. This result is applicable to various types of cancer cell lines. One option to extend this model would be to derive the cell-cycle time from a single experimental measurement. Second, we have applied our mathematical model to interpret and derive dynamic-depicting parameters of five melanoma cell lines exposed to radiotherapy. The mathematical result suggests there are shortcomings in the experimental methods and provides an insight into the cancer cell population dynamics during post radiotherapy. Finally, a mathematical model depicting a theoretical cancer cell population that comprises two sub-populations with different kinetic properties is presented to describe the transition of a primary culture to a cell line cell population.

0. ABSTRACT

Deputy Vice-Chancellor's Office
Postgraduate Office

UNIVERSITY OF CANTERBURY
Te Whare Wānanga o Waitaha
CHRISTCHURCH NEW ZEALAND

Co-Authorship Form

This form is to accompany the submission of any PhD thesis that contains research reported in co-authored work that has been published, accepted for publication, or submitted for publication. A copy of this form should be included for each co-authored work that is included in the PhD thesis. Completed forms should be included at the front (after the thesis abstract) of each copy of the thesis submitted for examination and library deposit (including electronic copy).

Please indicate the chapter/section/pages of this thesis that are extracted from co-authored work and provide details of the publication or submission from the extract comes:

Chapter 4 contains most of the work published in the Bulletin of Mathematical Biology, Volume 74 under the title "Mathematical determination of cell population doubling times for multiple cell lines", co–authored with David J.N. Wall, Bruce C. Baguley and Britta Basse.

Please detail the nature and extent (%) of contribution by the PhD candidate:

Contributed with data analysis, numerical simulations and the text in 80% range.

Certification by Co-authors:
If there is more than one co-author then a single co-author vcan sign on behalf of all
The undersigned certifys that:

- The above statement correctly reflects the nature and extent of the PhD candidate's contribution to this co-authored work
- In cases where the PhD candidate was the lead author of the co-authored work he or she wrote the text

Name:	Signature:	Date:
David Wall		19/12/12

Deputy Vice-Chancellor's Office
Postgraduate Office

UNIVERSITY OF CANTERBURY
Te Whare Wānanga o Waitaha
CHRISTCHURCH NEW ZEALAND

Co-Authorship Form

This form is to accompany the submission of any PhD thesis that contains research reported in co-authored work that has been published, accepted for publication, or submitted for publication. A copy of this form should be included for each co-authored work that is included in the PhD thesis. Completed forms should be included at the front (after the thesis abstract) of each copy of the thesis submitted for examination and library deposit (including electronic copy).

Please indicate the chapter/section/pages of this thesis that are extracted from co-authored work and provide details of the publication or submission from the extract comes:

Chapter 6 contains most of the work published in the Journal of Theoretical Biology, Volume 260 under the title "Using stem cell and progeny model to illustrate the relationship between cell cycle times of in vivo human tumour cell tissue populations, in vitro primary cultures and the cell lines derived from them", co–authored with David J.N. Wall, Bruce C. Baguley and Britta Basse.

Please detail the nature and extent (%) of contribution by the PhD candidate:

Contributed with data analysis, numerical simulations and the text in 80% range.

Certification by Co-authors:

If there is more than one co-author then a single co-author vcan sign on behalf of all

The undersigned certifys that:

- The above statement correctly reflects the nature and extent of the PhD candidate's contribution to this co-authored work
- In cases where the PhD candidate was the lead author of the co-authored work he or she wrote the text

Name:	Signature:	Date:
David Wall	D Wall	19/12/12

0. ABSTRACT

Acknowledgements

I would like to acknowledge The Department of Mathematics and Statistics at the University of Canterbury for their generous financial support over the years.

I'm grateful to my supervisors Professor David Wall and Professor Bruce Baguley at the University of Auckland for the exciting research project and patience and guidance throughout my study. I'm thankful to Dr. Britta Basse for her valuable mentoring and support during the beginning of my research.

Thank you to all the staff and the lovely and talented postgraduate students in the Mathematics and Statistics Department and other departments at the University of Canterbury, for the great talks about numbers, life, and sharing their great research topics and ideas that have left me feeling that there is no greater joy than tapping into the unknown.

Thanks to the city of Christchurch and the wonderful people that showed me what Kiwis and Cantabrians are about after the February Earthquake in 2011.

Thanks to my new family in New Zealand - Josh, Wendy, Craig and Georgie, for the support and warm welcome into their home, especially during the last year.

Thanks to my friends Zane and Janis, and everyone in my extended family for staying close to me and encouraging me through the years and making me feel less homesick by waking up at 5am to have a silly phone call.

And most of all, thanks to my parents Elza and Jazeps for their love and immense support.

0. ACKNOWLEDGEMENTS

List of Published Papers

1. Daukste, L., Basse, B., Baguley, B.C. & Wall, D.J.N. (2009). Using a stem cell and progeny model to illustrate the relationship between cell cycle times of *in vivo* human tumour cell tissue populations, *in vitro* primary cultures and the cell lines derived from them. *Journal of Theoretical Biology*, 260, 563 – 571. Daukste *et al.* (2009)

2. Daukste, L., Basse, B., Baguley, B.C. & Wall, D.J.N. (2012). Mathematical determination of cell population doubling times for multiple cell lines. *Bulletin of Mathematical Biology*, 74, 2510 – 2534. Daukste *et al.* (2012)

Contents

Glossary

Cell population model parameters

parameter	description	units
t	time	hours
τ	age	hours
$_p$	index in subscript denoting a phase	
τ_p	required cell growing/aging time in phase p	hours
T	maximum cell age in each phase	hours
T_d	population doubling time	hours
T_a	average cell-age of the population	hours
T_{rm}	average cell-removal time	hours
T_c	average cell-cycle time	hours
T_p	average cell age in phase p	hours
T_p^*	average transit time in phase p	hours
$r_{p\to p+1}$	transition rate from phase p to $p+1$	hours^{-1}
μ_p	death rate from phase p	hours^{-1}
λ	growth rate of the population	hours^{-1}
$n_p(t,\tau)$	cell number density function in phase p	$[\tau]^{-1}$
$\widehat{n}_p(\tau)$	cell number density function in phase p at BEG	$[\tau]^{-1}$
N_p	cell number in phase p	
N_{tot}	total cell number of the population	
$\pi_p(t,\tau)$	probability density function in phase p	$[\tau]^{-1}$
$\widehat{\pi}_p(\tau)$	probability density function in phase p at BEG	$[\tau]^{-1}$
Π_p	proliferating cell population proportion in phase p	
P_p	cell population proportion in phase p	

Abbreviations

BEG	balanced exponential growth
PDE	partial differential equation
ODE	ordinary differential equation
DAE	differential algebraic equation
DDE	delay differential equation

Function spaces

$C^{-1}([0,\infty)\times[0,T))$	discontinuous functions on the interval $[0,\infty)\times[0,T)$
$L^{\infty}[0,T)$, $L^{1}[0,T)$	Lebesgue function spaces

Chapter 1

Introduction

1.1 Mathematics in cancer research

The role of mathematics in cancer research has steadily increased over time and the future of this discipline is both exciting and critical as new patients are diagnosed with cancer every day. In New Zealand, around 51 people are diagnosed with cancer every day and around 22 cancer deaths occur (statistics provided by the Cancer Society of New Zealand, www.cancernz.org.nz). Multidisciplinary collaboration in cancer research is essential and mathematical applications can contribute significantly to many areas of cancer research. Mathematical models can provide insight and establish a framework for understanding properties of cancer cells, e.g., by modelling the biochemical behaviour within a single cancer cell or by modelling a tumour growth. This thesis presents the mathematical modelling of the cancer cell population grown out of human body, called cell lines. Several mathematical models that have been derived in close collaboration with the Auckland Cancer Society Research Centre serve as an additional tool for biologists. These models can be used to either give understanding of a plausible dynamics of cancer cell populations or to gain more effective methods of estimating parameters depicting the dynamics of cancer cell populations. We shall continue by introducing biological concepts that will be frequently referred to in the subsequent chapters.

1.2 Cell cycle and apoptosis

A cell cycle is a progression of a cell through steps of growth and chromosome duplication to complete cell division. The cell cycle of a eukaryotic cell is traditionally divided in four phases - G_1, S, G_2 and M. Phases G_1, S and G_2 together are called the interphase. A gap phase G_1 (G for gap) is an interval before the DNA synthesis (S-phase) that is followed by another gap phase named G_2, where the cell keeps growing until mitosis takes place (M-phase). A cell cycle consists of various cyclins and cyclin-dependent kinases that have to react at certain cell-cycle control checkpoints. During its cell cycle, a cell makes two vital decisions: first, the decision of "entering into S-phase" is made in late G_1-phase, called G_1 checkpoint. DNA replication begins when the cell is ready to undergo the entire cell cycle. Second decision is the "entry into mitosis", mitosis will proceed through all its stages once initiated, called G_2 checkpoint. The cell-cycle control system, the key proteins of the control system, initiates and controls the progression of the cell cycle and can arrest it at specific checkpoints. Cells in a cell cycle are called dividing or proliferating cell. If a cell is non-dividing or quiescent it is said to be in G_0-phase. A cell in G_0-phase can return to the G_1-phase again under the influence of mitogenic signals (growth factors, tumour viruses etc.), see Alberts *et al.* (1994). A diagram outlining cell-cycle

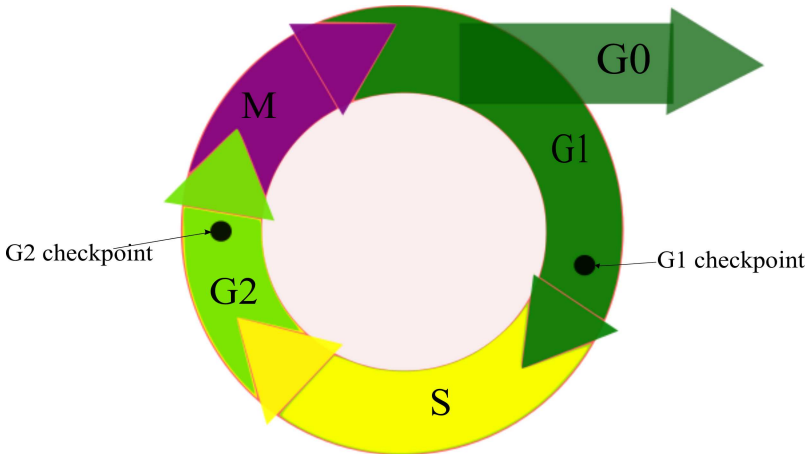

Figure 1.1: The cell-cycle control diagram. During G_1-phase cell grows then DNA is replicated and new chromatin is formed, denoted as S-phase. During G_2-phase cell prepares for mitosis or M-phase, where it divides into two daughter cells. A cell passing through the cell-cycle control checkpoints in G_1 and G_2 phases and completing cell division is called proliferating. G_0 depicts the non-proliferating cell phase.

control with key checkpoints is shown in Figure 1.1. Some non-dividing cells like neurons and skeletal muscle fibre cells are unable to re-enter the cell cycle. Others, like fibroblasts and lymphocytes are ordinarily in the G_0 - phase but can be activated by external agents.

Cells have the potential to undergo genetically programmed cell death, or apoptosis. Apoptosis is the "tidy" breakdown and disposal of cells without causing an inflammatory response in the body. Apoptosis is common during embryonic development, but also occurs in a response to severe cellular damage, viral infections and somatic mutations. Apoptosis is a protective mechanism that eliminates many virus-infected and genetically altered cells, Meisenberg & Simmons (1998).

We continue by introducing two parameters: doubling time and cell-cycle time. Doubling time is defined as the time required to double in number. Cell-cycle time is the time required to complete a cell cycle. For a single cell, doubling time and cell-cycle time are evidently equal. However, in the case of a cancer cell population, this is not necessarily true, we investigate this closer in Chapter 2. Cell-cycle length varies greatly during interphase from cell to cell with M-phase duration considered to be short compared to the other phases.

1.3 Cancer cell population: primary culture and cell line

Gene mutation can turn a normal cell into a cancer cell. What cell mechanisms exactly trigger these mutations is unclear. A cancer cell is considered to be more aggressive and faster growing than a cell from normal tissue. Tumour cells divide without inhibition, i.e., they do not stop dividing after they come into contact with neighbouring cells, and increasingly act as individuals with the goal of maximizing their own proliferation, see Nagl (2006). Great variation in the duration of the G_1-phase among different cancer cells produces a variety of cell-cycle times of the cancer cells that, effectively, influence the response to any type of cancer treatment.

In this thesis, our interest in cancer cell populations will be mainly focused on *in vitro* (out of

body) cell populations, and melanoma cell populations in particular. Cancer cells, taken from a tumour tissue sample (removed at surgery), to be examined *in vitro* are called primary culture. Tumour tissue can be grown in culture and measurements of primary culture cell-cycle times show a range of 3 days to several weeks, which is similar to that observed *in vivo* (in body), see Baguley & Marshall (2004); Furneaux *et al.* (2008). After several months, by a variety of culture techniques designed to preserve the viability of tumour cells and suppress the growth of host cells, particularly of fibroblasts, which are naturally activated in the wounding response generated by the tissue disaggregation, the clinical tumour material exhibits stable growth and is referred to as cell lines, Baguley *et al.* (2002). Established cancer cell lines exhibit shorter cell-cycle times thus reacting to the treatment much faster than cells in the primary cultures. It is considered that cells in cell lines divide indefinitely. The patients from whom the tissue samples were collected are often outlived by cancer cell lines.

Human tumour cell lines have been used extensively in the discovery and characterisation of new chemotherapeutic drugs, Baguley & Marshall (2004, 2008). A potential disadvantage of cancer cell lines is that they may have lost important properties originally present *in vivo*. Cell-cycle times are different between tumours and cell lines, and, as mentioned before, cell-cycle times of primary cultures cover the same wide range as estimated *in vivo* cell-cycle times. Responses of primary cultures to cancer treatment also differ from those of cell lines, suggesting that the process of developing a cell line can result in the loss of important cellular responses. The identification of cell lines that preserve potential targets is an important goal in cancer biology and research. Using primary cultures will help in this identification, Baguley & Marshall (2004).

Mathematical models have been applied to cancer cell populations taken from cell lines in this thesis. However, further work is necessary to extend the models presented in the subsequent chapters to describe the dynamics of cells in a primary culture, thus giving more insight into *in vivo* population growth and response to treatments.

Stem cells differ from other cells by two properties: firstly, stem cells has a self renewal property, meaning they can go through cell division many times whilst preserving their undifferentiated state. Secondly, stem cells have the potential to differentiate into other types of cells. It is hypothesised that a small proportion of cancer stem cells drive the growth of cancer in humans Dittmat & Zanker (2009); Schatton & Frank (2007); Sole *et al.* (2008). In Chapter 5, we develop a mathematical model that describes the behaviour of system with two cell populations with different kinetic characteristics, to provide a framework for understanding the behaviour of cancer tissue that is sustained by a minor population of proliferating stem cells.

1.4 Mathematical modelling of the growth of a cell population

The mathematical models are often predetermined by the available experimental data. In Steel (1977), G.G. Steel presented two principles that prevent unrestricted model-building. First, Occam's Razor states: "We should always choose the simplest model that will satisfactorily fit the data. Any increase in sophistication beyond this takes us into the realm of imagination rather than science". Second, Principle of Analogy: "A model whose parameters relate to experimentally measurable quantities is to be preferred to one that has abstract parameters. A model that is a close analogue to the actual cell system more readily enables predictions to be made about as yet undetected responses".

With an objective to model a cell population taken from a cell line, we first must observe that such a population does not respond to spatial constraints, thus, it exhibits balanced exponential growth (BEG), Bell (1968). We note here that cells in primary cultures do not exhibit exponential growth. Applied mathematics presents various methods of examining exponentially growing populations such

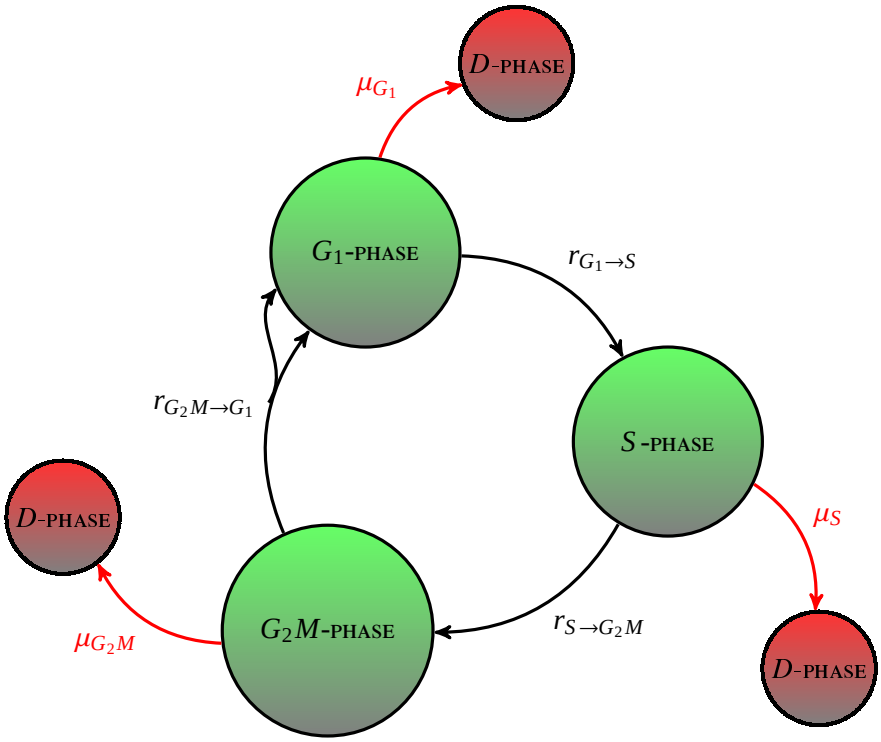

Figure 1.2: Diagram of the cell-cycle control of *in vitro* tumour cells showing the proportions in each phase. Parameters described in the Glossary.

as discrete and continuous, deterministic and stochastic methods.

Our choice lies in continuous deterministic models, with a focus on age-structured population models. Our mathematical model is initially designed to depict the growth of cancer cell population in the BEG state, i.e., population that has not been exposed to any cancer treatment. We assume that all cells in the population are proliferating and can be viewed as subdivided among phases G_1, S, G_2, and M. Due to presented experimental data, explained in Section 1.5, we combine subpopulations in G_2 and M phases and refer to it as G_2M-phase. Cells move from one phase to the next with a certain transition probability rate (r). Age (τ) is considered to be the time spent by a given cell in its current phase. Thus, each cell is at age zero when entering into a new phase of cell growth. No cells are in the non-proliferating state or G_0-phase. Although cells from cell lines exhibit immortality properties, we have incorporated a probability of apoptosis in each phase (μ). Figure 1.2 presents a schematically illustrated cancer cell population in BEG.

Apoptosis is genetically programmed cell death without inflammatory breakdown and disposal of cells. Cell necrosis occurs due to physical or chemical damage. Throughout this thesis, we define cell death or loss as a process of cells undergoing apoptosis. We declare that cells are proliferating or non-proliferating until they undergo apoptosis. We remark that notions cell death, apoptosis and cell loss are interchangeable in this thesis.

Detailed derivation of an age-structured model can be found in Chapter 2. Potential cancer treatment effects can be incorporated into mathematical equations by examining the effect of the treatment on the cell-cycle control. For example, a chemotherapeutic drug, that is said to stop mitosis, can be incorporated into the mathematical model by setting the transition probability rate from M-phase to

G_1-phase to zero. Similarly, after ionised radiation DNA damage can occur and cells might repair it and re-enter the cell cycle or might undergo apoptosis (the p53 protein - the product of tumour suppressor gene - promotes apoptosis and thus helps to eliminate the defective cell). These effects can be incorporated into our model by altering the transition rates between respective phases.

With the aim of providing "shortcuts" to estimate parameters that are experimentally unobtainable or not sufficiently accurate, we have derived mathematical models in the following chapters that would be beneficial for biologists and clinicians. We have kept in mind Occam's Razor and Principle of Analogy when simplifying a more general model in Chapters 3, 4, 5 in order to fit experimental data.

1.5 Flow cytometry

We have dedicated this section to introduce an experimental measurement technique with flow cytometry apparatus. Analysis of a cell population in a state of replication can be achieved by fluorescence labelling of the cell nuclei in suspension and subsequently analysing the fluorescence properties of each cell in the population. G_1-phase cells will have one copy of DNA and will therefore have 1x the fluorescence intensity. Cells in the G_2 and M phases will have two copies of DNA and, accordingly, will have 2x the intensity. Flow cytometry cannot distinguish between G_2 and M phases, therefore, we combine them for our mathematical models, derived in the following chapters, and refer to it as G_2M-phase. Because the cells in the S-phase are synthesizing DNA, they will have fluorescence values between 1x and 2x the population's. The flow cytometry histogram shown in Figure 1.3 (in blue) is obtained from labelled cells transiting through the laser beam and their fluorescence signal ultimately generating a voltage pulse by the fluorescence detector (photomultiplier tube). The horizontal axis in Figure 1.3 depicts the total cell fluorescence noted in the literature as FL2-A ("A" for area). The vertical axis shows the number of cells with a respective total fluorescence value. We can extract estimates of population proportions in each phase from the flow cytometry profiles. Population distribution in the respective phases is shown in coloured-in segments. In this thesis, we analyse flow cytometry profiles using Cylchred software provided by Cytonet, UK. When population is unexposed to the cancer treatment, i.e., exhibiting BEG, the flow cytometry profiles remain unchanged at all experimental observation points. We discuss steady population-distribution conditions in Chapter 2.

1.6 Thesis outline

Chapter 2
In this chapter, we derive and analyse an age-structured cell population model. We show an implicit analytical solution of the McKendrick-von Foerster partial differential equation (PDE) with side conditions: an initial condition and a boundary condition. Moreover, we prove the existence of that solution using methods developed for the Volterra integral equation of the second kind. We examine two kinds of transition probability rates between two consecutive phases of the cell cycle: constant and piecewise constant. A piecewise constant transition rate is biologically more relevant because cells must grow (age) in particular phases of the cell cycle before being able to transit into the next phase. Because a cancer cell population, when taken from a cancer cell line culture, exhibits the BEG state, we demonstrate a condition for the existence of BEG by using the Perron-Frobenius theorem. Later in this process, we derived formulae of the constant population proportions among cell cycle phases at BEG state. We show the reduction of a PDE model to an ordinary differential equation (ODE) system and a delay differential equation (DDE) system. A general PDE model allows us to derive vital parameters in cancer research, such as population doubling time and average cell-cycle time.

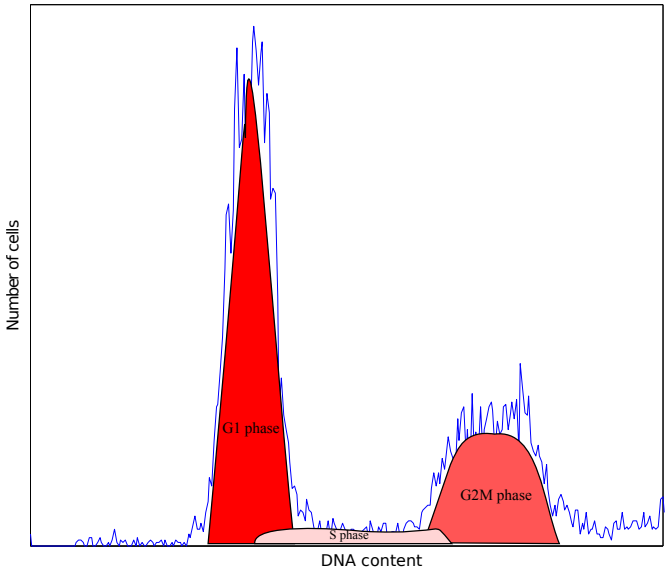

Figure 1.3: An example of a flow cytometryprofile of an unperturbed cell line population. The proportions of cell population in the G_1, S, and G_2M phases are shown in the diagram. The horizontal axis label FL2-A ("A" for area) depicts the total cell fluorescence. The vertical axis shows the number of cells with a respective total fluorescence value.

Results of this chapter provide an insight into the relationship between population doubling time and average cell-cycle time. A mathematical distinction is shown between two biological understandings: the expected average age in the phase and the expected removal time from the phase.

Chapter 3

This chapter introduces a new approach of determining population doubling time using a single experimental observation. A method for experimental estimation of cell-cycle times or doubling times of cultured cancer cell populations, based on addition of paclitaxel (an inhibitor of cell division) has been proposed in literature. We use a mathematical model to investigate relationships between essential parameters of the cell division cycle following inhibition of cell division. The reduction in the number of cells engaged in DNA replication reaches a plateau as the concentration of paclitaxel is increased; this can be determined experimentally. From our model, we have derived a plateau log reduction formula for proliferating cells and established that there are linear relationships between the plateau log reduction values and the reciprocal of doubling times (i.e. growth rates of the populations). We have therefore provided theoretical justification of an important experimental technique to determine cell doubling times. Furthermore, we have applied Monte Carlo experiments to justify the suggested linear relationships used to estimate doubling time from 5-day cell culture assays. We show that our results are applicable to cancer cell populations with cell loss present. Our mathematical model result provides a shortcut for estimating the population doubling time and we hope to extend this model for the cell-cycle estimation from a single experimental measurement.

Most of the results presented in this chapter have been published in Daukste *et al.* (2012).

Chapter 4

In this chapter, we examine the response of a cancer cell population to a one-time ionised irradiation dose treatment. We show that, by changing the PDE system of the number density function to the probability density function, our model tracks the variability of proportions in each phase of the cell

cycle and is compatible with the experimental estimates of proportions in each phase after a variety of cancer treatments. Our results agree with the previous studies of irradiated cancer cell lines, i.e., a cancer cell population undergoes little apoptosis after radiotherapy. Therefore, this study's experimentally observed decrease in the expected number of cells is due to the long-term arrest of the cell cycle. Our model provides an interval of the initial surviving fraction of the cell population for each cell line, i.e., the proportion of cells that keep proliferating after the application of radiotherapy. In the discussion section, we explain why the survival fraction estimated via our mathematical model does not agree with the experimentally estimated one.

Chapter 5

This chapter examines the application of the two-population model. This mathematical model describes the behaviour of a system with two cell populations with different kinetic characteristics. The results provide a framework for understanding the growth behaviour of cancer tissue that is sustained by a minor population of proliferating stem cells. The Perron-Frobenius theorem is used to prove the existence of a BEG state of a two population model.

The results from this chapter have been published in Daukste *et al.* (2009).

Chapter 2

One-Compartment Age-Structured Model of Cancer Cell Population Growth

In this chapter, we derive and analyse an age-structured cell population model. We show an implicit analytical solution of the McKendrick-von Foerster partial differential equation (PDE) with side conditions: an initial condition and a boundary condition. Moreover, we prove the existence of that solution using methods developed for the Volterra integral equation of the second kind. We examine two kinds of transition probability rates between two consecutive phases of the cell cycle: constant and piecewise constant. A piecewise constant transition rate is biologically more relevant because cells must grow (age) in particular phases of the cell cycle before being able to transit into the next phase. Because cancer cell population, when taken from the cancer cell line culture, exhibits the balanced exponential growth (BEG) state, we demonstrate a condition for the existence of BEG by using the Perron-Frobenius theorem. Later in the process, we derived formulae of the constant population proportions among cell cycle phases at BEG state. This mathematical model allows us to derive vital parameters in cancer research, such as population doubling time and average cell-cycle time. Results of this chapter provide an insight into the relationship between population doubling time and average cell-cycle time. A mathematical distinction is shown between two biological understandings: the expected average age in the phase and the expected removal time from the phase.

2.1 Introduction

Our objective is to mathematically model the dynamics of a cancer cell population taken from the cancer cell line culture. The mathematical modelling of a cancer cell population taken from the primary culture, which effectively exhibits *in vivo* properties, is of great interest in the cancer research; however, because such a population does not demonstrate balanced exponential growth (BEG) Bell (1968) properties, our main focus will stay on cell line cultures throughout this thesis.

The criteria for developing the mathematical models presented in the following chapters (such as those posed in Metz & Diekmann (1986)) are the biological relevance and mathematical tractability. Mathematical modelling has been applied to a large spectrum of the cancer cell proliferation problems, starting from the cycle-control biochemical modelling of a single cell to the modelling of the cancer cell population, looking into both - *in vivo* and *in vitro* cases. A single cell growth models open prospects for the multiscale modelling. Review papers Byrne (2010); Deisboeck *et al.* (2011) on cancer tumour modelling can be found in the literature. An overview paper on structured cell population dynamics Arino (1995) stated that during the 1970s, mathematical modelling was more focused on

nonlinear equation (such as Gompertz equation) applications to cancer cell population growth. In the 1980s, focus switched to the linear age-structured models. Linear partial differential equations have an advantage of being simple for analysis and are also applicable to the mathematical modelling of the cancer cell population.

A cell compartment method can analyse the formation of cancer cells from stem cells. In Ganguly & Puri (2006), it was concluded that mutations in stem cells rather than in early progeny cells lead to faster growth of the abnormal progeny. Moreover, a model shows that a repeated insult to mature cells leads to an increased growth rate of the abnormal progeny cells.

Compartmentalized cell population by cell kinetic properties, e.g. assuming that cells exit in one of two kinetic states: proliferating and non-proliferating has been used to examine cell motion in the tumour, Tindalla & Please (2007). It is assumed that the dominant mechanism for cell motion is due to chemical gradients. Multicellular tumour spheroids are used in this study because they exhibit many of the characteristics of *in vivo* tumours. The model in Tindalla & Please (2007) shows the commonly held view of the cell cycle distributions within spheroids - proliferating cells are near the boundary and the quiescent cells are in the core.

Cell compartment method has also been used to analyse the time- and dose-dependent effects of antitumour agent RHPS4 on the cancer cell line HCT116, in Johnson *et al.* (2011). In this study, experimental estimates of quite a few parameters have been used, i.e., the proportions in each phase as well as the proportion of senescent cells, the total number of cells at certain time and the overall population growth rate. In Johnson *et al.* (2011), telomerase inhibition RHPS4 increases the rate at which cells become senescent state but, rather surprisingly, actually inhibits the rate of cell death detects.

Mathematical models derived in this thesis have been previously examined to some extent in Basse & Ubezio (2007); Basse *et al.* (2003, 2004a,b, 2005). In this chapter, we introduce a theoretical background of the age-structured models and extend it beyond the analytical derivations published in other literature including models by Basse & Ubezio (2007); Basse *et al.* (2003, 2004a,b, 2005). We have derived analytical expressions for the average cell age in the phase and the average removal or transit time through the phase, which is a novel result and has not been published before. The existence and the uniqueness of the solution have been shown in the literature before just as the conditions for the balanced exponential growth. We have shown results for the piecewise-constant transition rates and analytically derived formulae for dynamical parameters. A DDE system has been derived from an age-structured system as used by Simms *et al.* (2012).

As mentioned before, cancer cell population taken from the cancer cell line culture exhibits BEG if unexposed to any cancer treatment methods. In the literature, BEG is also referred to as an asynchronous exponential growth (AEG), the steady-state distribution (SSD), or steady age distribution (SAD), but we will use notion BEG throughout the thesis. Age-structured models have the capacity to describe the underlying structure of a cancer cell population at BEG and provide an opportunity to estimate vital parameters in cancer research via mathematical models as an alternative to experimental observations.

Solely for the purposes of the experimental data used in our research, we subdivide cell cycle into the respective G_1, S, and a combined G_2M phases, as shown in Figure 1.2 in the Introduction. Our models are to be utilised for flow cytometry profiles, and because the flow cytometry apparatus/method cannot distinguish the difference between the G_2 and M phases (due to the fact that DNA contents in both phases are twice that of S-phase), phases G_2 and M are combined in a G_2M-phase in our mathematical model.

In this chapter, we present the derivation of the one-population (also denoted as a one-compartment, in this thesis term compartment does not refer to a phase of the cell cycle) age-structured model and

the proof of the existence for the solution from the theory of the Volterra equations of the second kind. Furthermore, the existence of the BEG state is proved by Perron-Frobenius theorem. Later, we express parameters that depict the dynamics of a cancer cell population, such as population doubling time and expected or average cell-cycle time of the cancer cell population, that have not been exposed to any cancer treatment. From the results obtained in this chapter, we gain an insight into the relationship between population doubling time and average cell-cycle time.

2.2 Age-structured model of a cancer cell population

Our objective is to model the dynamics of a cancer cell population in order to derive parameters that describe the kinetics of the population, which has not been exposed to treatment, as well as parameters that describe the effects of various cancer treatments.

A cell cycle of cancer cell population is modelled assuming that cells from this cancer cell population produce daughter cells with similar kinetic properties. In our model, cell cycle is subdivided into three phases: G_1, S, and G_2M (with combined phases G_2 and M because we apply our model to flow cytometry [FC] profiles, and FC measurements cannot distinguish between G_2 and M phases because DNA contents in both phases are twice that of S-phase). Age is considered to be the time spent by a given cell in its current phase. Thus, each cell has age zero when entering into a new phase of cell growth.

Derivation of an age-structured partial differential equation is as follows. First, let us assume that there is a continuous function $\mathbf{n}(t,\tau)$ that represents the number density of the cancer cell population and is a vector quantity, with

$$\mathbf{n}(t,\tau) = [n_{G_1}(t,\tau) \quad n_S(t,\tau) \quad n_{G_2M}(t,\tau)]^T. \tag{2.2.1}$$

Here vector components $n_p(t,\tau)$ with $p \in \{G_1, S, G_2M\}$ are continuous functions, where $n_p : [0,\infty) \times [0,T) \to [0,\infty)$, that shows the number density of cells with age τ at time t in a cell cycle phase p. Age τ states the duration of a cell in particular phase p. We impose a maximum age of cells, $T > 0$, after which cells are assumed to have died. In fact, *in vitro* studies are seldom longer than 2 weeks, so most of the time, T need not be larger than this number Baguley & Marshall (2004). The assumption of a maximum age is for mathematical simplicity; T can be set arbitrarily large. Furthermore, derivatives of $n_p(t,\tau)$ exist and are also continuous functions on $[0,\infty) \times [0,T)$. If time t is increased by h units (and we assume that time unit $h = \triangle t = \triangle\tau$), then cells have aged by h units. Given that function $n_p(t,\tau)$ has a continuous derivative, then we obtain the following equation:

$$\begin{aligned}\lim_{h\to 0} \frac{n_p(t+h,\tau+h) - n_p(t,\tau)}{h} &= \lim_{h\to 0} \frac{n_p(t+h,\tau+h) - n_p(t,\tau+h)}{h} + \frac{n_p(t,\tau+h) - n_p(t,\tau)}{h} \\ &= \frac{\partial}{\partial t} n_p(t,\tau) + \frac{\partial}{\partial \tau} n_p(t,\tau).\end{aligned}$$

Second, let us assume that the probability rate at which cells leave phase p is given by term $b_p(t,\tau)$. Assumptions that the transition probability depends on time t and age τ and is a non-negative piecewise continuous function, are comprehensible in biological terms. Here, transition rate $b_p(t,\tau)$ with

$p \in \{G_1, S, G_2M\}$ is defined as follows:

$$\begin{aligned} b_{G_1}(t,\tau) &= r_{G_1\to S}(t,\tau) + \mu_{G_1}(t,\tau), \\ b_S(t,\tau) &= r_{S\to G_2M}(t,\tau) + \mu_S(t,\tau), \\ b_{G_2M}(t,\tau) &= r_{G_2M\to G_1}(t,\tau) + \mu_{G_2M}(t,\tau), \end{aligned} \tag{2.2.2}$$

where $r_{G_1\to S}(t,\tau)$, $r_{S\to G_2M}(t,\tau)$, and $r_{G_2M\to G_1}(t,\tau)$ are the transition probability rates (probability per time unit per cell) between two consecutive phases and $\mu_p(t,\tau)$ depicts the death rate from the phase p. Description of variables used in our mathematical model that has been schematically depicted in Figure 1.2 have been explained in the Glossary. We have assumed, for now, that the transition probability rates and death rates are dependent on time t and age τ. We also assume that cancer cells taken from cancer cell lines have a potential undergoing apoptosis at any phase of the cell cycle. The conservation law states that the variation of the population number density in p phase in time is caused by a transition to the next phase or death; thus, the following linear partial differential equation can be derived:

$$\frac{\partial}{\partial t}n_p(t,\tau) + \frac{\partial}{\partial \tau}n_p(t,\tau) = -b_p(t,\tau)n_p(t,\tau). \tag{2.2.3}$$

Conservation between the various phases and the death phase, which is not explicitly modelled, follows from the continuity of the derivatives on the domain. This is particularly important when considering proportions in each phase rather than number of cells.

Third, additional conditions for equation (2.2.3) are provided: the initial number density distribution and renewal condition (also called Lotka equation) for each phase. The initial age distribution is defined as:

$$n_p(t=0,\tau) = n_p^0(\tau), \tag{2.2.4}$$

with the initial distribution $n_p^0(\tau)$ in $(L^1 \cap L^\infty)[0,T)$. Lotka showed Lotka (1922) that a boundary condition expressed as an integral with respect to cell population age will then result in the solution being depend on the boundary condition itself. The Lotka boundary condition turns the problem described with (2.2.3) and (2.2.4) into a bounded and, subsequently, a compact problem. The boundary or renewal condition states that cells in each phase start from age zero. Furthermore, all cells at age zero have transferred from the previous phase and are expressed as follows:

$$n_p(t,\tau=0) = \int_0^T a_{p-1}(t,\tau)n_{p-1}(t,\tau)\,d\tau, \tag{2.2.5}$$

where transition rate $a_p(t,\tau)$ with $p \in \{G_1, S, G_2M\}$ is defined as:

$$\begin{aligned} a_{G_1}(t,\tau) &= r_{G_1\to S}(t,\tau), \\ a_S(t,\tau) &= r_{S\to G_2M}(t,\tau), \\ a_{G_2M}(t,\tau) &= 2r_{G_2M\to G_1}(t,\tau). \end{aligned} \tag{2.2.6}$$

Cells are presumed to be in the G_1-phase immediately after division. Here, subscript $p-1$ in equation (2.2.5) is taken to signify the following:

$$G_1 - 1 = G_2M; \quad S - 1 = G_1; \quad G_2M - 1 = S.$$

We note that for the G_1 - phase, the renewal condition (2.2.5) is as follows:

$$n_{G_1}(t, \tau = 0) = \int_0^T 2r_{G_2M \to G_1}(t, \tau) n_{G_2M}(t, \tau) d\tau, \tag{2.2.7}$$

where 2 refers to each cell that has completed mitosis producing two daughter cells.

It is assumed that $r_{p \to p+1}, \mu_p \in C^{-1}([0, \infty) \times [0, T))$ for all $p \in \{G_1, S, G_2M\}$, and, in addition, they are bounded and strictly positive. We also assume that derivatives of $r_{p \to p+1}(t, \tau)$ and $\mu_p(t, \tau)$ for all $p \in \{G_1, S, G_2M\}$ are bounded and piecewise continuous in t and τ. Finally, we assume that there exists a positive lower bound. Note that for biological realism, we also assume $\mu_p(t, \tau)$ is non-negative. The simplicity of the model is due to the linearity that is present when dealing with a cancer cell population that grows *in vitro* exponentially without any environmental constraints. In the subsequent sections, we provide the analytical solution of the problem (2.2.3) - (2.2.5) and show the condition for the existence of such solution.

2.2.1 Analytical solution of an age-structured model

2.2.1.1 Single-phase model

We focus on a single-phase model in this section to demonstrate the derivation of the analytical solution via the method of characteristics. We impose change in variables: now arguments t and τ depend on parameter z. Thus, the number density function can be rewritten as follows:

$$\bar{n}_p(z) = n_p(t(z), \tau(z)). \tag{2.2.8}$$

Hence, the derivative of $\bar{n}_p(z)$ with respect to new variable z can be expressed as follows:

$$\frac{d\bar{n}_p}{dz} = \frac{d}{dz} n_p(t(z), \tau(z)) = \frac{\partial n_p}{\partial t}\frac{dt}{dz} + \frac{\partial n_p}{\partial \tau}\frac{d\tau}{dz},$$

where z varies along the following characteristic lines:

$$\frac{dt}{dz} = 1, \qquad \frac{d\tau}{dz} = 1, \tag{2.2.9}$$

$$\tau = z + t. \tag{2.2.10}$$

Thus, equation (2.2.3) can be rewritten as

$$\frac{d\bar{n}_p}{dz}(z) + b_p(t(z), \tau(z))\bar{n}_p(z) = 0. \tag{2.2.11}$$

We choose point (t_0, τ_0) along the characteristic lines (2.2.9). This point can be any point in the first quadrant, as shown in Figure 2.1. Thus, the following expressions are derived:

$$t = t_0 + z, \qquad \tau = \tau_0 + z.$$

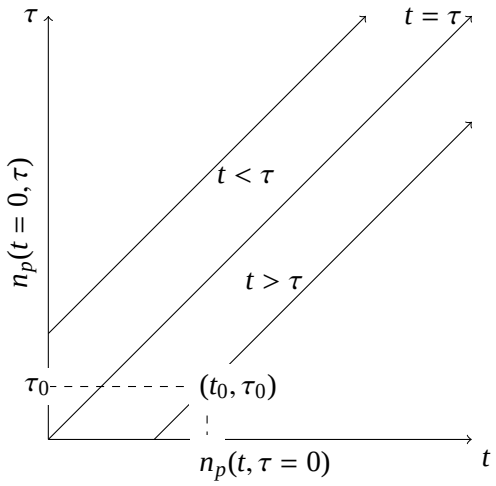

Figure 2.1: Characteristic lines of McKendrick-von Foerster equation analytical solution, where number density function $n_p(t,\tau)$ on horizontal axis represents the renewal condition, and $n_p(t,\tau)$ on vertical axis depicts the initial condition.

For simplicity, we define the number density function n_p at point (t_0,τ_0) as $n_p(t_0,\tau_0) = n_0$. Therefore, equation (2.2.11) can be solved by integrating along the characteristic lines as follows:

$$\begin{aligned}\bar{n}_p(z) &= n_0\, e^{-\int_0^z b_p(t(\xi),\tau(\xi))\,d\xi} = n_0\, e^{-\int_0^z b_p(t_0+\xi,\tau_0+\xi)\,d\xi} = \\ &= n_0\, e^{-\int_{\tau_0}^{\tau_0+z} b_p(s+t_0-\tau_0,s)\,ds},\end{aligned} \tag{2.2.12}$$

where $s = \tau_0 + \xi$. Further, we subdivide analysis of the solution into two cases: $t < \tau$ and $t > \tau$, as depicted in Figure 2.1. In the case of $t < \tau$, we express solution of $\bar{n}_p(z)$ as:

$$\begin{aligned} t &= 0 + z, \qquad \tau = \tau_0 + z, \\ \bar{n}_p(z) &= n_p(z, \tau_0 + z) = n_p(0,\tau_0)\, e^{-\int_{\tau_0}^{\tau_0+z} b_p(s-\tau_0,s)\,ds}. \end{aligned}$$

Thus, the number density $n_p(t,\tau)$ for the case $t < \tau$ can be expressed as follows:

$$n(t,\tau) = n_p(0,\tau - t)\, e^{-\int_{\tau-t}^{\tau} b_p(s+t-\tau,s)\,ds}, \quad t < \tau. \tag{2.2.13}$$

We note that the analytical solution of the problem (2.2.3) - (2.2.5), in the case of $t > \tau$, portrays the growth of the cancer cell population taken from the cancer cell line culture, i.e., the time it takes for the cell population to grow is longer than the age τ that cells have spend in phase p. For the case $t > \tau$, solution of $\bar{n}_p(z)$ is as follows:

$$\begin{aligned} t &= t_0 + z, \qquad \tau = z, \\ \bar{n}_p &= n_p(t_0 + z, z) = n_p(t_0, 0)\, e^{-\int_0^z b_p(s+t_0,s)\,ds}. \end{aligned}$$

Here, the variable change gives us cell number density function $n_p(t,\tau)$, for the case $t > \tau$, as:

$$n_p(t,\tau) = n_p(t-\tau,0)\, e^{-\int_0^\tau b_p(s+t-\tau,s)\,ds}, \quad t > \tau. \tag{2.2.14}$$

Thus, by using the renewal condition (2.2.5), equation (2.2.14) can be rewritten in its general form as a representation of the asymptotic solution of the problem (2.2.3) - (2.2.5) as follows:

$$n_p(t,\tau) = \int_0^T a_{p-1}(t-\tau,s)\, n_{p-1}(t-\tau,s)\,ds\; e^{-\int_0^\tau b_p(s+t-\tau,s)\,ds}, \quad t > \tau. \tag{2.2.15}$$

2.2.1.2 Multiple-phase model

For the purposes of mathematical analysis in the subsequent sections, we rewrite the problem of cancer cell population growth with more general notation using vector function $\mathbf{n}(t,\tau)$, as defined in (2.2.1).

The cancer cell population taken from the cancer cell line culture exhibits BEG state. Because there are no environmental constraints on the cancer cell population growth, a linear partial differential equation is suitable for depicting such cell population dynamics. In more general notation, McKendrick - von Foerster equation (2.2.3) can be rewritten as:

$$\frac{\partial}{\partial t}\mathbf{n}(t,\tau) + \frac{\partial}{\partial \tau}\mathbf{n}(t,\tau) = -\mathbf{D}_{\text{out}}(t,\tau)\mathbf{n}(t,\tau), \quad 0 < t < \infty, \quad 0 < \tau < T, \tag{2.2.16}$$

with respective side conditions defined as follows:

$$\mathbf{n}(t=0,\tau) = \mathbf{n}^0(\tau), \quad \text{initial age distribution}, \tag{2.2.17}$$

$$\mathbf{n}(t,\tau=0) = \int_0^T \mathbf{D}_{\text{in}}(t,\tau)\mathbf{n}(t,\tau)\,d\tau, \quad t > 0, \quad \text{renewal distribution}. \tag{2.2.18}$$

The matrix $\mathbf{D}_{\text{out}}$ represents the loss of cells from the various phases via death and transfer to other phases, and is defined as:

$$\mathbf{D}_{\text{out}}(t,\tau) = \begin{bmatrix} r_{G_1\to S} + \mu_{G_1} & 0 & 0 \\ 0 & r_{S\to G_2M} + \mu_S & 0 \\ 0 & 0 & r_{G_2M\to G_1} + \mu_{G_2M} \end{bmatrix}(t,\tau). \tag{2.2.19}$$

The renewal matrix $\mathbf{D}_{\text{in}}$ represents the gain of cells at age $\tau = 0$ in each phase and is caused by transfer from other phases. $\mathbf{D}_{\text{in}}$ is defined as:

$$\mathbf{D}_{\text{in}}(t,\tau) = \begin{bmatrix} 0 & 0 & 2r_{G_2M\to G_1} \\ r_{G_1\to S} & 0 & 0 \\ 0 & r_{S\to G_2M} & 0 \end{bmatrix}(t,\tau). \tag{2.2.20}$$

Transition rates $r_{p\to p+1}$ and μ_p for $p \in \{G_1, S, G_2M\}$ are described in the Glossary, with the cell-cycle control depicted in Figure 1.2. Solution to the governing differential equation (2.2.16) along the characteristic lines, already expressed for each component of vector function $\mathbf{n}(t,\tau)$ in equations (2.2.13) and (2.2.14), is as follows:

$$\mathbf{n}(t,\tau) = \begin{cases} \exp\left(-\int_{\tau-t}^{\tau} \mathbf{D}_{\text{out}}(s+t-\tau,s)\;ds\right)\mathbf{n}^0(\tau-t), & 0 \le t \le \tau, \\ \exp\left(-\int_0^{\tau} \mathbf{D}_{\text{out}}(s+t-\tau,s)\;ds\right)\mathbf{n}(t-\tau,0), & 0 \le \tau < t. \end{cases} \tag{2.2.21}$$

2.3 Existence of a unique solution

Analytical solution of McKendrick-von Foerster equation (2.2.16) assumes that the solution on the boundary $\tau = 0$ has been given. However, in our problem, we are given the renewal boundary condition (2.2.18). Substituting the formal solution from (2.2.21) into the boundary condition (2.2.18) gives us a Volterra integral equation of the second kind for $\mathbf{n}(t, 0)$:

$$\mathbf{n}(t,0) = \mathcal{F}(t) + \int_0^t K(t,s)\mathbf{n}(s,0)\ ds, \tag{2.3.1}$$

where

$$\mathcal{F}(t) = \int_t^T \mathbf{D}_{\text{in}}(t,\tau)\exp\left(-\int_{\tau-t}^{\tau}\mathbf{D}_{\text{out}}(s+t-\tau,s)\ ds\right)\mathbf{n}^{\mathbf{0}}(\tau-t)\ d\tau, \tag{2.3.2}$$

and kernel of integro-equation is defined as follows:

$$K(t,s) = \mathbf{D}_{\text{in}}(t,t-s)\exp\left(-\int_0^{t-s}\mathbf{D}_{\text{out}}(\xi+s,\xi)\ d\xi\right). \tag{2.3.3}$$

By the assumptions made in our problem, we know that $\mathbf{D}_{\text{out}}(t,\tau)$ and $\mathbf{D}_{\text{in}}(t,\tau)$ are piecewise continuous: therefore, $K(t,s)$ is piecewise continuous. Furthermore, because the components of $\mathbf{n}^0(\tau)$ are in $(L^1 \cap L^\infty)[0,T)$ and the components of $\mathbf{D}_{\text{in}}(t,\tau)$ are bounded, we find that $\mathcal{F}(t)$ exists. We observe, by the piecewise continuity of $\mathbf{D}_{\text{out}}$ and $\mathbf{D}_{\text{in}}$, that $\mathcal{F}(t)$ is continuous. Because kernel $K(t,s)$ is piecewise continuous, we use method of continuation to first establish existence and uniqueness in some interval $[0,T_1]$, and then show that this solution can be continued to successive intervals $[T_1,T_2]$, $[T_2,T_3]$, and so on. Eventually the whole interval $[0,T)$ is covered. We rewrite kernel $K(t,s)$ as $p(t,s)\widetilde{K}(t,s)$, where $\widetilde{K}(t,s)$ is continuous and $p(t,s)$ represents the piecewise continuous part (effectively $p(t,s)$ is the same as equation (2.3.3)); thus, we may apply theorem from Linz (1985), showed in the Appendix A.1, which tells us there is a unique continuous solution to equation (2.3.1) on $[0,T)$ for any $T > 0$.

Theorem 2.3.1. *There exists a unique non-negative solution* $\mathbf{n}(t,\tau)$ *(along characteristic lines) to problem* (2.2.16) *such that each component of* $\mathbf{n}(t,\tau)$ *belongs to* $(L^1 \cap L^\infty)([0,\infty)\times[0,T))$ *for any* $T > 0$*, and each component of* $\mathbf{n}(t,\cdot)$ *belongs to* $(L^1 \cap L^\infty)[0,\infty)$ *for all* $t \geq 0$*. The solution is given by equation* (2.2.21)*, where* $\mathbf{n}(t,0)$ *is continuous for all* $t \geq 0$*.*

2.4 Steady age distribution at BEG state

We now show the existence of steady age distributions, given that problem (2.2.16)-(2.2.18) has age-dependent transition probability rates. We note here that it would not be possible to show BEG state for time-dependent transition rates. This corresponds to the unperturbed, i.e., unexposed to cancer treatment, proliferating cancer cell line colonies that are exhibiting BEG, so $\mathbf{D}_{\text{in}}$ and $\mathbf{D}_{\text{out}}$ are possible functions of τ. We apply the results from Section 2.3 to show that steady age distributions, referred to as $\widehat{\mathbf{n}}(\tau)$, exist and are stable when $\mathbf{D}_{\text{out}}$ and $\mathbf{D}_{\text{in}}$ are functions of age τ only. We find in Theorem 2.4.1 proved by the Perron-Frobenius theorem that given any initial conditions in $((L^1 \cap L^\infty)[0,T))^3$, the shape of the solution $\mathbf{n}(t,\tau)$ to the problem will tend to a steady age distribution $\widehat{\mathbf{n}}(\tau)$ (different methods of proof can be found in Basse & Ubezio (2007); Begg *et al.* (2010)). As the renewal (boundary) equation involves a compact operator, a consequence is, it is characterized by a discrete spectrum of eigenvalues and the solution can be expressed as a superposition of eigenfunctions, Keyfitz & Keyfitz (1997). A positive dominant eigenvalue depicts the asymptotic growth rate of the population, i.e., the

population growth rate at BEG state. This will mean that there is a constant proportion of cells in each phase: a fact that is observed experimentally *in vitro*. This result is important in showing our mathematical model exhibits a unique steady age distribution, as is observed experimentally *in vitro* via cell flow cytometry. In Figure 2.5, we show an example of such a steady age distribution structure. Observe the exponential decay in the population as the age advances. It should be noted that by finding stationary solutions to our problem, we are finding solutions to the problem of the following form:

$$\mathbf{n}(t,\tau) = e^{\lambda t}\widehat{\mathbf{n}}(\tau), \tag{2.4.1}$$

and, therefore, $\widehat{\mathbf{n}}(\tau)$ is a steady age distribution of the problem because the age distribution of cells, $\mathbf{n}(t,\tau)$, retains the same shape $\widehat{\mathbf{n}}(\tau)$, whereas the overall number of cells may be growing or decaying depending upon the sign of growth constant λ (also called Malthusian parameter). This scenario corresponds to the unperturbed cancer cell line, where the transition and death probabilities in each phase are purely a function of the age in that phase.

Theorem 2.4.1. *There exists some double* $(\lambda_0, \widehat{\mathbf{n}})$ *such that* λ_0 *is a real, positive dominant eigenvalue to the characteristic equation* $Q(\lambda) = 1$, *and* $\widehat{\mathbf{n}}(\cdot) \in (L^1 \cap L^\infty)^3[0,T)$ *is a strictly positive stationary solution to* (2.4.1).

When the ansatz (2.4.1) is substituted into equation (2.3.1), we obtain the following expression:

$$\Big[\mathbb{A}(\lambda) - \mathbb{I}\Lambda\Big]\widehat{\mathbf{n}}(0) = 0, \tag{2.4.2}$$

with $\mathcal{F}(t) \to 0$, as $t \to \infty$ and $\Lambda = 1$. Thus, a necessary condition for the solution (2.4.1) to exist is the existence of such λ that the nonlinear eigenvalue problem (2.4.2) admits an eigenvalue $\Lambda = 1$ for some λ. The matrix $\mathbb{A}$ is defined as follows:

$$\mathbb{A} = \int_0^T \mathbf{D}_{\text{in}}(s)\exp\Big(-\int_0^s [\mathbf{D}_{\text{out}}(s') + \mathbb{I}\lambda]\,ds'\Big)\,ds. \tag{2.4.3}$$

Thus, we need to know if there is a $\Lambda = 1$ for the parameter $\lambda = \lambda_0$. Now it can be shown that the structure of $\mathbb{A} \geq 0$ is as:

$$\mathbb{A} = \begin{bmatrix} 0 & 0 & \kappa_{G_2M} \\ \kappa_{G_1} & 0 & 0 \\ 0 & \kappa_S & 0 \end{bmatrix}, \tag{2.4.4}$$

where κ_p denotes a positive element and is defined as follows:

$$\kappa_p = \int_0^T a_p(s)\exp\Big(-\int_0^s [b_p(\xi) + \lambda]\,d\xi\Big)\,ds, \tag{2.4.5}$$

with $p \in \{G_1, S, G_2M\}$ and a_p, b_p defined in equations (2.2.6) and (2.2.2), respectively. We note that transition probability rates a_p and b_p are now assumed to be a function of τ only. A non-negative matrix is irreducible if and only if its life cycle graph contains a path from every node to every other node,Caswell (2001). We can see that matrix $\mathbb{A}$ is irreducible, as its strongly connected graph shows in Figure 2.2. This matrix is imprimitive, see Section A.2 in the Appendix for more detail. Thus, from the Perron-Frobenius theorem on irreducibe but imprimitive matrices A.2.1, there exists a real positive eigenvalue λ_0, which is a simple root of the characteristic equation $\det[\mathbb{A}(\lambda) - \mathbb{I}\Lambda] = 0$ and the associated eigenvector, namely $\widehat{\mathbf{n}}(\mathbf{0})$, is positive. Expression $\det[\mathbb{A}(\lambda) - \mathbb{I}\Lambda] = 0$ reduces to the

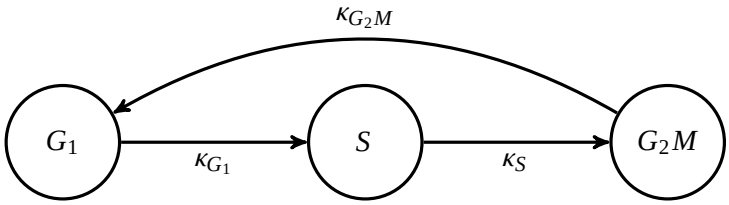

Figure 2.2: Diagram of irreducible matrix $\mathbb{A}$.

following equality:

$$1 = \Lambda^3 = Q(\lambda), \tag{2.4.6}$$

where

$$Q(\lambda) = \prod_p \int_0^T a_p(s) \exp\left(-\int_0^s [b_p(\xi) + \lambda]\, d\xi\right) ds. \tag{2.4.7}$$

The equation (2.4.6) states that the necessary condition for existence of a BEG is described by the following characteristic equation:

$$Q(\lambda) = 1. \tag{2.4.8}$$

Solution (2.2.21) with only age-dependent transition rates can be rewritten as follows:

$$\mathbf{n}(t, \tau) = \exp\left(-\int_0^\tau \mathbf{D}_{\text{out}}(s)\, ds\right) \mathbf{n}(t - \tau, 0), \quad \tau < t. \tag{2.4.9}$$

Taking into account equation (2.4.1), we can express the steady age distribution of the cancer cell population at BEG state as:

$$\widehat{\mathbf{n}}(\tau) = \exp\left(-\int_0^\tau (\mathbf{D}_{\text{out}}(s) + \lambda \mathbb{I})\, ds\right) \widehat{\mathbf{n}}(0). \tag{2.4.10}$$

This shows that $\widehat{\mathbf{n}}(\tau)$ will effectively have compact support provided $\mathbf{D}_{\text{out}}(s) + \lambda \mathbb{I} > 0$. Later, we derive a characteristic equation $Q(\lambda) = 1$ for constant and piecewise constant transition rates. In the following sections, we show derivations of numerous parameters that are used frequently in the cancer research.

2.5 Parameters: constant proportions, doubling time, and cell-cycle time

For further analysis of the unperturbed cancer cell population exhibiting BEG, we assume that transition rates $r_{p \to p+1}$ and death rates μ_p are piecewise continuous functions with respect to τ only. On the premise that each proliferating cell grows (ages) in G_1, S and G_2M phases before transferring into the next phase, we find that by defining transition probability rates as piecewise constant adds to our mathematical model viability. Further, we derive several vital parameters in the cancer research.

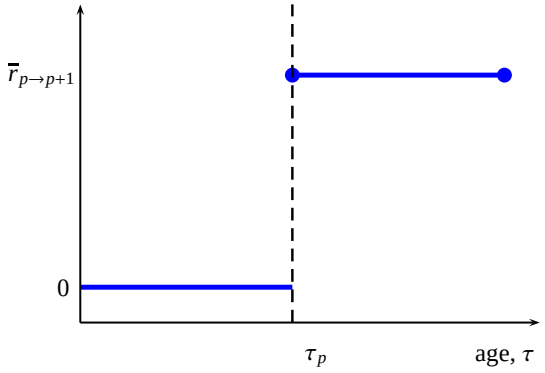

Figure 2.3: Piecewise constant transition rate $r_{p\to p+1}(\tau)$.

2.5.1 The total number of cells

The total number of cells in each phase p, denoted by N_p, is defined by integrating the number density over the age as follows:

$$N_p(t) = \int_0^T n_p(t,\tau)\, d\tau, \tag{2.5.1}$$

where the total cell number of the population at any given time t, denoted as N_{tot}, is the sum of the total cell number over the phases of the cell cycle, described as follows:

$$N_{tot}(t) = \sum_p N_p(t), \quad \text{with} \quad p \in \{G_1, S, G_2M\}. \tag{2.5.2}$$

We note here that at the total number of cell population at BEG state is as follows:

$$N_{tot}(t) = N_{tot}(0)e^{\lambda t}. \tag{2.5.3}$$

2.5.2 Piecewise constant transition probability rates

We define piecewise constant transition probability rates, taking into account that cells have zero transition probability while they grow (age) for a certain time (denoted as τ_p), as follows:

$$r_{p\to p+1}(\tau) = \begin{cases} 0, & \text{if } \tau < \tau_p, \\ \overline{r}_{p\to p+1}, & \text{if } \tau \geq \tau_p, \end{cases} \tag{2.5.4}$$

where $p \in \{G_1, S, G_2M\}$, as depicted in Figure 2.3.

We have assumed that death probability rate μ_p is a piecewise constant function, i.e., cells may undergo apoptosis only after growing for time τ_p in each phase, thus,

$$\mu_p(\tau) = \begin{cases} 0, & \text{if } \tau < \tau_p, \\ \overline{\mu}_p, & \text{if } \tau \geq \tau_p, \end{cases} \tag{2.5.5}$$

where $p \in \{G_1, S, G_2M\}$.

We remark that transition rates a_p and b_p, defined in equations (2.2.6) and (2.2.2), respectively, are then expressed as follows:

$$a_p(\tau) = \begin{cases} 0, & \text{if } \tau < \tau_p, \\ \overline{a}_p, & \text{if } \tau \geq \tau_p, \end{cases} \tag{2.5.6}$$

$$b_p(\tau) = \begin{cases} 0, & \text{if } \tau < \tau_p, \\ \overline{b}_p, & \text{if } \tau \geq \tau_p. \end{cases} \tag{2.5.7}$$

Although biologically age-dependent transition rates are a more realistic option, it is not simple enough for numerical calculations with the experimental data provided. Thus, we do neglect this in our model applications in Chapters 3, 4 and 5 because of the lack of experimental estimates that would be needed if one would want to include a minimum time each cell averagely spends in a phase before leaving the phase. By taking the limit when $\tau_p \to 0$, we can transfer from piecewise constant transition rates $r_{p\to p+1}(\tau)$ to constant transition probability rates $\overline{r}_{p\to p+1}$, thus stating that cells can possibly transfer to the consecutive phase as soon as they enter present phase p.

2.5.3 Characteristic equation

Characteristic equation (2.4.8) is a condition imposed on our model that describes the population at BEG state. In the case of the piecewise transition rates, we can show from equation (2.4.7) this condition explicitly as the following nonlinear transcendental expression:

$$Q(\lambda) = \frac{\overline{a}_{G_1}\overline{a}_S\overline{a}_{G_2M}}{(\overline{b}_{G_1}+\lambda)(\overline{b}_S+\lambda)(\overline{b}_{G_2M}+\lambda)} \exp\Big(-\lambda[\tau_{G_1}+\tau_S+\tau_{G_2M}]\Big) = 1. \tag{2.5.8}$$

We remind the reader that cells have a probability of transferring to the consecutive phase or die after ages τ_{G_1}, τ_S, and τ_{G_2M} in G_1, S and G_2M phases, respectively.

By taking potential aging times τ_p in every phase equal to zero, we can derive the BEG condition for the constant transition probability rates, depicted in Figure 2.4, as follows:

$$Q(\lambda) = \frac{\overline{a}_{G_1}\overline{a}_S\overline{a}_{G_2M}}{(\overline{b}_{G_1}+\lambda)(\overline{b}_S+\lambda)(\overline{b}_{G_2M}+\lambda)} = 1. \tag{2.5.9}$$

For the simplicity in numerical simulations later in thesis, we introduce new variable $F(\lambda)$ and define it as:

$$F(\lambda) = \frac{1}{Q(\lambda)} = 1. \tag{2.5.10}$$

Examination of equation (2.5.10) shows the following evaluations:

$$\lim_{\lambda\to\infty} F(\lambda) \to \infty, \quad \lim_{\lambda\to-\infty} F(\lambda) = -\infty, \tag{2.5.11}$$

and because $F(\lambda)$ is a continuous function, the intermediate value theorem shows that at least one solution to the equation $Q(\lambda) = 1$ exists. Figure 2.4 illustrates the characteristic equation for three theoretical cell lines with constant transition rates.

2.5.4 Constant proportions of cell population at BEG

To derive constant proportion formulae, we start by introducing a new notation: the probability density function $\pi(t,\tau)$ that depicts the probability density for a certain cell to be in the phase p of age τ at

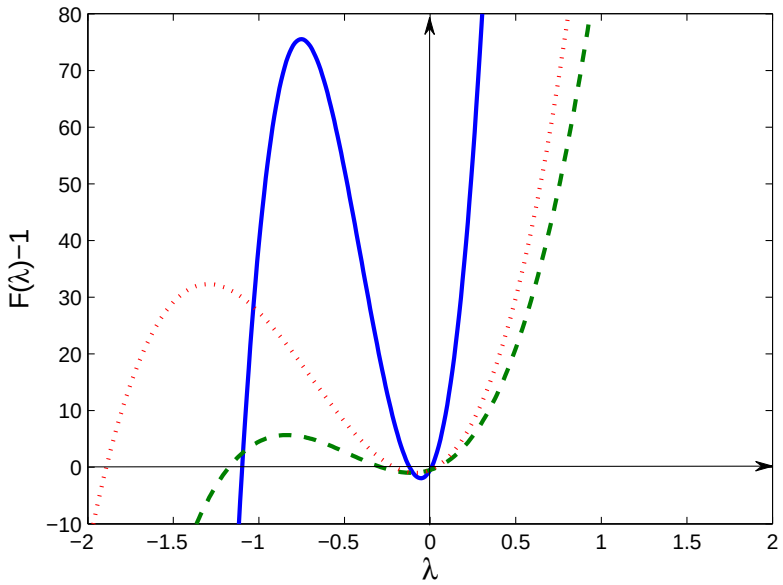

Figure 2.4: Characteristic equation $F(\lambda) = 1$ is plotted for three random sets of constant transition rates, where $\overline{r}_{G_1S} < \overline{r}_{SG_2M}$. Here red dotted line depicts a cell line with transition rates $\overline{r}_{G_1} = 0.025$, $\overline{r}_S = 0.25$ and $\overline{r}_{G_2M} = 1.9$. Blue solid line $\overline{r}_{G_1} = 0.009$, $\overline{r}_S = 0.11$ and $\overline{r}_{G_2M} = 1.1$. Green dashed line $\overline{r}_{G_1} = 0.02$, $\overline{r}_S = 0.35$ and $\overline{r}_{G_2M} = 1.2$.

time t. From equations (2.4.1) and (2.5.2), the probability density function, in the general case of population growth, is defined as number density divided by the total mass of the system as follows:

$$\pi_p(t,\tau) = \frac{n_p(t,\tau)}{N_{tot}(t)}. \tag{2.5.12}$$

From equations (2.5.1), (2.5.2), and (2.5.12), the proportion in p phase, denoted as $\Pi_p(t)$, is given by the following expression:

$$\Pi_p(t) = \int_0^T \pi_p(t,\tau)\,d\tau = \frac{\int_0^T n_p(t,\tau)\,d\tau}{N_{tot}(t)} = \frac{N_p(t)}{N_{tot}(t)}, \tag{2.5.13}$$

thus, the following identity (essential in our later models) arises:

$$\sum_p \int_0^T \pi_p(t,\tau)d\tau = \sum_p \Pi_p(t) = 1, \quad \text{for} \quad t \geq 0, \tag{2.5.14}$$

where $p \in \{G_1, S, G_2M\}$.

We continue by showing that, for the case of population in BEG state, from equations (2.5.12) and (2.5.3), the probability density function, denoted as $\widehat{\pi}_p(\tau)$, is expressed as follows:

$$\widehat{\pi}_p(\tau) = \frac{\widehat{n}_p(\tau)}{N_{tot}(0)}, \tag{2.5.15}$$

observing that from equation (2.4.1), we can express numerical density function at BEG state in each phase p as follows:

$$n_p(t,\tau) = e^{\lambda t}\widehat{n}_p(\tau). \tag{2.5.16}$$

We proceed by presenting the constant population formulae, from equations (2.5.13) and (2.5.14), for the population at BEG as follows:

$$\Pi_p = \int_0^T \widehat{\pi}_p(\tau)\,d\tau = \frac{\int_0^T \widehat{n}_p(\tau)\,d\tau}{N_{tot}(0)}, \quad \text{where} \quad \sum_p \Pi_p = 1. \tag{2.5.17}$$

We go on to explicitly show the number density, the probability density functions, and, subsequently, formulae of the constant proportions in each phase on the cell cycle. Remembering that the transition probability rates a_p and b_p are assumed to be piecewise constant functions, as discussed in Section 2.5.2.

We begin by rewriting general steady age-distribution equation (2.4.10) for each phase p of the cell cycle separately, where $p \in \{G_1, S, G_2M\}$ as follows:

$$\widehat{n}_p(\tau) = \int_0^T a_{p-1}(s)\widehat{n}_{p-1}(s)\,ds\; e^{-\int_0^\tau (b_p(s)+\lambda)\,ds}, \qquad t > \tau. \tag{2.5.18}$$

From Section 2.5.1, we show that the total cell number in the respective phase is as follows:

$$\begin{aligned} N_p(t) &= \int_0^T n_p(t,\tau)\,d\tau, \\ &= e^{\lambda t}\int_0^T \widehat{n}_p(\tau)\,d\tau, \\ &= \int_0^{\tau_p} n_p(t,\tau)\,d\tau + \int_{\tau_p}^T n_p(t,\tau)\,d\tau, \\ &= \widetilde{N}_p(t) + \overline{N}_p(t), \\ &= e^{\lambda t}(\widetilde{N}_p + \overline{N}_p), \end{aligned}$$

where we define $\widetilde{N}_p = \int_0^{\tau_p}\widehat{n}_p(s)ds$ as the total cell number in phase p at age $\tau < \tau_p$ and $\overline{N}_p = \int_{\tau_p}^T \widehat{n}_p(s)ds$ as the cell number in phase p at age $\tau \geq \tau_p$, when T is assumed to be very large. Thus, we can rewrite steady age-distribution equation (2.5.18) for each phase p of the cell cycle, depicted in Figure 2.5 as:

$$\widehat{n}_p(\tau) = \overline{a}_{p-1}e^{-\lambda\tau}\overline{N}_{p-1} \quad \begin{cases} 1, & \tau < \tau_p \\ e^{-\overline{b}_p(\tau-\tau_p)}, & \tau \geq \tau_p. \end{cases} \tag{2.5.19}$$

We note here that to obtain the number density function for the case of constant transition probability rates, the growth age in each phase τ_p is set to zero, thus giving $\widehat{n}_p(\tau) = \overline{a}_{p-1}\overline{N}_{p-1}e^{-(\overline{b}_p+\lambda)\tau}$. By taking into account that $\lim_{\tau\to T} e^{-\tau} = 0$, where T is the maximum age in a phase (as would be seen in the

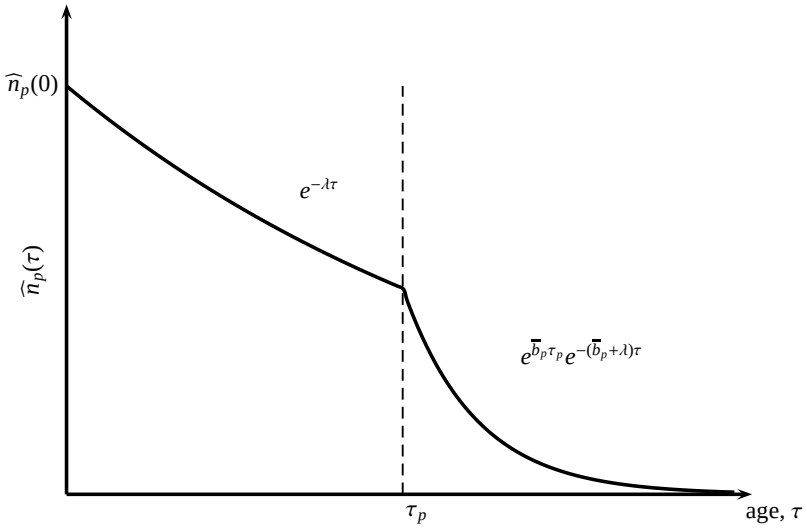

Figure 2.5: A diagram showing the piecewise differentiable number density $\widehat{n}_p(\tau)$ at the BEG state for piecewise constant transition rates a_p and b_p.

case of $T \to \infty$), the total number of cells in p phase at time t can be expressed as follows:

$$\begin{aligned} N_p(t) &= \widetilde{N}_p(t) + \overline{N}_p(t), \\ &= e^{\lambda t}\overline{a}_{p-1}\overline{N}_{p-1}\left[\frac{1-e^{-\lambda\tau_p}}{\lambda} + \frac{e^{-\lambda\tau_p}}{\lambda+\overline{b}_p}\right]. \end{aligned} \tag{2.5.20}$$

From equation (2.5.20), we can establish that $\widetilde{N}_p = \overline{a}_{p-1}\overline{N}_{p-1}\frac{1-e^{-\lambda\tau_p}}{\lambda}$ and $\overline{N}_p = \overline{a}_{p-1}\overline{N}_{p-1}\frac{e^{-\lambda\tau_p}}{\lambda+\overline{b}_p}$.
We proceed by writing out population number density functions for phases G_1, S, and G_2M as follows:

$$\widehat{n}_{G_1}(\tau) = \begin{cases} \widehat{n}_{G_1}(0)e^{-\lambda\tau}, & \tau < \tau_{G_1}, \\ \widehat{n}_{G_1}(0)e^{-\lambda\tau}e^{-\overline{b}_{G_1}(\tau-\tau_{G_1})}, & \tau \geq \tau_{G_1}, \end{cases} \tag{2.5.21}$$

$$\widehat{n}_S(\tau) = \begin{cases} \overline{a}_{G_1}\overline{N}_{G_1}e^{-\lambda\tau}, & \tau < \tau_S, \\ \overline{a}_{G_1}\overline{N}_{G_1}e^{-\lambda\tau}e^{-\overline{b}_S(\tau-\tau_S)}, & \tau \geq \tau_S, \end{cases} \tag{2.5.22}$$

$$\widehat{n}_{G_2M}(\tau) = \begin{cases} \overline{a}_S\overline{N}_S e^{-\lambda\tau}, & \tau < \tau_{G_2M}, \\ \overline{a}_S\overline{N}_S e^{-\lambda\tau}e^{-\overline{b}_{G_2M}(\tau-\tau_{G_2M})}, & \tau \geq \tau_{G_2M}, \end{cases} \tag{2.5.23}$$

where $\widehat{n}_{G_1}(0) = \overline{a}_{G_2M}\overline{N}_{G_2M}$, see Figure 2.5. Furthermore, we can express $\overline{N}_{G_1}$ as:

$$\begin{aligned}\overline{N}_{G_1} &= \int_{\tau_{G_1}}^{T} \widehat{n}_{G_1}(s)\,ds,\\ &= \widehat{n}_{G_1}(0)\frac{e^{-\lambda\tau_{G_1}}}{\overline{b}_{G_1}+\lambda},\end{aligned} \tag{2.5.24}$$

and then $\overline{N}_S$ as follows:

$$\overline{N}_S = \widehat{n}_{G_1}(0)\frac{\overline{a}_{G_1}}{(\overline{b}_{G_1}+\lambda)(\overline{b}_S+\lambda)}e^{-\lambda(\tau_{G_1}+\tau_S)}. \tag{2.5.25}$$

Thus, from equations (2.5.20), (2.5.24),(2.5.25) and taking into account that $\widehat{n}_{G_1}(0) = \overline{a}_{G_2M}\overline{N}_{G_2M}$, the total number in G_1, S, and G_2M phases for the population at BEG are given as follows:

$$N_{G_1}(t) = e^{\lambda t}\widehat{n}_{G_1}(0)\left[\frac{1-e^{-\lambda\tau_{G_1}}}{\lambda} + \frac{e^{-\lambda\tau_{G_1}}}{\lambda+\overline{b}_{G_1}}\right], \tag{2.5.26}$$

$$N_S(t) = e^{\lambda t}\widehat{n}_{G_1}(0)\frac{\overline{a}_{G_1}}{\lambda+\overline{b}_{G_1}}e^{-\lambda\tau_{G_1}}\left[\frac{1-e^{-\lambda\tau_S}}{\lambda} + \frac{e^{-\lambda\tau_S}}{\lambda+\overline{b}_S}\right], \tag{2.5.27}$$

$$N_{G_2M}(t) = e^{\lambda t}\widehat{n}_{G_1}(0)\frac{\overline{a}_{G_1}\overline{a}_S}{(\lambda+\overline{b}_{G_1})(\lambda+\overline{b}_S)}e^{-\lambda(\tau_{G_1}+\tau_S)}\left[\frac{1-e^{-\lambda\tau_{G_2M}}}{\lambda} + \frac{e^{-\lambda\tau_{G_2M}}}{\lambda+\overline{b}_{G_2M}}\right]. \tag{2.5.28}$$

We remind here that transition rates are defined as $\overline{a}_{G_1} = \overline{r}_{G_1\to S}$, $\overline{a}_S = \overline{r}_{S\to G_2M}$, $\overline{a}_{G_2M} = 2\overline{r}_{G_2M\to G_1}$ and $\overline{b}_p = \overline{r}_{p\to p+1} + \overline{\mu}_p$ with $p \in \{G_1, S, G_2M\}$. Because $N_{tot}(t) = N_{G_1}(t) + N_S(t) + N_{G_2M}(t)$, we can rewrite equation (2.5.3) as follows:

$$N_{tot}(t) = e^{\lambda t}\widehat{n}_{G_1}(0)C_\lambda, \tag{2.5.29}$$

observing that $N_{tot}(0) = \widehat{n}_{G_1}(0)C_\lambda$ and $\widehat{n}_{G_1}(0) = \overline{a}_{G_2M}\overline{N}_{G_2M}$. Furthermore, our constant C_λ is defined as follows:

$$\begin{aligned}C_\lambda = \frac{1-e^{-\lambda\tau_{G_1}}}{\lambda} + \frac{e^{-\lambda\tau_{G_1}}}{\lambda+\overline{b}_{G_1}} + \frac{\overline{a}_{G_1}}{\lambda+\overline{b}_{G_1}}e^{-\lambda\tau_{G_1}}\left[\frac{1-e^{-\lambda\tau_S}}{\lambda} + \frac{e^{-\lambda\tau_S}}{\lambda+\overline{b}_S}\right] +\\ + \frac{\overline{a}_{G_1}\overline{a}_S}{(\lambda+\overline{b}_{G_1})(\lambda+\overline{b}_S)}e^{-\lambda(\tau_{G_1}+\tau_S)}\left[\frac{1-e^{-\lambda\tau_{G_2M}}}{\lambda} + \frac{e^{-\lambda\tau_{G_2M}}}{\lambda+\overline{b}_{G_2M}}\right].\end{aligned} \tag{2.5.30}$$

We have to note here that by using characteristic equation (2.5.8), after some algebraic manipulation, we can show that equation (2.5.30) can be simplified to the following identity:

$$C_\lambda = \frac{1}{2\lambda}. \tag{2.5.31}$$

From equations (2.5.12) and (2.5.21) to (2.5.25), the probability density functions for G_1, S, and G_2M phases can be expressed as follows:

$$\pi_{G_1}(\tau) = \begin{cases}\frac{1}{C_\lambda}e^{-\lambda\tau}, & \tau < \tau_{G_1},\\ \frac{1}{C_\lambda}e^{\overline{b}_{G_1}\tau_{G_1}}e^{-(\overline{b}_{G_1}+\lambda)\tau}, & \tau \geq \tau_{G_1},\end{cases} \tag{2.5.32}$$

$$\pi_S(\tau) = \begin{cases} \frac{1}{C_\lambda}\frac{\overline{a}_{G_1}}{\overline{b}_{G_1}+\lambda} e^{-\lambda\tau_{G_1}} e^{-\lambda\tau}, & \tau < \tau_S, \\ \frac{1}{C_\lambda}\frac{\overline{a}_{G_1}}{\overline{b}_{G_1}+\lambda} e^{-\lambda\tau_{G_1}} e^{\overline{b}_S\tau_S} e^{-(\overline{b}_S+\lambda)\tau}, & \tau \geq \tau_S, \end{cases} \tag{2.5.33}$$

$$\pi_{G_2M}(\tau) = \begin{cases} \frac{1}{C_\lambda}\frac{\overline{a}_{G_1}\overline{a}_S}{(\overline{b}_{G_1}+\lambda)(\overline{b}_S+\lambda)} e^{-\lambda(\tau_{G_1}+\tau_S)} e^{-\lambda\tau}, & \tau < \tau_{G_2M}, \\ \frac{1}{C_\lambda}\frac{\overline{a}_{G_1}\overline{a}_S}{(\overline{b}_{G_1}+\lambda)(\overline{b}_S+\lambda)} e^{-\lambda(\tau_{G_1}+\tau_S)} e^{\overline{b}_{G_2M}\tau_{G_2M}} e^{-(\overline{b}_{G_2M}+\lambda)\tau}, & \tau < \tau_{G_2M}. \end{cases} \tag{2.5.34}$$

We introduce new variables $\widetilde{\Pi}_p$ and $\overline{\Pi}_p$, where $\widetilde{\Pi}_p$ shows the proportion of the population in a particular phase that is in the required phase growing state, and $\overline{\Pi}_p$ denotes the proportion of the population that is able to transition onto the next phase. These notions are defined as follows:

$$\widetilde{\Pi}_p = \int_0^{\tau_p} \pi_p(\tau)\, d\tau, \tag{2.5.35}$$

$$\overline{\Pi}_p = \int_{\tau_p}^{T} \pi_p(\tau)\, d\tau, \tag{2.5.36}$$

with the total proportion in each phase as $\Pi_p = \widetilde{\Pi}_p + \overline{\Pi}_p$. Finally, the constant proportions in each cell cycle phase for the population at BEG state are expressed as follows:

$$\Pi_{G_1} = \frac{1}{C_\lambda}\left[\frac{1-e^{-\lambda\tau_{G_1}}}{\lambda} + \frac{e^{-\lambda\tau_{G_1}}}{\lambda+\overline{b}_{G_1}}\right], \tag{2.5.37}$$

$$\Pi_S = \frac{1}{C_\lambda}\frac{\overline{a}_{G_1}}{\lambda+\overline{b}_{G_1}} e^{-\lambda\tau_{G_1}}\left[\frac{1-e^{-\lambda\tau_S}}{\lambda} + \frac{e^{-\lambda\tau_S}}{\lambda+\overline{b}_S}\right], \tag{2.5.38}$$

$$\Pi_{G_2M} = \frac{1}{C_\lambda}\frac{\overline{a}_{G_1}\overline{a}_S}{(\lambda+\overline{b}_{G_1})(\lambda+\overline{b}_S)} e^{-\lambda(\tau_{G_1}+\tau_S)}\left[\frac{1-e^{-\lambda\tau_{G_2M}}}{\lambda} + \frac{e^{-\lambda\tau_{G_2M}}}{\lambda+\overline{b}_{G_2M}}\right], \tag{2.5.39}$$

where $\widetilde{\Pi}_p$ is the first term of the sum, and $\overline{\Pi}_p$ is the second term of the summation in the square brackets for corresponding phases $p \in \{G_1, S, G_2M\}$.
We remind the reader here that in order to convert previous formulae for the population with constant transition rates among phases, aging times τ_{G_1}, τ_S, and τ_{G_2M} must be set to zero.

2.5.5 Population doubling time and average cell-age

We define the doubling time of the cell population, denoted by T_d, as a time unit taken for a population to double its cell number. When population is at the BEG state and grows at a constant rate λ, from (2.5.3), we see that $2N_{tot}(0) = N_{tot}(0)e^{\lambda T_d}$. Thus, we express population doubling time as follows:

$$T_d = \frac{ln2}{\lambda}. \tag{2.5.40}$$

We continue by defining the expected cell age in each phase p, denoted as T_p, of the cell population at BEG as follows:

$$T_p = \int_0^T \tau\pi_p(\tau)d\tau = \int_0^{\tau_p} \tau\pi_p(\tau)d\tau + \int_{\tau_p}^T \tau\pi_p(\tau)d\tau. \tag{2.5.41}$$

We can express the average cell-age for phases G_1, S, and G_2M as follows:

$$T_{G_1} = \frac{1}{C_\lambda}\left[\frac{1-e^{-\lambda\tau_{G_1}}}{\lambda^2} - \frac{\tau_{G_1}e^{-\lambda\tau_{G_1}}}{\lambda}\right] + \frac{1}{C_\lambda}\frac{e^{-\lambda\tau_{G_1}}}{\lambda+\overline{b}_{G_1}}\left[\tau_{G_1} + \frac{1}{\lambda+\overline{b}_{G_1}}\right], \tag{2.5.42}$$

$$T_S = \frac{1}{C_\lambda}\frac{e^{-\lambda\tau_{G_1}}}{\lambda+\overline{b}_{G_1}}\left[\frac{1-e^{-\lambda\tau_S}}{\lambda^2} - \frac{\tau_S e^{-\lambda\tau_S}}{\lambda}\right] + \frac{1}{C_\lambda}\frac{\overline{a}_{G_1}e^{-\lambda(\tau_{G_1}+\tau_S)}}{(\lambda+\overline{b}_{G_1})(\lambda+\overline{b}_S)}\left[\tau_S + \frac{1}{\lambda+\overline{b}_S}\right], \tag{2.5.43}$$

$$T_{G_2M} = \frac{1}{C_\lambda}\frac{\overline{a}_{G_1}e^{-\lambda(\tau_{G_1}+\tau_S)}}{(\lambda+\overline{b}_{G_1})(\lambda+\overline{b}_S)}\left[\frac{1-e^{-\lambda\tau_{G_2M}}}{\lambda^2} - \frac{\tau_{G_2M}e^{-\lambda\tau_{G_2M}}}{\lambda}\right] + \frac{1}{C_\lambda}\frac{1}{\overline{a}_{G_2M}}\left[\tau_{G_2M} + \frac{1}{\lambda+\overline{b}_{G_2M}}\right], \tag{2.5.44}$$

where the characteristic equation (2.5.8) was used to simplify the second term of T_{G_2M}. Thus, the average cell-age of the cancer cell population at BEG, denoted as T_a, is the sum of the average cell-age times of each phase of the cell cycle, defined as follows:

$$T_a = T_{G_1} + T_S + T_{G_2M}. \tag{2.5.45}$$

We expect that the average age of cells in the population T_a is smaller than the population doubling time T_d. Since the relationship between average cell age T_a and population doubling time T_d is not explicitly observable from our formulae, we created a following simulation: we chose random (and biologically realistic) transition rates $\overline{r}_{p\to p+1}$, death rates $\overline{\mu}_p$ and aging times τ_p, for $p \in \{G_1, S, G_2M\}$. The results shown in Figure 2.6. The relationship between the doubling time and average cell-age is as follows:

$$T_a < T_d. \tag{2.5.46}$$

For the simulations shown in Figure 2.6, random uniformly distributed transition rates $\overline{r}_{p\to p+1}$, aging times τ_p and death rates $\overline{\mu}_p$ were chosen. The intervals picked were $\overline{r}_{G_1\to S} \in [0.0001, 0.2]$, $\overline{r}_{S\to G_2M} \in [0.0001, 0.2]$, $\overline{r}_{G_2M\to G_1} \in [0.05, 2]$, $\tau_{G_1} \in [3, 25]$,$\tau_S \in [2, 25]$, $\tau_{G_2M} \in [0.01, 10]$, and $\overline{\mu}_p \in [10^{-4}, 10^{-3}]$, for $p \in \{G_1, S, G_2M\}$ with units for these variables presented in the Glossary. We remark that for Figure 2.6, a constraint $T_d < 168$ was imposed because population doubling time for cells growing *in vitro* is rarely exceeds 168 hours (or 1 week). We observe that from equation (2.5.8) the growth rate value λ is affected by transition rates $\overline{r}_{p\to p+1}$, aging times τ_p and death rates μ_p; therefore variations in the nine-dimension space of transition rates, aging times and death rates results in stochastic like changes in doubling time T_d values and the average cell age T_a, as can be seen in Figure 2.6.

2.5.6 Expected cell removal time, i.e., cell-cycle time

We introduce a new parameter - the average (expected) age of cells removed from a phase, denoted as T_p^*. A cell removed from a phase p is considered as either transferred to the next phase $p+1$ or dead. We note that the average cell-age in phase p, namely T_p, is not equal to the average cell removal-age from phase p, T_p^*. We examine the relationship between these two terms in this section.

The removal time is the time cells at age zero in phase p, namely $\widehat{n}_p(0)$, take to transit through phase p. Let us assign some constant σ_R to the magnitude of the cell number density at age zero that we want to track, so $\sigma_R = \widehat{n}_p(0)$. This number density of cells will grow (age) for at least τ_p hours and then transfer onto the next phase or die. Because the cell population continues to grow for time τ_p, the initially observed number density σ_R will be reduced because the total number of cells in phase p, namely N_p, would have grown at a rate λ; thus, scaling the initially observed number density σ_R by

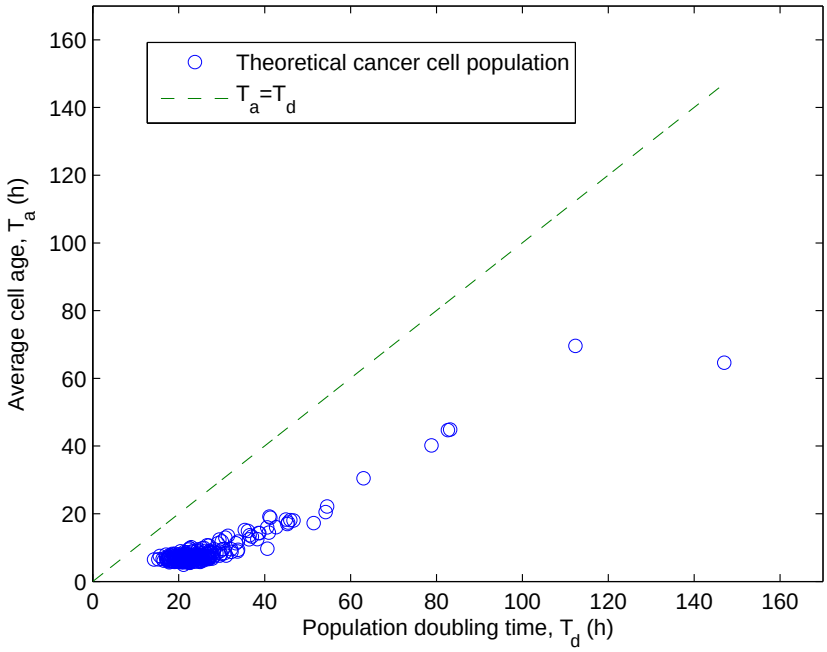

Figure 2.6: Diagram representing relationship between cell doubling time T_d and average cell-age T_a for theoretical cancer cell populations. Transition rates $\overline{r}_{p\to p+1}$, aging times τ_p, and death rates $\overline{\mu}_p$ are randomly chosen from uniform distribution from the following intervals: $\overline{r}_{G_1\to S} \in [0.0001, 0.2]$, $\overline{r}_{S\to G_2M} \in [0.0001, 0.2]$, $\overline{r}_{G_2M\to G_1} \in [0.05, 2]$, $\tau_{G_1} \in [3, 25]$,$\tau_S \in [2, 25]$, and $\tau_{G_2M} \in [0.01, 10]$, with death rates $\overline{\mu}_{G_1} \in [10^{-4}, 10^{-3}]$, $\overline{\mu}_S \in [10^{-4}, 10^{-3}]$, and $\overline{\mu}_{G_2M} \in [10^{-4}, 10^{-3}]$. A constraint of $T_d < 168$ hours is imposed for biological realism.

$e^{\lambda\tau_p}$. Therefore, the number density equations (2.5.21)-(2.5.23) have to be scaled by $e^{\lambda\tau}$ when dealing with the removal time expressions. These normalised number density functions for each phase are referred as $\widehat{n}^*_p$, so $\widehat{n}^*_p(\tau) = \widehat{n}_p(\tau)e^{\lambda\tau}$. We define the number of cells leaving phase p per unit time at age τ, denoted as $H_p(\tau)$, as follows:

$$H_p(\tau) = \widehat{n}^*_p(0) - \widehat{n}^*_p(\tau), \qquad p \in \{G_1, S, G_2M\}, \tag{2.5.47}$$

we remark to the reader that the initially observed/tracked total number of cells is $\widehat{n}^*_p(0)$, thus the total cell number removed, denoted by H^{tot}_p, is $H^{tot}_p = \widehat{n}^*_p(0)$ when $\tau \to T$. From equations (2.5.21)-(2.5.23) and the scaling factor $\widehat{n}^*_p(\tau) = \widehat{n}_p(\tau)e^{\lambda\tau}$, we can derive $\widehat{n}^*_p(\tau)$ as:

$$\widehat{n}^*_p(\tau) = \begin{cases} \widehat{n}^*_p(0), & \tau < \tau_p, \\ \widehat{n}^*_p(0)\, e^{-\overline{b}_p(\tau-\tau_p)}, & \tau \geq \tau_p, \end{cases} \tag{2.5.48}$$

for $p \in \{G_1, S, G_2M\}$. We remark that $\widehat{n}^*_p(0) = \widehat{n}_p(0)$. We continue by introducing the rate at which

the number density of cells changes due to removal from phase p, denoted by $\widehat{h}_p(\tau)$, as follows:

$$\widehat{h}_p(\tau) = -\frac{d\widehat{n}_p^*(\tau)}{d\tau}. \tag{2.5.49}$$

The function $\widehat{h}_p(\tau)$ is piecewise differentiable with respect to τ. Furthermore, we introduce a variable for the probability density function for cells that are removed at age τ, refer to it as $\widehat{\gamma}_p(\tau)$, and define as:

$$\widehat{\gamma}_p(\tau) = \frac{\widehat{h}_p(\tau)}{H_p^{tot}} = -\frac{1}{\widehat{n}_p(0)}\frac{d\widehat{n}_p^*(\tau)}{d\tau}, \tag{2.5.50}$$

then the probability of being removed from phase p at age τ, denoted as $\Gamma_p(\tau)$, is defined as follows:

$$\Gamma_p(\tau) = \int_0^\tau \widehat{\gamma}_p(s)\, ds, \tag{2.5.51}$$

where $\lim_{\tau\to T}\Gamma_p(\tau) = 1$. Considering that the probability density function $\widehat{\gamma}_p$ is decreasing in interval $[\tau_p, T)$, we express the expected time of cell removal from phase p as follows:

$$\begin{aligned} T_p^* &= \int_0^T \tau\widehat{\gamma}_p(\tau)\, d\tau = \int_0^{\tau_p} \tau\widehat{\gamma}_p(\tau)d\tau + \int_{\tau_p}^T \tau\widehat{\gamma}_p(\tau)d\tau, \\ &= \int_0^{\tau_p} \tau\Big[-\frac{1}{\widehat{n}_p(0)}\frac{d\widehat{n}_p^*(\tau)}{d\tau}\Big]d\tau + \int_{\tau_p}^T \tau\Big[-\frac{1}{\widehat{n}_p(0)}\frac{d\widehat{n}_p^*(\tau)}{d\tau}\Big]d\tau. \end{aligned} \tag{2.5.52}$$

For simplicity, we define normalised number of cells in each phase p as:

$$\begin{aligned} \widetilde{N}_p^* &= \int_0^{\tau_p} \widehat{n}_p^*(\tau)\, d\tau, \qquad \tau < \tau_p, \\ \overline{N}_p^* &= \int_{\tau_p}^T \widehat{n}_p^*(\tau)\, d\tau, \qquad \tau \geq \tau_p. \end{aligned} \tag{2.5.53}$$

Finally, by integrating equation (2.5.52) and incorporating (2.5.53), we derive the following expression for the time of removal from phase p:

$$T_p^* = \frac{\widetilde{N}_p^*}{\widehat{n}_p(0)} + \frac{\overline{N}_p^*}{\widehat{n}_p(0)}. \tag{2.5.54}$$

We proceed by deriving explicit formulae for expected removal times in each phase. Taking into account equations (2.5.48) and (2.5.53), we obtain the following expressions:

$$T_{G_1}^* = \tau_{G_1} + \frac{1}{\overline{b}_{G_1}}, \tag{2.5.55}$$

$$T_S^* = \tau_S + \frac{1}{\overline{b}_S}, \tag{2.5.56}$$

$$T_{G_2M}^* = \tau_{G_2M} + \frac{1}{\overline{b}_{G_2M}}. \tag{2.5.57}$$

We remind the reader that cancer cell population is composed of proliferating cells with some un-

dergoing cell death; thus, all cells in each phase will either transit to the next phase or die. When comparing the average age in the particular phase T_p with the average removal age T_p^*, we can see that the following is true :

$$T_p^* > T_p.$$

We have not shown this result analytically. Here we define the expected time of cell removal from all phases, denoted as T_{rm}, as the sum of the removal times of all three phases:

$$T_{\text{rm}} = T_{G_1}^* + T_S^* + T_{G_2M}^* = \tau_{G1} + \tau_S + \tau_{G_2M} + \frac{1}{\overline{b}_{G_1}} + \frac{1}{\overline{b}_S} + \frac{1}{\overline{b}_{G_2M}}. \tag{2.5.58}$$

The relationship between the population doubling time T_d and the expected removal time from all phases T_{rm} (or expected transit time through all phases) is as follows:

$$T_d \leq T_{\text{rm}}. \tag{2.5.59}$$

We ran a Monte Carlo simulation for equation (2.5.58) versus population doubling time (see Figure 2.7) for theoretical cell lines with the same random values for the transition rates, aging times and death rates as in Figure 2.6 and obtained the following expression:

$$T_{\text{rm}} = \theta T_d, \qquad \text{with} \qquad \theta \in [1, 1.3]. \tag{2.5.60}$$

If no cell death μ_p or aging times τ_p are incorporated in the model, the expression (2.5.60) would still hold as the magnitude of the growth rate λ, calculated from the characteristic equation (2.5.8), is affected by the apoptosis rate and aging time variations. Clearly, the average cell age in the phase T_a is always smaller than the average removal time of the cell cycle T_{rm}.

The notions, the average cell-removal time and the average cell-cycle time, are intertwined when relating to cell growth times and can also be called the cell transit time through cell cycle. In the following chapters of this thesis, we will assume that notions of expected cell-removal time, cell-transit time and cell-cycle time are interchangeable and will refer to it as T_c, i.e., $T_{\text{rm}} = T_c$.

As mentioned before, the estimation of the cell-cycle time of a cancer population is of a particular interest for biologists as it relates to patients survival prognosis; shorter cell-cycle times relate to poor prognoses for the cancer patient. Mathematical model that could evaluate the cell-cycle time from a single experimental observation, would be valuable to clinicians.

In experimental observations, biologists often assume that the cell-cycle time is equal to the population doubling time, which is calculated from the constructed growth curve. This data is then used for the empirical estimate of the transition rate probability between certain phases of the cell cycle. We note that this empirical method does not take into account the possibility of cell death. Our mathematical model agrees that the population doubling time can be equal to the cell-cycle time for some cell lines. However, in general case, the average cell-cycle time of the population is greater or equal to the population doubling time.

Several mathematical methods of the cell-cycle time estimation for the cancer cell population at the BEG state can be found in the literature. The identical expression for the average cell-cycle time ($T_c = T_{\text{rm}}$) derived from our model, shown in equation (2.5.58), can be found in Basse & Ubezio (2007); Basse *et al.* (2005); Simms *et al.* (2012). However, in these publications, the cell-cycle time expression has been guessed and then verified by using a discrete computational simulation Simms *et al.* (2012). An alternative method for estimating cell-cycle time can be found in Chiorino *et al.* (2001), where the desynchronization of the population growth has been incorporated into the age-

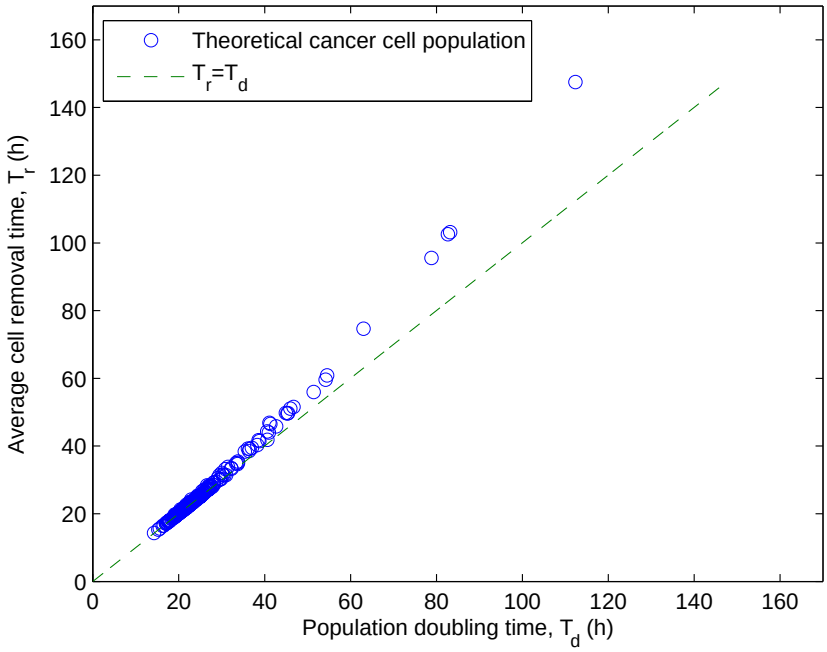

Figure 2.7: Diagram representing relationship between cell doubling time T_d and expected removal time T_{rm} for theoretical cancer cell populations. Transition rates $\overline{r}_{p\to p+1}$, aging times τ_p, and death rates $\overline{\mu}_p$ are randomly chosen from uniform distribution from the following intervals: $\overline{r}_{G_1\to S} \in [0.0001, 0.2]$, $\overline{r}_{S\to G_2M} \in [0.0001, 0.2]$, $\overline{r}_{G_2M\to G_1} \in [0.05, 2]$, $\tau_{G_1} \in [3, 25]$,$\tau_S \in [2, 25]$, and $\tau_{G_2M} \in [0.01, 10]$, with death rates $\overline{\mu}_{G_1} \in [10^{-4}, 10^{-3}]$, $\overline{\mu}_S \in [10^{-4}, 10^{-3}]$, and $\overline{\mu}_{G_2M} \in [10^{-4}, 10^{-3}]$. A constraint of $T_d < 168$ hours is imposed for biological realism.

structured model and then related to the mean cell cycle duration. The computational results of this model showed that, for two cell lines examined, the population doubling times and the average cell-cycle times are approximately the same in their magnitude, thus strongly agreeing with our model result. We note that the model in Chiorino *et al.* (2001) requires many experimental observation points to monitor the desynchronized population's convergence to the exponential growth state. The stochastic approach of the desynchronization rate method has been shown in Bronk *et al.* (1968); Olofsson & McDonald (2009). In the classic work Steel (1977), analytical methods for estimating the duration of particular phases have been derived from an age-structured model, where phases G_1, S and G_2 have been combined into one, therefore the transition rate probabilities between these phases have not been included into the model. For example, from this method, the duration of the S-phase can be calculated from the experimental estimates of the doubling time, the growth rate and the labelling index (the number of cells in the S-phase of the growth cycle divided by the total cells in the population, namely what we refer to as Π_S). Many papers utilise analytical results from Steel (1977) to estimate the transit times of the particular phases Fried (1973); Larsson *et al.* (2007); Terry & White (2006); White & Terry (2000).

2.6 Conversion of age distribution model to ordinary differential equation model

In further chapters of this thesis, we apply experimental data to several ODE models. Transition from PDE to the ordinary differential equation (ODE) is done with the assumption of homogeneity of individual cells within the particular phases p. Taking into account equation (2.5.1), we find by integrating McKendrick-von Foerster equation (2.2.16) over $0 \le \tau \le T$ the following ODE system:

$$\frac{d\mathbf{N}(t)}{dt} = \mathbf{n}(t,\tau=0) - \int_0^T \mathbf{D}_{\text{out}}(t,\tau)\mathbf{n}(t,\tau)\,d\tau, \quad 0 < t < \infty, \tag{2.6.1}$$

$$= \int_0^T \mathbf{D}_{\text{in}}(t,\tau)\mathbf{n}(t,\tau)\,d\tau - \int_0^T \mathbf{D}_{\text{out}}(t,\tau)\mathbf{n}(t,\tau)\,d\tau, \tag{2.6.2}$$

where we used expression $\mathbf{N}(t,\tau \to T) = 0$ and the renewal condition (2.2.18) to derive the result above.

The only possible form of the matrices $\{\mathbf{D}_{\text{in}}, \mathbf{D}_{\text{out}}\}$, in order to convert this equation into an ODE system, is to have these matrices independent of τ; then we obtain the following ODE system:

$$\frac{d\mathbf{N}(t)}{dt} = B\mathbf{N}(t), \quad \mathbf{N}(0) = \int_0^T \mathbf{n}(0,\tau)\,d\tau, \quad 0 < t < \infty, \tag{2.6.3}$$

and for the $\mathbf{D}_{\text{in}}$, $\mathbf{D}_{\text{out}}$ matrices also independent of time t, we have the constant matrix

$$\begin{aligned} B &= (\mathbf{D}_{\text{in}} - \mathbf{D}_{\text{out}}), \\ &= \begin{bmatrix} -(\overline{r}_{G_1\to S} + \overline{\mu}_{G_1}) & 0 & 2\overline{r}_{G_2M\to G_1} \\ \overline{r}_{G_1\to S} & -(\overline{r}_{S\to G_2M} + \overline{\mu}_S) & 0 \\ 0 & \overline{r}_{S\to G_2M} & -(\overline{r}_{G_2M\to G_1} + \overline{\mu}_{G_2M}) \end{bmatrix}. \end{aligned}$$

In Chapters 3 and 5, we use ODE systems as main modelling tools. In Chapter 4, we derive an ODE system describing the variations of cell population proportions over time that with an additional constraint, showed in equation (2.5.14), becomes a differential-algebraic equation (DAE) system.

2.7 Delay differential equation system

The transition from an age-structure model with piecewise constant transition rates to a DDE system is done by integrating the corresponding PDE equations over the age (as shown in Section 2.6). Thus, by integrating McKendrick-von Foerster equation (2.2.3) over interval $\tau \in [0, \tau_p)$, we can obtain the following expression:

$$\begin{aligned} \frac{\partial}{\partial t}\int_0^{\tau_p} n_p(t,\tau)\,d\tau &= -n_p(t,\tau_p) + n_p(t,0) - \int_0^{\tau_p} b_p(\tau)n_p(t,\tau)\,d\tau, \\ \frac{d\widetilde{N}_p(t)}{dt} &= -n_p(t,\tau_p) + \int_0^T a_{p-1}(\tau)n_{p-1}(t,\tau)\,d\tau - \int_0^{\tau_p} b_p(\tau)n_p(t,\tau)d\tau, \\ &= -n_p(t,\tau_p) + \overline{a}_{p-1}\overline{N}_{p-1}(t), \end{aligned} \tag{2.7.1}$$

with the initial condition $\widetilde{N}_p(0) = \int_0^{\tau_p} n_p(0,\tau)\,d\tau$. We remind the reader from Section 2.5.4 notion $\widetilde{N}_p(t)$ is the total number of cells in phase p at time t between ages 0 and τ_p, and notion $\overline{N}_p(t)$ is the

total number of cells in phase p at time t after age τ_p. Integrating over interval $\tau \in [\tau_p, T]$, we get the following:

$$\begin{aligned}\frac{\partial}{\partial t}\int_{\tau_p}^{T} n_p(t,\tau)\,d\tau &= -n_p(t,T) + n_p(t,\tau_p) - \int_{\tau_p}^{T} b_p(\tau) n_p(t,\tau)\,d\tau,\\ \frac{d\overline{N}_p(t)}{dt} &= n_p(t,\tau_p) - \int_{\tau_p}^{T} b_p(\tau) n_p(t,\tau)\,d\tau,\\ &= n_p(t,\tau_p) - \overline{b}_p \overline{N}_p(t), \end{aligned} \tag{2.7.2}$$

with the initial condition as follows $\overline{N}_p(0) = \int_{\tau_p}^{T} n_p(0,\tau)\,d\tau$.

The number density of the population in phase p, from equation (2.2.15) when population is not at BEG and transition rates are only age-dependent, is as follows:

$$n_p(t,\tau) = \int_0^T a_{p-1}(s) n_{p-1}(t-\tau, s)\,ds\, e^{-\int_0^\tau b_p(s)\,ds}, \tag{2.7.3}$$

$$= \begin{cases} \overline{a}_{p-1}\int_0^T n_{p-1}(t-\tau,s)\,ds, & \tau < \tau_p,\\ \overline{a}_{p-1}\int_0^T n_{p-1}(t-\tau,s)\,ds\, e^{\overline{b}_p(\tau-\tau_p)}, & \tau \geq \tau_p, \end{cases} \tag{2.7.4}$$

where, from equation (2.5.1), we can express the integral in equation (2.7.4) as $\overline{N}_{p-1}(t-\tau) = \int_0^T n_{p-1}(t-\tau,s)\,ds$. Thus, we can conclude that the number density of cells at age τ_p, in phase p at time t, can be calculated as follows:

$$n_p(t,\tau_p) = \overline{a}_{p-1}\overline{N}_{p-1}(t-\tau_p). \tag{2.7.5}$$

A DDE model tracks, first, the total cell number that are in a required growth state, namely $\widetilde{N}_p(t)$, at time t in each phase p, and, second, the total cell number that are in transition to the next phase, namely $\overline{N}_p(t)$, at time t in each phase p. We continue by deriving a DDE system, by using equations (2.7.1), (2.7.2), and (2.7.5) to express the cell number variations in time as follows:

$$\frac{d\widetilde{N}_{G_1}}{dt} = \overline{a}_{G_2M}\overline{N}_{G_2M}(t) - \overline{a}_{G_2M}\overline{N}_{G_2M}(t-\tau_{G_1}), \tag{2.7.6}$$

$$\frac{d\overline{N}_{G_1}}{dt} = \overline{a}_{G_2M}\overline{N}_{G_2M}(t-\tau_{G_1}) - \overline{b}_{G_1}\overline{N}_{G_1}(t), \tag{2.7.7}$$

$$\frac{d\widetilde{N}_{S}}{dt} = \overline{a}_{G_1}\overline{N}_{G_1}(t) - \overline{a}_{G_1}\overline{N}_{G_1}(t-\tau_S), \tag{2.7.8}$$

$$\frac{d\overline{N}_{S}}{dt} = \overline{a}_{G_1}\overline{N}_{G_1}(t-\tau_S) - \overline{b}_{S}\overline{N}_{S}(t), \tag{2.7.9}$$

$$\frac{d\widetilde{N}_{G_2M}}{dt} = \overline{a}_{S}\overline{N}_{S}(t) - \overline{a}_{S}\overline{N}_{S}(t-\tau_{G_2M}), \tag{2.7.10}$$

$$\frac{d\overline{N}_{G_2M}}{dt} = \overline{a}_{S}\overline{N}_{S}(t-\tau_{G_2M}) - \overline{b}_{G_2M}\overline{N}_{G_2M}(t), \tag{2.7.11}$$

where $\overline{a}_{G_1} = \overline{r}_{G_1\to S}$, $\overline{a}_S = \overline{r}_{S\to G_2M}$, $\overline{a}_{G_2M} = 2\overline{r}_{G_2M\to G_1}$, and $\overline{b}_p = \overline{r}_{p\to p+1} + \overline{\mu}_p$, $p \in \{G_1, S, G_2M\}$. With

the following initial conditions:

$$\widetilde{N}_{G_1}(0) = \widetilde{N}^0_{G_1}, \tag{2.7.12}$$

$$\overline{N}_{G_1}(0) = \overline{N}^0_{G_1}, \tag{2.7.13}$$

$$\widetilde{N}_S(0) = \widetilde{N}^0_S, \tag{2.7.14}$$

$$\overline{N}_S(0) = \overline{N}^0_S, \tag{2.7.15}$$

$$\widetilde{N}_{G_2M}(0) = \widetilde{N}^0_{G_2M}, \tag{2.7.16}$$

$$\overline{N}_{G_2M}(0) = \overline{N}^0_{G_2M}. \tag{2.7.17}$$

Since, biologically, cells have to grow/age in certain phases before transferring to the next phase, a mathematical model incorporating this property would be preferable to the ODE model, in the literature linear DDEs. Such mathematical models often require estimates of aging times τ_p that experimentally can be observed via mitotic selection method, a linear DDE model investigating the breast cancer cell line growth dynamics can be seen in Simms *et al.* (2012). Mitotic selection is a synchronization method that does not affect the cell cycle. Upon entering mitosis, cells are not firmly attached to the surrounding medium and can be collected after agitation (by shaking a culture vessel like petri dish). This method is applicable only to cells that grow in monolayer culture, see Pagano (1995). Cells that are tightly adherent to the surface of the culture vessel or to each other cannot be synchronized by mitotic selection.
The DDE model in Simms *et al.* (2012) depicts a cell-cycle that has been subdivided into seven phases, our DDE system (2.7.6) verifies the model proposed in the literature as the model in Simms *et al.* (2012) can be reduced to a six-phase DDE system. In system (2.7.6) three equations out of six decouple, the total number of cells leaving the storage phases have been incorporated into the delay terms of the transiting number of cells. Population dynamics described with the delay differential equation system represents the population growth at BEG state.
We have not been provided with the experimental estimates of aging times τ_p from the mitotic selection for the melanoma cancer cell lines. Thus in the following chapters, we utilise ODE systems because the data that can be extracted from the flow cytometry profiles is not sufficient to apply the DDE model.

2. ONE-COMPARTMENT AGE-STRUCTURED MODEL OF CANCER CELL POPULATION GROWTH

Chapter 3

Determination of Cell Population Dynamics Using Plateau Log Reduction Method

Cell-cycle times are vital parameters in cancer research and short cell-cycle times are often related to poor survival of cancer patients. A method for experimental estimation of cell-cycle times or doubling times of cultured cancer cell populations, based on addition of paclitaxel (an inhibitor of cell division) has been proposed in literature. In this chapter, we use a mathematical model to investigate relationships between essential parameters of the cell division cycle following inhibition of cell division. The reduction in the number of cells engaged in DNA replication reaches a plateau as the concentration of paclitaxel is increased; this can be determined experimentally. From our model, we have derived a plateau log reduction formula for proliferating cells and established that there are linear relationships between the plateau log reduction values and the reciprocal of doubling times (i.e., growth rates of the populations). We have therefore provided theoretical justification of an important experimental technique to determine cell doubling times. Furthermore, we have applied Monte Carlo experiments to justify the suggested linear relationships used to estimate doubling time from 5-day cell culture assays. We show that our results are applicable to cancer cell populations with cell loss present.

3.1 Introduction to the plateau log reduction method

In this chapter, we develop analytical methods to interpret the growth of cancer cells in culture, thus providing insights into the measurement of cancer growth *in vitro* unexposed to any cancer treatment. An age-structured model with constant transition rates (derived in Section 2.6) has been reduced to the ODE model and used in study of the cell population dynamics.

We remind the reader that our mathematical model depicts the dynamics of cell population in BEG state. Cancer cell population has no microenvironmental constraints when growing in vitro. As discussed before, mammalian cells proliferating in culture progress through a series of four phases during the cell division cycle, namely G_1, S (DNA replication), G_2 and M (mitosis) phases. It seems relatively straightforward to determine experimentally at least two of the basic parameters of proliferating cells, namely population doubling time and the proportion of cells in each phase. The population doubling time T_d can be measured by counting the number of cells at different times to produce a growth curve, and the proportion of cells in each phase can be measured by staining the DNA with a fluores-

cent dye such as propidium iodide and analysing the population by flow cytometry. This latter method does not distinguish G_2 and M-phase cells (which have the same DNA content) and these analyses therefore often measure three phases G_1, S and a combined G_2M-phase, as discussed in Section 1.5. Determination of transit times for each of the phases and the cycle time of the overall population is complicated by two issues:

1. Although the numbers of proliferating cells increase exponentially with time, the phase transit times are not just simply related to the proportion of cells as determined by flow cytometry. A direct relationship has been thought to be so in some of the literature Barnes *et al.* (2001); Taylor *et al.* (1983).

2. The transit times of individual mammalian cells in individual phases are variable, particularly in G_1 phase. This has the effect that in a proliferating cell population, some cells may remain for long periods in G_1 phase and thus appear as non-proliferating cells. In previous studies, this issue has been addressed by modelling the cell cycle using a system of differential equations and incorporating transition probabilities from one phase to another for the onset of DNA replication and cell division Basse *et al.* (2003, 2004b), and we utilise similar approach in this chapter.

A further practical issue in the determination of cell cycle parameters of a proliferating cell population is the incidence of apoptosis Baguley (2011). Many, perhaps all, cell lines in culture have a finite probability of undergoing this programmed cell death mechanism which begins within seconds with blebbing of the cytoplasm and continues for about 3 hours Andrade *et al.* (2010), leading to complete fragmentation of the cell and to loss of DNA, thus making them almost invisible to microscopy and DNA-based flow cytometry. Therefore, simple counting of cells cannot estimate this cell loss factor, which would lead to errors in the calculation of population doubling times.

An alternative method, from the method explained above, for the estimation of cell cycle parameters is the so-called stathmokinetic method, where the cell cycle is blocked at a particular point (such as mitosis) and the consequent changes in proportions in the cell phases are measured by flow cytometry. Cell cycle can be blocked by using a mitotic inhibitor chemotherapy drug - paclitaxel. It interferes with the normal breakdown of microtubules during cell division. Because the transition to apoptosis is thought to be essentially independent of the cycle phase, this method provides a good basis for calculating cell cycle parameters. This method has been previously applied by using the drug paclitaxel, which arrests cells in mitosis and prevents cell division. A complication of this approach is that cells arrested by paclitaxel subsequently enter a state, which we termed A-phase, where DNA is slowly but progressively degraded. In Basse *et al.* (2004a), the A-phase is included to exhibit process of slow DNA loss.

A simplification of the above stathmokinetic methodology is to measure the incorporation of radioactive labelled thymidine (^{3}H-TdR) into cellular DNA at a selected time after addition of paclitaxel. This method provides an estimate of the number of cells in the population that have recently (less than 6 hours) entered the S-phase. The method uses comparison of cell populations grown in the presence and absence of labelled thymidine to derive the cell cycle data. Comparison of measurements of the population doubling time (by cell counting) and the described thymidine incorporation following addition of paclitaxel provided a significant correlation in Baguley *et al.* (1995). This result has led to the development of a technique to more accurately estimate doubling time of cell populations. Moreover, the derivation of population doubling time, by counting, does not take cell loss into account. The method based on this simplification, as outlined in this chapter, overcomes this problem by use of the measured uptake of ^{3}H-TdR into DNA of cultured cells. Then a 'plateau' reduction value

(P_{LR}) for ^{3}H-TdR incorporation, at paclitaxel concentrations above a value that completely inhibits cell division, can be used to estimate doubling time.

We address the question here, of whether the transition probability model can be used to derive a direct relationship between cell doubling time and thymidine incorporation data. This chapter provides the theoretical justification and a further extension of this ^{3}H-TdR technique, which was pioneered in Baguley *et al.* (1995, 1999). Central to our results here, and in flow cytometry experiments, is the determination of transition rates between the phases that are used in our mathematical model from the measurement of percentages in each phase and the cell population doubling time. In subsequent sections, we address the existence and uniqueness of this mathematical mapping and its inverse map (from the transition rates to the cell proportions). We suggest the replacement of the direct counting measurement of the doubling time for cultures of proliferating cells by its calculation from the plateau logarithm reduction measurement discussed here.

We provide in Section 3.2 respective adjustments to our general mathematical model derived in Chapter 2. In Section 3.2.1, we utilise the analytical formulae, from Chapter 2, for the relationships between transition rates, total population growth rate and proportions in each phase at BEG state in order to provide theoretical justification and extensions which are discussed in Section 3.3. We show our results of a Monte Carlo simulation of the full equations to justify the linear reciprocal relationship between P_{LR} and T_d derived asymptotically in in Section 3.3.2.1. In Section 3.3.4 we summarise our results showing the simple affine relationship that exists between T_d and P_{LR}. This result is particularly important for oncology.

3.2 The model for *in vitro* human tumour cell population kinetics

We reduce our age-structured model (introduced in Chapter 2) to the ODE model due to limited amount of experimental estimates. In Section 2.6, it was shown that the dynamics of the total number of cells in each phase are subsumed by the ODE model. In this case, transition rate probabilities are not functions of age. In this chapter, transition rates are constant and we refer to them as $r_{p\to p+1}$ throughout this chapter with $p \in \{G_1, S, G_2M\}$ (in Chapter 2 we referred to them as $\overline{r}_{p\to p+1}$). We observe that mathematical model has to incorporate the effects of chemotherapy drug paclitaxel, thus appropriate adjustments to the ODE model in Section 2.6 have been made. Consider a population of cells, with structure classification as G_1, S, G_2M and A, according to their corresponding phase of the cell cycle and with the probability that cells can transfer from one phase to the next according to transition rates $\{r_{G_1\to S}, r_{S\to G_2M}, r_{G_2M\to G_1}, r_A\}$ between phases. A cell arrest or apoptosis phase A is also included as a removal class, and this occurs from the G_2M-phase so that it can model the effect of paclitaxel. In case of an A-phase consisting of arrested cancer cells, we refer to it as non-proliferating cells of the population. Whereas, for an A-phase representing apoptosis we refer to it as cell death.

The resulting dynamical system, depicted in Figure 3.1, can be described with three ODEs — one equation for the number of cells in each phase $\{N_{G_1}(t), N_S(t), N_{G_2M}(t)\}$ as a function of time (t) as follows:

$$\frac{dN_{G_1}(t)}{dt} = 2r_{G_2M\to G_1}N_{G_2M}(t) - r_{G_1\to S}N_{G_1}(t), \tag{3.2.1a}$$

$$\frac{dN_S(t)}{dt} = r_{G_1\to S}N_{G_1}(t) - r_{S\to G_2M}N_S(t), \tag{3.2.1b}$$

$$\frac{dN_{G_2M}(t)}{dt} = r_{S\to G_2M}N_S(t) - r_{G_2M\to G_1}N_{G_2M}(t) - r_AN_{G_2M}(t), \tag{3.2.1c}$$

parameter	description	units
$r_{G_1 \to S}$	rate transition G_1 to S-phase	hours^{-1}
$r_{S \to G_2M}$	rate transition S to G_2M-phase	hours^{-1}
$r_{G_2M \to G_1}$	rate transition G_2M to G_1-phase	hours^{-1}
r_A	arrest or apoptosis rate	hours^{-1}

Table 3.1: Model parameters with descriptions and units. It should be observed for biological cell lines that generally the transition probabilities satisfy $0 < r_{G_1 \to S} < r_{S \to G_2M} < r_{G_2M \to G_1}$ with the rare exception of $0 < r_{S \to G_2M} < r_{G_1 \to S} < r_{G_2M \to G_1}$.

where the transition between the phases (included the A-phase) is determined by the probability parameters as listed in Table 3.1. It should be noted that the 2 on the right-hand-side of equation (3.2.1a) indicates that 2 daughter cells are produced for every cell leaving the G_2M-phase. Each equation is a conservation equation for the rate of change of the number of cells in that phase per unit time with transition rates per unit time between phases. Furthermore, defining

$$N_{prolif}(t) = N_{G_1}(t) + N_S(t) + N_{G_2M}(t), \tag{3.2.2}$$

where we see that the total number of proliferating cells, N_{prolif}, in the three phases is not conserved but grows or decays depending on the sign of $(r_{G_2M \to G_1} - r_A)$. The total population, N_{tot}, in the four classes satisfies

$$N_{tot}(t) = N_{prolif}(t) + N_A(t), \tag{3.2.3}$$

where the term N_A represents the number of cells in the A-phase.

The number of cells removed from the proliferating cell population (N_A) satisfies:

$$\begin{aligned} \frac{dN_A}{dt} &= r_A N_{G_2M}, \\ N_A(0) &= 0, \end{aligned} \tag{3.2.4}$$

where it follows that N_A grows exponentially when $r_A \neq 0$.

3.2.1 Phase solutions in BEG with constant transition rates

When a cell line is being cultured for flow cytometry experiments the cell population exhibits balanced exponential growth of the form

$$N_p(t) = \overline{N}_p e^{\lambda t}, \tag{3.2.5}$$

where $\overline{N}_p$, $p \in \{G_1, S, G_2M\}$ is a constant for each phase. The form of the expression (3.2.5) shows that the cell phase population grows exponentially with a growth rate λ and asymptotically the population has a stable phase distribution which is independent of the initial phase distribution. Furthermore, it is asynchronous as the percentage of cells in each phase are not in general the same but depend upon the transition rates. We have shown the characteristic equation for the population in the BEG state

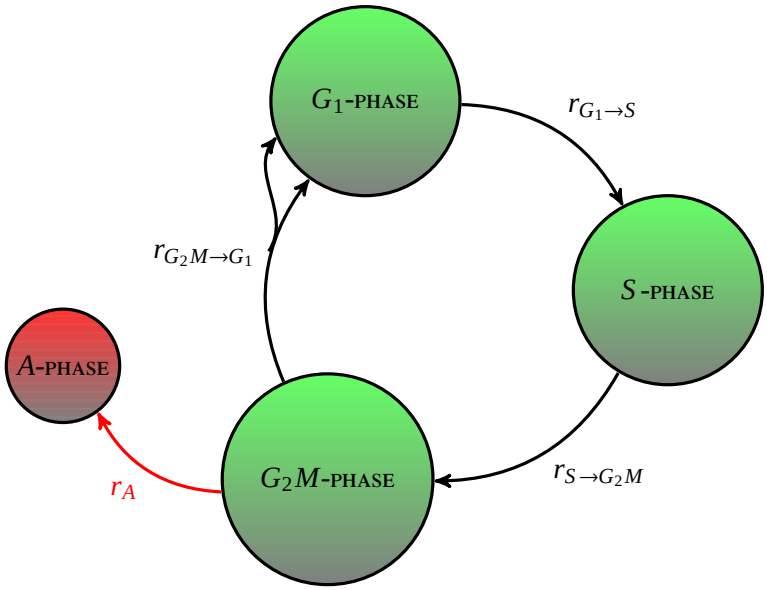

Figure 3.1: A diagram of cell-cycle control of a cell line cell population. The population is subdivided into G_1, S, G_2M and A phases with the possibility that cells can transfer from one phase to the next according to transition rates (Table 3.1) between phases. Response of cancer cell population to paclitaxel is shown when transition rate $r_{G_2M \to G_1}$ is equal to zero.

with constant transition rates in equations (2.5.9) and (2.5.10). The condition for the exponential growth of population with parameters used in system (3.2.1) is as follows:

$$F(\lambda) = \frac{(r_{G_2M \to G_1} + r_A + \lambda)(r_{G_1 \to S} + \lambda)(r_{S \to G_2M} + \lambda)}{2 r_{G_2M \to G_1} r_{G_1 \to S} r_{S \to G_2M}} = 1. \tag{3.2.6}$$

The function $F(\lambda)$ is a cubic polynomial with zeros at $-r_{G_1 \to S}$, $-r_{S \to G_2M}$, and $-(r_{G_2M \to G_1} + r_A)$, and it intersects the ordinate at $(1 + r_A / r_{G_2M \to G_1})/2$ and moreover[1] F is monotone increasing for $\lambda > 0$. An alternative proof has been discussed in Basse *et al.* (2004a).

Figure 2.4 in Chapter 2 shows a series of typical graphs of $F(\lambda)$. Further considerations of the graph of F shows that if $r_A < r_{G_2M \to G_1}$, then $F(\lambda) - 1$ always has just one positive root for λ, and this value determines the cell population growth. The case $r = r_{G_2M \to G_1}$, which defines constant population growth, is the boundary value of λ leading to proliferating population (N_{prolif}) decline when $r_A > r_{G_2M \to G_1}$. In addition, it is seen that λ defines the doubling time of the population cell line through the well known equation

$$T_d = \frac{\ln(2)}{\lambda}. \tag{3.2.7}$$

This time is central to understanding the dynamics of the cell line in that it also defines the population cell-cycle time (equivalent to the population cell transit time) as the time it takes 1 cell to become 2 cells *etc.* When the proliferating cell population is considered to be in BEG, as given by equation (3.2.5), then we can easily calculate the proportions in each phase, which will become asymptotically constant, as shown in equations (2.5.37)-(2.5.39) in Chapter 2. Constant proportions in the phases

[1] See Appendix B.1 equation (B.1.2a)

are obtained experimentally in cell lines when the cell cultures are maintained in exponential growth. For simplicity in the remainder of this section we consider $r_A \equiv 0$, so that $N_{tot} = N_{prolif}$. We can reduce the constant proportion formulae (2.5.37)-(2.5.39) for the case of constat transition rates by taking $\tau_p \to 0$ for $p \in \{G_1, S, G_2M\}$. Then let Π_{G_1} be the proportion of cells in the G_1-phase, namely $\Pi_{G_1} = N_{G_1}(t)/N_{tot}$, and similar notation for the other phases, then

$$\Pi_{G_1} = \frac{1}{C_\lambda(r_{G_1\to S} + \lambda)}, \tag{3.2.8a}$$

$$\Pi_S = \frac{1}{C_\lambda(r_{G_1\to S} + \lambda)} \frac{r_{G_1\to S}}{r_{S\to G_2M} + \lambda}, \tag{3.2.8b}$$

$$1 = \Pi_{G_1} + \Pi_S + \Pi_{G_2M}, \tag{3.2.8c}$$

where from equation (2.5.30)

$$C_\lambda = \frac{1}{r_{G_1\to S} + \lambda} + \frac{r_{G_1\to S}}{(r_{S\to G_2M} + \lambda)(r_{G_1\to S} + \lambda)} + \frac{r_{G_1\to S} r_{S\to G_2M}}{(r_{S\to G_2M} + \lambda)(r_{G_2M\to G_1} + \lambda)(r_{G_1\to S} + \lambda)}, \tag{3.2.9}$$

so that

$$\frac{\Pi_S}{\Pi_{G_1}} = \frac{r_{G_1\to S}}{r_{S\to G_2M} + \lambda}, \tag{3.2.10a}$$

$$\frac{\Pi_{G_2M}}{\Pi_S} = \frac{r_{S\to G_2M}}{r_{G_2M\to G_1} + \lambda}, \tag{3.2.10b}$$

$$1 = \Pi_{G_1} + \Pi_S + \Pi_{G_2M}. \tag{3.2.10c}$$

Now N_{prolif} satisfies

$$\frac{dN_{prolif}}{dt} = (r_{G_2M\to G_1} - r_A)N_{G_2M}, \tag{3.2.11}$$

$$= (r_{G_2M\to G_1} - r_A)\Pi_{G_2M}N_{prolif}, \tag{3.2.12}$$

so that besides the characteristic equation (3.2.6) for the population growth rate we have $\lambda = (r_{G_2M\to G_1} - r_A)\Pi_{G_2M}$.

From the equations of this section for an established cell line we have a relationship between proportions in each phase, the rate transitions between phases, the population doubling time. The equations (3.2.6), (3.2.7), and (3.2.10) form a system of five equations in the eight variables

$$\{r_{G_1\to S}, r_{S\to G_2M}, r_{G_2M\to G_1}, \lambda, \Pi_{G_1}, \Pi_S, \Pi_{G_2M}, T_d\}$$

but two of these five equations are reducible in that Π_{G_2M} can be eliminated with the last of equation (3.2.10) and similarly T_d can removed with equation (3.2.7). So we have an implicit three-system of equations for the six variables in the three-groupings $\mathbf{r} = \{r_{G_1\to S}, r_{S\to G_2M}, r_{G_2M\to G_1}\}$, and $\boldsymbol{\sigma} = \{\Pi_{G_1}, \Pi_S, \lambda\}$ hence the implicit three-system can be written

$$\mathbf{G}(\mathbf{r}, \boldsymbol{\sigma}) = \mathbf{0}, \tag{3.2.13}$$

where $\mathbf{G} : \mathbb{R}^3_+ \times \mathbb{R}^3_+ \to \mathbb{R}^3$, as we are only interested in $\lambda > 0$. For the Monte Carlo simulation considered in Section 3.3.3 the $\mathbf{r}$'s are known and we wish to know whether this implicit function, $\mathbf{G}$, determines the $\boldsymbol{\sigma}$ uniquely. That is, given the three transition rates is there a unique mapping to

the proportions and λ (effectively T_d). We now show for this direct problem that we have a local differentiable mapping, R, defined by $\boldsymbol{\sigma} = R(\mathbf{r})$ that uniquely determines the $\boldsymbol{\sigma}$. Another important question for determination of cell kinetics is: Does measurement of $\boldsymbol{\sigma}$ uniquely determine the $\mathbf{r}$? That is, can we write $\mathbf{r} = R^{-1}(\boldsymbol{\sigma})$? Both these answers are proven in Appendix B.1 by the implicit function theorem, and in the following statement of this result the matrices J_σ, $J_\mathbf{r}$ are defined as appropriate sub-matrices of the jacobian of $\mathbf{G}$. We can now express the results found for both maps in the following theorem:

Theorem 3.2.1. *(a) The mapping, $R(\mathbf{r})$, exists locally as $\det J_\sigma > 0$ on S, a bounded and open subset of $\{r_{G_1\to S}, r_{S\to G_2M}, r_{G_2M\to G_1}\} \in \mathbb{R}^3_+$, and it is uniquely locally defined on S, and the local maps are continuously differentiable.*

(b) The mapping $R^{-1}(\boldsymbol{\sigma})$ exists locally as $\det J_\mathbf{r} > 0$ on S', a bounded and open subset of $\{\Pi_{G_1}, \Pi_S, \lambda\} \in \mathbb{R}^3_+$, and it is uniquely locally invertible on S', and the local maps are continuously differentiable.

We observe that from the flow cytometry data the Π_p, $p \in \{G_1, S, G_2M\}$ can be measured, and T_d can be determined by cell counting thus yielding λ. This means that the $\mathbf{r}$'s are uniquely determined by Theorem 3.2.1(b).

These results are central to our model's usefulness in predicting the cell dynamics from flow cytometry measurements.

3.3 Results

3.3.1 Experimental paclitaxel dose-response effects

The cell-cycle times of human tumour cells vary considerably among different individuals Prescott (1987), and for several cancer types, where short cycle times are related to poor survival times of patients Furneaux *et al.* (2008); Rew & Wilson (2000). Hence it is important to estimate cell-cycle times of *in vivo* tumours. However, the determination of *in vivo* potential doubling times (T_{pot}) is not currently ethically justifiable, since it involves the administration of a potential mutagen (bromodeoxyuridine an analogue of thymidine) and subsequent tumour biopsy. An alternative approach to estimate cell doubling time is to culture clinical material in a short-term (7 day) assay Baguley *et al.* (1999) and to measure the effect of cell division arrest, typically carried out by adding a mitotic poison such as paclitaxel. On subsequent uptake of ^{3}H-TdR into DNA of cultured cells, a measured 'plateau' reduction value for ^{3}H-TdR incorporation, at paclitaxel concentrations above a value that completely inhibits cell division Baguley *et al.* (1999); Furneaux *et al.* (2008) can be used to estimate doubling time. The method relies on the intrinsic variability of cell-cycle time, much of which is in the G_1-phase of the cell cycle and thus occurs before the onset of DNA replication Prescott (1987). The range of values determined using this method is surprisingly similar to that obtained using *in vivo* the T_{pot} method. Previous studies have shown that the kinetic behaviour of cultured cells, as measured by flow cytometry, can be modelled effectively by incorporating transition probabilities for the onset of DNA replication and cell division Basse *et al.* (2003, 2004b). This technique is analysed here for cell lines, but a further application of it would allow this method to be extended to cultured clinical tumour material.

We observe that the chemotherapy drug paclitaxel is an antimitotic agent that stabilises the assembly of microtubules by preventing depolymerisation, thus arresting cells prior to or during mitoses. In Baguley *et al.* (1995), the chemosensitivity of cell lines to paclitaxel was assayed by exposing the

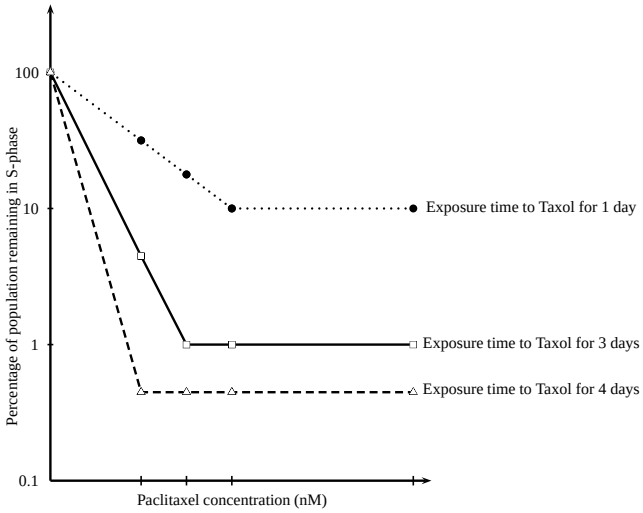

Figure 3.2: Diagrammatic representation of the paclitaxel concentration-dependent phase of the dose-response semilog-curves.

tumour cell lines to paclitaxel for 5 days and the remaining proliferative cells quantitated by ^{3}H-TdR incorporation. This subsequent incorporation of ^{3}H-TdR is proportional to the number of proliferating cells in the S-phase and the level of this incorporation is measured using a liquid scintillation counter. The resulting measurement then is proportional to the amount of cell proliferation.

$P_S(t)$ is defined as the time dependent (t hours) percentage of the S-phase cells after exposure to paclitaxel. We name this important quantity the *plateau log reduction* with the symbol, P_{LR}, which is $\log_{10}$ units of the normalised value of $P_S(t)$. In Baguley *et al.* (1995) experimental measurements were made and various P_{LR} values and their corresponding measurements of population doubling time, T_d were calculated for 21 cell lines (after exposing them to paclitaxel for 5 days) and it was shown that when these quantities were plotted against each other they showed a significant linear dependence. The wide range of P_{LR} found shows how different cell lines can have a different responses to chemotherapy, and this stems from the possible wide range of values for transition rates between phases. In particular, it is the transition rate from G_1 to S-phase that produces a wide range of G_1-phase transit times.

The dose-response curves, obtained in Baguley *et al.* (1995), were biphasic on a semi-logarithmic plot with a linear decrease in incorporation up to a particular drug concentration, and above which no further decrease was evident (see diagrammatic representation of dose-response curves in Figure 3.2). The plateau defines the P_{LR} measurement. We observe in Figure 3.2 that, firstly, the initial decreasing region of the dose response curve as the paclitaxel concentration increases results in a decreasing proportion of proliferating cells, hence fewer cells in the S-phase. Secondly, the plateau corresponds to the concentration level where the cell is arrested in mitosis. Also we observe that the position of the elbow in the curve is dependent upon the concentration because for a shorter exposure time to paclitaxel the concentration must be higher to stop cells cycling. Thirdly, the plateau is a measure of the remaining cells in the S-phase at the exposure time. Fourthly, we observe the depth of the plateau is deeper with longer exposure times. This is because there are fewer remaining proliferating cells, in the S-phase, with longer paclitaxel exposure times. This is borne out by our mathematics in Section 3.3.2.1 where it is shown that once mitosis has been inhibited the number of cells in the

S-phase declines exponentially as a function of exposure time.

Baguley *et al.* (1995) hypothesised a model for this dose-response behaviour as: firstly, the cell killing in response to paclitaxel occurs only during metaphase arrest (i.e., in M-phase), while the rate of progress through other phases in the cell cycle is close to normal. Secondly, that the number of proliferating cells is proportional to the ^{3}H-TdR incorporation. Then, their model of the experimental results was that during the linear reduction in number of cells, in the dose-response dependence range, a proportion of the cells undergo paclitaxel induced irreversible arrest once they enter mitosis while the remaining cells continue through mitosis to another cell cycle. Whereas, over the plateau concentration range, where the dose-response is independent of concentration, all cells undergo irreversible paclitaxel-induced arrest or death once they enter mitosis. Furthermore, they suggested that the plateau effect shows the number of S-phase cells, fixed at a time, which is resultant on the entry of cells from the G_1-phase and exit into the G_2M-phase, and will be independent of paclitaxel concentration. Moreover, the exact number of remaining S-phase cells will be strongly dependent upon the exposure time to paclitaxel and this hypothesis is supported by their experiments. These behavioural characteristics are shown in Figures 3.2. Our model, which is predicated upon the phase cycle of the cell, further supports their hypothesis from our mathematical results in Section 3.3.2.

3.3.1.1 Previous experimental work results

In Baguley *et al.* (1995), it was shown that the cancer cell population doubling time significantly correlated with the maximum plateau reduction. In particular, they postulated that if an exponential rate of departure of cells from G_1-phase is assumed, the proportion (P_{G_1}) of G_1-phase cells at any time after exposure to paclitaxel at concentrations high enough to block cell division will be described by the relationship:

$$P_{G_1} = P_0 e^{-kt/\widetilde{T}}, \tag{3.3.1}$$

where P_0 is the proportion of G_1-phase cells at zero time, k is a constant and $\widetilde{T}$ is the doubling time. After an interval (corresponding approximately to the S-phase transit time) the proportion of S-phase cells will have a similar dependence on t. So following Baguley *et al.* (1995), taking the logarithm of equation (3.3.1), when in the plateau logarithmic reduction dose-response concentration we have

$$\ln \frac{P_S(t)}{P_s(0)} = -\frac{k}{\widetilde{T}}t, \tag{3.3.2}$$

where $P_S(t)/P_s(0)$ is the change in the proportion of cells in the S-phase. So their model predicts that the logarithm of the remaining S-phase cells at time t after paclitaxel exposure should be linear function of $t/\widetilde{T}$. This formula can be rewritten (without loss of generality) in logarithm to base 10 units, and observing that $100 \times P_S(t)/P_s(0)$ is the percentage of the S-phase fraction giving *plateau log reduction* (which we denote by P_{LR}) it implies that the logarithm reduction formula is:

$$\begin{aligned} P_{LR} &= \log_{10} \frac{P_S(0)}{P_S(t)} \\ &= -\log_{10} \frac{P_S(t)}{P_S(0)} = \log_{10} 100 - \log_{10} \left[100 \frac{P_S(t)}{P_S(0)} \right], \\ &= k_1 t/\widetilde{T}, \end{aligned} \tag{3.3.3}$$

where $k_1 = k \log_{10} e$. Furthermore, they found that on their plotting the experimental data from 21 tumour cell lines, which were sub-cultured in exponential phase over 5 days with the doubling times

estimated by counting the cells in a haemocytometer, and using a linear regression polynomial to this data a positive correlation existed (with $r = 0.90; p < 0.001$). From this an empirical formula was derived in Baguley *et al.* (1995) as

$$\widetilde{T} = \frac{K_1}{P_{LR}}, \tag{3.3.4}$$

where $K_1 = k_1 t_1$, with $k_1 = 0.45$, and $t_1 = 5$ days, this value of k_1 is our least squares fit from their 21 cell lines from the tabulated data in their Table 2 (in Baguley *et al.* (1995)), and thus $K_1 = 2.25$ for these cell lines. Whereas, based on their Figure 6 (in Baguley *et al.* (1995)), which has 37 cell lines, one can obtain a value $k_1 = 0.473$, and with $t_1 = 5$ days, get $K_1 = 2.365$ for these cell lines. We observe for reference, for primary cultures with a paclitaxel exposure time of 7 days, the value of K_1 is 3.78 (as cited in Furneaux *et al.* (2008)). Further application of formula (3.3.4) to short-term cultures of tumour samples taken at surgery from patients with brain cancer in Furneaux *et al.* (2008) yields a value of K_1 up to 4.8. This formula between P_{LR} and $1/\widetilde{T}$, for a fixed time t, implies that for cell cultures with a long doubling time (or cycle time) P_{LR} is small. But for those cell cultures with a short doubling time P_{LR} is large. It should observed that this formula can be only valid over restricted ranges of P_{LR} and $\widetilde{T}$ as will be made apparent in Section 3.3.3.

The fundamental experimental hypothesis made in Baguley *et al.* (1995) is that the plateau log reduction value obtained, at high enough paclitaxel concentration, is directly proportional to the paclitaxel exposure time and inversely proportional to the doubling time. We show similar correlations, based on our theories, between $\widetilde{T} = T_d$ and P_{LR} in Section 3.3.2.1

3.3.2 Deriving a simple empirical method of calculating the cell doubling time for cell lines using a phase structured model

We use our mathematical model to derive a simple empirical method for calculating the cell population doubling time T_d for cell lines as follows. First, we model the response to the mitotic inhibitor paclitaxel, by setting the transition rate from the combined G_2M-phase to G_1-phase equal to zero, and deriving a temporal expression for the remaining S-phase cells. We then apply the model to a range of theoretical cell lines and show that P_{LR} is approximately proportional to the exposure time divided by cell doubling time for a range of values.

In this section, we will justify mathematically the results of Baguley *et al.* (1995), namely equation (3.3.3), and their hypotheses through our phase ODE system (3.2.1). Hence we now model the effects of adding paclitaxel at a concentration to ensure entry into the plateau region of the dose-response. We therefore note that in the plateau region there are no proliferating cells so we simulate the paclitaxel concentration by setting the transfer rate from G_2M to G_1 phase to zero, i.e., $r_{G_2M\to G_1} = 0$. Then BEG will be broken and there will be *no* constant proportions in the phases, so that the number of cells in the various phases will be described by the equations in Appendix B.3. We aim to show that the relationship described in equation (3.3.1) holds for our model. Namely, that after addition of paclitaxel the proportion of cells in S-phase will decline exponentially:

$$\frac{N_S(t)}{N_{total}(0)} = \frac{N_{G_1}(0)}{N_{total}(0)} \frac{r_{G_1\to S}}{r_{S\to G_2M} - r_{G_1\to S}} \left(e^{-r_{G_1\to S} t} - e^{-r_{S\to G_2M} t} \right) + \frac{N_S(0)}{N_{total}(0)} e^{-r_{S\to G_2M} t}. \tag{3.3.5}$$

We observe that $t = 0$ corresponds to the paclitaxel concentration having just stopped cell division so that N_{total} is given by equation (3.2.2), when $r_A = 0$, for BEG at $t = 0_-$. For the rest of the chapter we will assume $r_{G_1\to S} \neq r_{S\to G_2M}$, in other words, the case $r_{G_1\to S} = r_{S\to G_2M}$, considered in equation (B.3.2), will not occur. This is true in our Monte Carlo simulations of Section 3.3.3, as this case has

zero probability of occurring as it is a boundary case.

Using notation P_S for the proportion of the total population of cells in the S-phase, equation (3.3.5) can be simplified to:

$$P_S(t) = P_{G_1}(0)\frac{r_{G_1\to S}}{r_{S\to G_2M} - r_{G_1\to S}}\left(e^{-r_{G_1\to S}t} - e^{-r_{S\to G_2M}t}\right) + P_S(0)e^{-r_{S\to G_2M}t}. \tag{3.3.6}$$

Furthermore, since $P_S(0)$ denotes the proportion of the total cell population in the S-phase at time $t = 0_-$, i.e. , just before paclitaxel incorporation, we can express the proportion of cells in the S-phase as follows:

$$\frac{P_S(t)}{P_S(0)} = \frac{P_{G_1}(0)}{P_S(0)}\frac{r_{G_1\to S}}{r_{S\to G_2M} - r_{G_1\to S}}\left(e^{-r_{G_1\to S}t} - e^{-r_{S\to G_2M}t}\right) + e^{-r_{S\to G_2M}t}. \tag{3.3.7}$$

As

$$\frac{P_{G_1}(0)}{P_S(0)} = \frac{\Pi_{G_1}}{\Pi_S},$$

we can use equation (3.2.10) to simplify equation (3.3.7) to

$$\frac{P_S(t)}{P_S(0)} = \frac{r_{S\to G_2M} + \lambda}{r_{S\to G_2M} - r_{G_1\to S}}\left(e^{-tr_{G_1\to S}} - e^{-tr_{S\to G_2M}}\right) + e^{-tr_{S\to G_2M}}. \tag{3.3.8}$$

Now to show the exponential decay of the percentage of cells in the S-phase, we must subdivide expression (3.3.8) into two cases. Firstly, in case of the transition rate from the G_1 to S-phase being slower than from the S to G_2M -phase, i.e., $r_{G_1\to S} < r_{S\to G_2M}$, we can express the percentage of the total cell population in the S-phase after a linearisation time T_L, where $T_L > T_s$, as:

$$\frac{P_S(t)}{P_S(0)} = \frac{r_{S\to G_2M} + \lambda}{r_{S\to G_2M} - r_{G_1\to S}}e^{-tr_{G_1\to S}} + \mathcal{O}(e^{-tr_{S\to G_2M}}), \quad 0 < r_{G_1\to S} < r_{S\to G_2M}, \quad t > T_L, \tag{3.3.9}$$

where T_L is large enough to ensure that the order term is exponentially small. Secondly, when $r_{G_1\to S} > r_{S\to G_2M}$, we can see that the following is true:

$$\frac{P_S(t)}{P_S(0)} = \frac{r_{G_1\to S} + \lambda}{r_{G_1\to S} - r_{S\to G_2M}}e^{-tr_{S\to G_2M}} + \mathcal{O}(e^{-tr_{G_1\to S}}), \quad 0 < r_{S\to G_2M} < r_{G_1\to S}, \quad t > T_L. \tag{3.3.10}$$

Thus, the percentage of cells in the S-phase is eventually exponentially decreasing regardless of the relationship between the transition rates $r_{G_1\to S}$ and $r_{S\to G_2M}$ and this is illustrated in Figure 3.3(a). In both of the cases previously considered, the graphs display simple exponential decay when $T_L > 50$ hours; see the log plot in Figure 3.3(b) showing when proportion of S-phase P_S decays in a linear fashion on time t.

3.3.2.1 Deriving the plateau log reduction formula

Using our model, we will show a plateau log reduction formula similar to equation (3.3.3), i.e., there is a direct relationship between population doubling time and the plateau log reduction value. From equation (3.3.8) at measurement time t_1 as

$$P_{LR} = -\log_{10}\frac{P_S(t_1)}{P_S(0)},$$

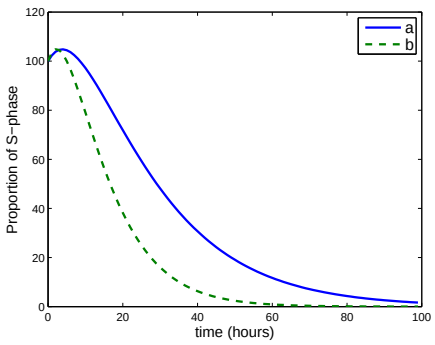

(a) Linear plot of proportion of cells in the S-phase. Cell cycle transfer rates were chosen for the case ***a***: where $r_{G_1\to S} < r_{S\to G_2M}$ - $r_{G_1\to S} = 0.05$, $r_{S\to G_2M} = 0.101$, $r_{G_2M\to G_1} = 1.5$. In the case ***b***: where $r_{G_1\to S} > r_{S\to G_2M}$ - $r_{G_1\to S} = 0.15$, $r_{S\to G_2M} = 0.101$, $r_{G_2M\to G_1} = 1.5$.

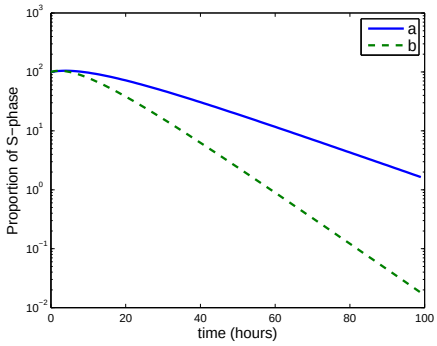

(b) Logarithmic plot of proportion of cells in the S-phase. Cell cycle transfer rates were chosen for the case ***a***: $r_{G_1\to S} < r_{S\to G_2M}$ - $r_{G_1\to S} = 0.05$, $r_{S\to G_2M} = 0.101$, $r_{G_2M\to G_1} = 1.5$. In the case ***b***: when $r_{G_1\to S} > r_{S\to G_2M}$ - $r_{G_1\to S} = 0.15$, $r_{S\to G_2M} = 0.101$, $r_{G_2M\to G_1} = 1.5$.

Figure 3.3: Proportion of cells in the S-phase after paclitaxel application will decrease exponentially. It can be seen that in cases of $r_{G_1\to S} > r_{S\to G_2M}$ proportion in S-phase will decay faster than in cases of $r_{G_1\to S} < r_{S\to G_2M}$.

it follows

$$P_{LR} = -\log_{10}\left(\frac{r_{S\to G_2M}+\lambda}{r_{S\to G_2M}-r_{G_1\to S}}(e^{-r_{G_1\to S}t_1} - e^{-r_{S\to G_2M}t_1}) + e^{-r_{S\to G_2M}t_1}\right). \tag{3.3.11}$$

Now remember t_1 is the end of the paclitaxel exposure time, and λ can be obtained from the solution of equation (3.2.6). So that asymptotically when $t_1 > T_L$, we can obtain two linear plateau log reduction formulae, and to this end add and subtract T_L from t. The first case being of $r_{G_1\to S} < r_{S\to G_2M}$, and from equation (3.3.9), it is

$$P_{LR} \approx -\log_{10}\left(\frac{r_{S\to G_2M}+\lambda}{r_{S\to G_2M}-r_{G_1\to S}}e^{-r_{G_1\to S}T_L}\right) + \log_{10}(e)\, r_{G_1\to S}\,(t_1 - T_L), \quad t_1 > T_L. \tag{3.3.12}$$

The second equation applies for when $r_{G_1\to S} > r_{S\to G_2M}$, and it is

$$P_{LR} \approx -\log_{10}\left(\frac{r_{G_1\to S}+\lambda}{r_{G_1\to S}-r_{S\to G_2M}}e^{-r_{S\to G_2M}T_L}\right) + \log_{10}(e)\, r_{S\to G_2M}\,(t_1 - T_L), \quad t_1 > T_L. \tag{3.3.13}$$

These formulae show directly the linear dependence of P_{LR} on t_1 and the two transition probabilities. Furthermore, in Figure 3.3(b) we plot an illustration of formulae (3.3.11) showing the linear dependence, as represented in equations (3.3.12), (3.3.13), when $t_1 > T_L$ for $T_L \approx 50$ hr. The formulae illustrate a linear increase in P_{LR} on the exposure time t_1 and the two transition rates.

Equations (3.3.12) and (3.3.13) should be compared with equation (3.3.3) with the understanding that the transition rates are related to $k_1/\widetilde{T}$ as is now shown. The remaining link with the results of Baguley *et al.* (1995) to be shown is how P_{LR} is approximately linearly dependent upon $1/T_d$. To show this, we need the dependence of λ on the transition rates. This can be done by examination of the nonlinear equation (3.2.6). In Appendix B.2, we show that there exists an approximate linear

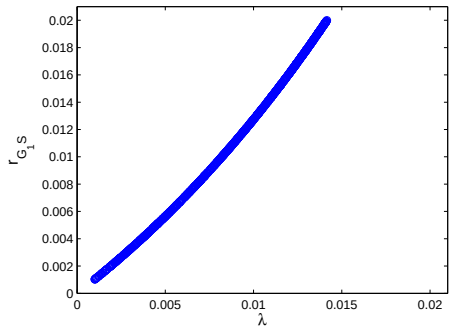

(a) Simulation to verify the linear dependence of λ on transition rate $r_{G_1 \to S}$ with condition $r_{G_1 S} < r_{S G_2 M}$. Transition rates were chosen as $r_{G_1 S} \in (0.02, 0.09)$, $r_{S G_2 M} = 0.09$ and $r_{G_2 M G_1} = 1.2$.

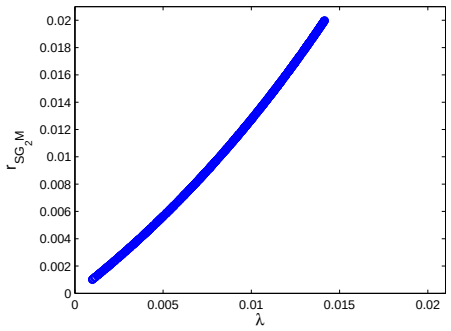

(b) Simulation to verify the linear dependence of λ on transition rate $r_{G_1 \to S}$ with condition $r_{G_1 S} > r_{S G_2 M}$. Transition rates were chosen as $r_{S \to G_2 M} \in (0.02, 0.09)$, $r_{G_1 \to S} = 0.09$ and $r_{G_2 M G_1} = 1.2$.

Figure 3.4: Simulations were carried out to verify statements postulated in equation (3.3.14).

dependence of λ on the two transition rates appearing in the above two equations as

$$\lambda \approx \begin{cases} r_{G_1 \to S}, & r_{G_1 \to S} < r_{S \to G_2 M}, \\ r_{S \to G_2 M}, & r_{G_1 \to S} > r_{S \to G_2 M}. \end{cases} \tag{3.3.14}$$

This result provides some mathematical justification of the often quoted approximation that the BEG growth rate is $r_{G_1 \to S}$. It is seen here that this is only true with the asymptotic assumptions made in Appendix B.2 and if $r_{G_1 \to S} < r_{S \to G_2 M}$. To further illustrate the approximate linear dependence of λ on the appropriate transition probability, we show in Figure 3.4 both cases considered in expression (3.3.14) of λ verses $r_{G_1 \to S}$, and $r_{S \to G_2 M}$ from the nonlinear equation (3.2.6). This figure shows that our analysis in Appendix B.2 holds true for an appropriate range of $r_{G_1 \to S}$. In Appendix B.2, a second order approximation is estimated.
So remembering equation (3.2.7), it is seen that we can find one asymptotic formula for the plateau log reduction formulae as

$$P_{LR} \approx -\log_{10}\left(\frac{r_{S \to G_2 M} + \lambda}{r_{S \to G_2 M} - r_{G_1 \to S}} e^{-r_{G_1 \to S} T_L}\right) + \frac{\ln 2}{\ln 10} \frac{(t_1 - T_L)}{T_d}, \quad t_1 > T_L. \tag{3.3.15}$$

Equation (3.3.15) is essential to our results as it shows that P_{LR} is approximately linearly dependent upon $1/T_d$ as it was proposed in the paper Baguley *et al.* (1995).

We note that to get agreement with Baguley *et al.* (1995), as given in equation (3.3.4) for $K_1 = 2.25$ the above equation implies that $T_L = 2.47$ days or 59.4 hours which is fairly close to our previously mentioned linearity estimate.
It is seen that equation (3.3.15) provides theoretical justification from our model of the experimental postulate of Baguley *et al.* (1995), for equation (3.3.3). In the next section, we provide a Monte Carlo simulation of the full equation (3.3.11) further justifying these conclusions.

3.3.3 Monte Carlo simulations

In this section, we present simulations of our model that were carried out in order to verify the linearity of logarithmic plateau reduction values and exposure times over cell doubling time. This simulation

uses the full equation (3.3.11), not the asymptotic equations, and so it will not only show justification of the experimental results of Baguley *et al.* (1995), but will also verify the asymptotic analysis of Section 3.3.2.

We chose approximately 500 random uniformly distributed transition rates within the intervals $0.0001 < r_{G_1 \to S} < 0.12$, $0.0001 < r_{S \to G_2 M} < 0.12$, $0.99 < r_{G_2 M \to G_1} < 2$ and $0.000001 < r_A < 0.0001$, which are appropriate to many cell lines and were provided by biologists. For the biologically significant case $r_{G_1 \to S} < r_{S \to G_2 M}$, in Figure 3.5(a) we show the results from equation (3.3.11) of our simulation from the randomly generated transition rates, with the abscissa depicting the ratio of exposure time to cell doubling time. Superimposed on the simulated data is our least squares affine regression line. In Figure 3.5(b), we incorporate a constant death rate in our simulations that results in cell loss of 2%-20% of the total population. The simulation uses the numerical solution of the ODE system (3.2.1) to determine the ratio $P_S(t)/P_S(0)$ as in this case the formula on the right-hand-side of equation (3.3.11) is not correct. When solving the ODE system, the term r_A is chosen from a uniform random distribution to result in the appropriate cell loss. We observe that our model with apoptosis Figure 3.5(b) gives the least square affine regression line equivalent to the second decimal place to the affine regression line of our model without apoptosis in Figure 3.5(a).

In our remaining simulations, we use the model without apoptosis effects in order to simplify the derivation of the analytical formulae. For the less biologically significant case where $r_{S \to G_2 M} < r_{G_1 \to S}$, we show in Figure 3.5(c) the results of our simulation from the randomly generated transition rates, with the abscissa the ratio of exposure time and cell doubling time. Also shown in this figure is the least squares affine regression line. Furthermore, we show for comparison in Figure 3.5(d), a reproduction of the experimental and least squares affine regression line from Baguley *et al.* (1995). To compare this figure with our results we must observe a few points. First, the experimental values of T_d in this figure are obtained by cell counting so that any apoptosis that occurs will ensure that the experimental value of T_d is too large. Second, the small number of data points in the experimental fit leads to considerable variability in the coefficients of the fit when compared to our final results shown in Figure 3.6.

We observe from equation (3.2.6) that the value of λ is affected by all three transition rates $r_{G_1 \to S}$, $r_{S \to G_2 M}$, $r_{G_2 M \to G_1}$, and thus changes in the three-dimensional space of transition rates result in a stochastic like changes in values of the doubling time T_d in the three simulated plots of Figure 3.5. It should be remembered that the doubling time is an inverse of λ. This will mean that all our simulation graphs will have stochastic-like appearance.

The nonlinear map R was used to map the randomly chosen $\mathbf{r}$'s onto λ the Π's with the subsequent calculation of T_d, and then P_{LR} through equations (3.2.7) and (3.3.11) to produce the results shown in Figures 3.5-3.6. The map R was solved numerically by use of the damped Newton method.

It is observed from the simulated graphs in Figure 3.5 that a wide range of T_d has been offered; this range is in excess of what is found biologically. So in Figure 3.6 we reject simulations that offer T_d outside the interval: $1.3 < \frac{5}{T_d} < 4.5$ (here T_d is in days). Figure 3.6(a) shows the results of our simulation from the randomly generated transition rates when used in equation (3.3.11), with the abscissa the ratio of exposure time to cell doubling time. Superimposed on the simulated data is our least squares affine regression line. In Figure 3.6(b) we invert the plots of Figure 3.6(a) by plotting the doubling time against the exposure time divided by the plateau log reduction value. Furthermore, a least square affine regression line is shown. These regression lines show that we can express the doubling time values through the reciprocal of the plateau log reduction values as follows:

$$T_d = c_1 \frac{t}{P_{LR}} + c_2. \tag{3.3.16}$$

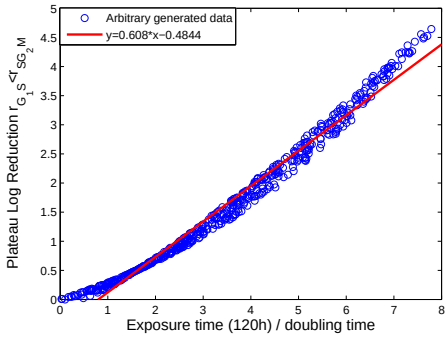

(a) The biologically more plausible case of $r_{G_1 \to S} < r_{S \to G_2 M}$ and $r_A = 0$. From this plot it can be concluded that doubling time can be obtained from linear expression $P_{LR} = m_1 t/T_d + m_2$,where $m_1 = 0.608$, $m_2 = -0.4844$ and $t = 120$ hours, thus $T_d = 72.96/(P_{LR} + 0.4844)$.

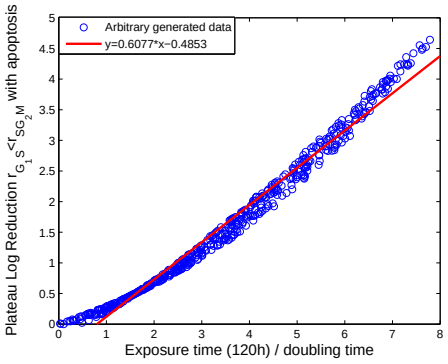

(b) The biologically more plausible case of $r_{G_1 \to S} < r_{S \to G_2 M}$ with apoptosis present after treatment with paclitaxel. The population doubling time can be obtained from linear expression $P_{LR} = m_3 t/T_d + m_4$,where $m_3 = 0.6077$, $m_4 = -0.4853$ and $t = 120$ hours, thus $T_d = 72.924/(P_{LR} + 0.4853)$.

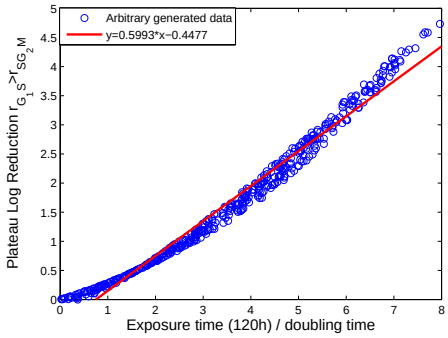

(c) For the case of $r_{G_1 \to S} > r_{S \to G_2 M}$, with $r_A = 0$, it be can see that the doubling time can be calculated using expression $P_{LR} = n_1 t/T_d + n_2$ with $n_1 = 0.5993$, $n_2 = -0.4477$ and $t = 120$ hours, thus $T_d = 71.916/(P_{LR} + 0.4477)$.

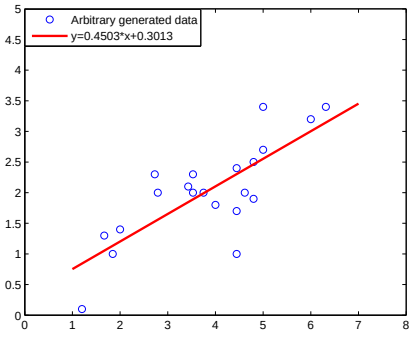

(d) An experimental cell line data and the experimental data in Table 2 from Baguley *et al.* (1995) is plotted for the comparison with the previous three figures. The doubling time can be estimated from the equation $P_{LR} = n_3 t/T_d + n_4$ with $n_3 = 0.4503$, $n_4 = 0.3013$ and $t = 120$ hours, thus $T_d = 54.036/(P_{LR} - 0.3013)$.

Figure 3.5: Plateau log reduction value is plotted against the exposure time/doubling time in order to show the linearity. Two cases - $r_{G_1 \to S} < r_{S \to G_2 M}$ and $r_{G_1 \to S} > r_{S \to G_2 M}$ were analysed. It can be concluded that the relation between transition rates $r_{G_1 \to S}$ and $r_{S \to G_2 M}$ has no effect on affine formula of the doubling time. Cases of no apoptosis and apoptosis present after paclitaxel addition are analysed and it can be seen that apoptosis presence has no effect on the affine formula of the doubling time. Each dot represents a cell line either experimental or theoretical.

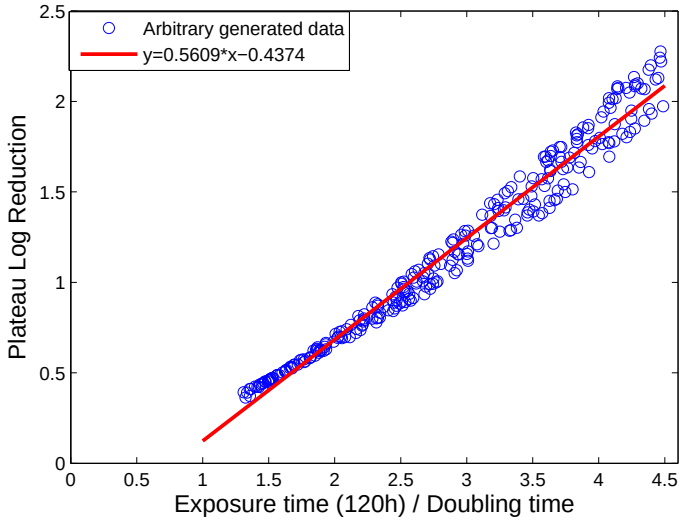

(a) Plateau log reduction values versus exposure time/ cell doubling time for cell line data, when $r_{G_1S} < r_{SG_2M}$. We can see that the doubling time can be calculated using expression $P_{LR} = a_1 t/T_d + a_2$ with $a_1 = 0.5609$, $t = 120$ hours and $a_2 = -0.4374$, thus we can express population doubling time through the plateau log reduction value as $T_d = 67.308/(P_{LR} + 0.4374)$.

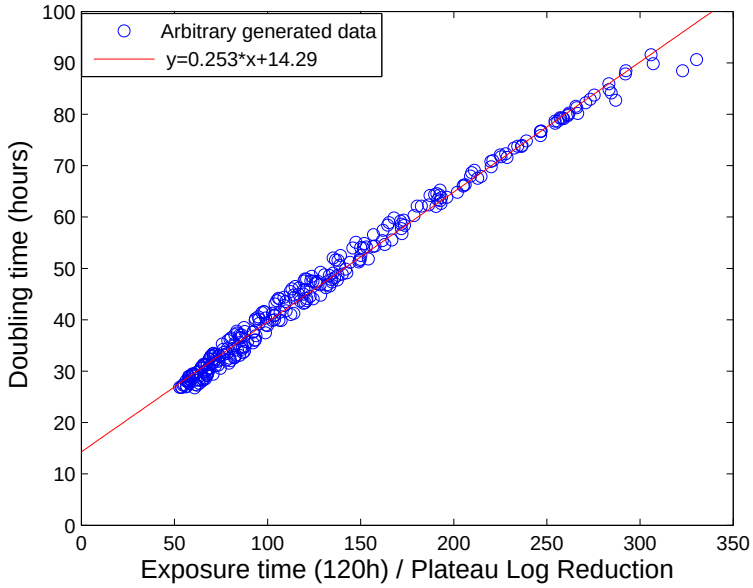

(b) Population doubling time values versus exposure time/ plateau log reduction for cell line data, when $r_{G_1S} < r_{SG_2M}$. We can see that the doubling time can be calculated using expression $T_d = c_1 t/P_{LR} + c_2$ with $c_1 = 0.253$, $t = 120$ hours and $c_2 = 14.29$ thus $T_d = 30.36/P_{LR} + 14.29$.

Figure 3.6: Simulations for estimating cell population doubling time for cell lines are shown. We have only considered case of $r_{G_1 \to S} < r_{S \to G_2 M}$ since there is no effect on choosing the opposite and also $r_A = 0$. From arbitrary generated data we have chosen only those that fall within the range $1.3 < \frac{5}{T_d} < 4.5$ for cell lines, here T_d is in days.

	Cell line	Cell line	Cell line
Exposure time (hours)	120	144	168
(days)	5	6	7
Doubling time (hours)	$T_d = \frac{30.36}{P_{LR}} + 14.29$	$T_d = \frac{36.288}{P_{LR}} + 16.42$	$T_d = \frac{42.2184}{P_{LR}} + 19.16$

Table 3.2: Affine formula for the cell doubling time calculation. Figure 3.6(b) was used to obtain the affine relation values. Observe that T_d is in hours.

We have derived a linear relationship between the plateau log reduction value and the cell doubling time (as found in Baguley *et al.* (1995)) of a cell line after being exposed to paclitaxel. The coefficient c_1 ($c_1 t = K$) is directly dependent on the exposure time, therefore the linear method is applicable only for the fixed exposure time of 5 to 7 days. Our simulations show that the linear relationship between T_d and P_{LR} exists. We have used the asymptotics in Section 3.3.2 on $P_{LR} \times T_d$ to show that for any random transition rates the coefficient c_1 value is the approximately the same.

3.3.4 Determination of population cell dynamics from plateau log reduction

We first observe that determination of λ from the experimentally obtained doubling time is problematic as it involves cell counting. The use of the experimental method analysed in this chapter to determine P_{LR} and then the use of the least squares regression line between P_{LR} and T_d, of the previous subsection, overcomes this difficulty. This then enables the determination of the transition probabilities with λ calculated from the doubling time and the nonlinear map described in Theorem 3.2.1(b). However, a superior method for short term assays to determine T_d is:

1. Find the plateau log reduction, P_{LR}, from the assay.
2. Use the results in Table 3.2 to find T_d from P_{LR}.

In Table 3.2, we list our overall affine regression results.

3.3.5 Population doubling time formulae in literature

A variety of methods of the doubling time estimation can be found in the literature. Table 3.3 depicts many crucial features that distinguish between different methods - firstly, whether or not cell death is taken into account when calculating population doubling time. T_d describes population doubling time with cell death present and T_{pot} is a measurement of cell population doubling time with no cell loss Steel (1977). Secondly, whether or not one needs to estimate apoptosis rate experimentally since cell death evaluation has come to be known as somewhat problematic Rew & Wilson (2000). Thirdly, whether experimental estimates used in population doubling time formulae are single time-point observations or multiple time-point observations.
We have included references to formulae of doubling times and short descriptions of variables used in theses formulae. For more detailed information, we ask readers to look at papers Baguley *et al.* (1995); Bertuzzi *et al.* (2002); Rew & Wilson (2000); Steel (1977); Terry & White (2006) as shown in Table 3.3.

Formula	Cell death included	Cell death measurement	Experimental methods	Authors	Variables	Single (ST) or multiple (MT) time-point observation
$T_d = c_1 \frac{t}{P_{LR}} + c_2$	Yes	No	Stathmokinetic $^3H - TdR$, Flow cytometry	Our method Baguley *et al.* (1995)	P_{LR} - plateau log reduction value c_1, c_2 -constant t - exposure time to paclitaxel	ST
$T_d = \frac{ln(2)}{rc}$	Yes	Yes	Relative motion (RM) BrdUrd, Flow cytometry	Terry & White (2006)	r - fraction of labelled cells completing division c - progression rate of labelled cells towards division	MT
$T_d = \frac{ln(2)}{\lambda}$	No	N/A	Growth curve	Many papers	λ - growth rate	MT
$T_{pot} = \frac{ln(2)T_S}{\nu}$	No	N/A	Relative motion (RM) BrdUrd, Flow cytometry	Steel (1977); Terry & White (2006) Bertuzzi *et al.* (2002); Rew & Wilson (2000)	T_S - duration of S-phase ν- labelling index	MT

Table 3.3: Population doubling time estimation methods in the literature. Second column indicates whether or not a particular method takes cell loss into account when estimating doubling time. Third column shows if cell death has to be determined experimentally (N/A stands for not applicable), fourth column provides key words of the experimental techniques applied. Fifth column points to references in literature. Sixth column briefly describes variables used in the particular formulae. Seventh column shows whether or not the particular method requires a single time-point measurement.

3.4 Conclusions

We have addressed the question here of whether the transition probability model can be used to derive a direct relationship between cell population doubling time and ^{3}H-TdR incorporation data. We have shown that indeed it can, and furthermore we can derive a direct relationship between cell doubling time and ^{3}H-TdR incorporation data.

In Baguley *et al.* (1995), a cell doubling time formula (3.3.4) was estimated using a simple model for cell growth. We use a more complicated phase structured model and obtain a similar linear dependence for the cell doubling time T_d. We have verified by asymptotics that the linear relationship between T_d and P_{LR} exists. We have derived that the coefficient K_t is dependent on the time a cell line has been exposed to paclitaxel. We have applied Monte Carlo experiments to justify and quantify the linear relationships used to estimate doubling time from 5-day cell culture assays, and we suggest these equations be used for application of the experimental technique. Furthermore, we have incorporated apoptosis in our simulations that would result in a cell loss of 2%-20% of the total population, through a constant death rate. We observed that our model with apoptosis and no apoptosis after paclitaxel incorporation had no difference in the least square affine regression lines. This implies our techniques are applicable to cell line populations with a small percentage of non-proliferating cells.

We also observe that the wide range of P_{LR} show how different cell lines can have a different responses to chemotherapy and this stems from the possible wide range of values for transition rates between phases, in particular the transition rate from G_1 to S-phase which produces to a wide range of G_1-phase transit times is a major factor in this. A further extension of this model for cancer cell lines would involve: first, incorporating aging times τ_p in each phase of the cell cycle to increase biological realism of the model. Second, derive expressions for estimating the cell-cycle time (or removal time in Chapter 2) from single experimental observation of the plateau log reduction value, similar to the ones presented in Table 3.2 for the doubling time.

We should point out that currently this type of linear relationship can be derived only for the cell lines, although it has been suggested in Baguley *et al.* (1999) such a relationship holds for primary cultures. The above model and method could be applied to primary cultures by using an extension of the model described Daukste *et al.* (2009). Further work would include deriving such formulae for primary cultures.

3. DETERMINATION OF CELL POPULATION DYNAMICS USING PLATEAU LOG REDUCTION METHOD

Chapter 4

Modelling Cancer Cell Population Perturbed by Irradiation

In this chapter, we examine the response of a cancer cell population to a one-time irradiation dose. We show that, by changing the PDE system of the number density function to the probability density function, our model tracks the variability of proportions of cancer cell population in each phase of the cell cycle and is compatible with the experimental estimates of proportions in each phase after a variety of cancer treatments. Our results agree with the previous studies of irradiated cancer cell lines, i.e., a cancer cell population undergoes little apoptosis after radiotherapy within the given experimental observation times. Therefore, we show that the experimentally observed decrease in the expected number of cells is due to the long-term arrest of the cell cycle. Our model provides an interval of the initial proliferating fraction of the cell population for each cell line, i.e., a proportion of cells that keeps proliferating after the application of radiotherapy. In the discussion section, we explain why the proliferating fraction estimated via our mathematical model does not agree with experimentally estimated surviving fraction.

4.1 Introduction

Radiation therapy is one of the main cancer treatment methods due to its ability to control cell growth: it causes DNA damage, leading to long-term cell cycle arrest and cell death. The aim of the model in this chapter is to determine the proliferating proportion of a cancer cell population of human melanoma cell lines after a one-time irradiation dose. It is considered that cell death or apoptosis takes place within a few hours of an irradiation dose Illidge (1998); Kerr *et al.* (1994); Meyn (1997). We observe here that, in biological nomenclature, cells are considered dead if they have lost ability to divide indefinitely. Cells that divide indefinitely are called clonogenic. Throughout this thesis, we define cell death or loss as process of cells undergoing apoptosis. We declare that cells are proliferating or non-proliferating until they undergo apoptosis. We remark that notions cell death, apoptosis and cell loss are interchangeable in this chapter. The difference between programmed cell death, apoptosis, and necrosis occurring after radiotherapy has been discussed in paper Illidge (1998). However, we do not differentiate between these notions in our mathematical model.

Numerous mathematical models have been developed to analyse the effects of radiotherapy Barazzoul *et al.* (2010); Basse *et al.* (2010); Enderling *et al.* (2006); Rockne *et al.* (2009). Many of the proposed methods involve the construction of a mathematical model to explain the flow cytometry data of cancer cell lines after irradiation. In this chapter, we are going to address and elaborate on

the methods derived in paper Basse *et al.* (2010). The model presented in Basse *et al.* (2010) demonstrated that an irradiation dose of 9 Gray (Gy) induced long-term cell cycle arrest. While a cancer cell population unperturbed by any treatment remains in balanced exponential growth (BEG) Bell (1968), a cancer cell population after exposure to any cancer treatment does not exhibit BEG.

We note here that, for various cancer types, cancer patients are given radiotherapy in fractions of $1.8 - 2.0$ Gy daily on weekdays for $5 - 7$ weeks Kim & Tannock (2005). Radiation dose 2 Gy is considered to cause a sub-lethal radiation damage to normal tissue. The total weekly radiation dose $9 - 10$ Gy is broken down to multiple smaller doses along the week to give time for a normal tissue to recover, which is named as one of the reasons of radiotherapy failures for some cancer types, see Kim & Tannock (2005). Our mathematical model is applied to five melanoma cell lines that have been exposed to one-time irradiation of 9 Gy. Cancer patients never receive radiation dose of total 9 Gy in a day due to potential sever toxic reactions.

We start by deriving an age-structured mathematical model of a cell population response to radiation therapy to analyse experimental data of human melanoma cell lines from the Auckland Cancer Society Research Centre. Identical data has been analysed in paper Basse *et al.* (2010), see Basse *et al.* (2010) for details on cell line derivation and experimental methods applied. Here we undertake the method presented in paper Guiotto & Ubezio (2000), i.e., we normalise the numerical density function (previously discussed in Chapter 2) and deal with the proportion density function in our age-structured model. We then apply our mathematical model to experimental data extracted from flow cytometry profiles. Such profiles show proportion distribution among cell cycle phases at different time points. The existence of the age-structured model solution has been discussed in Guiotto & Ubezio (2000).

Later, we reduce the model to a nonlinear differential - algebraic equation (DAE) system in order to determine the arrest and cell loss impact on the transition rates between the cell cycle phases. We use the DAE system because normalisation of the system, i.e., dealing with the varying proportions at each time step, leads to a constraint that the sum of proportions in all phases combined is equal to one at every time step. The aim of this model is to determine the initial proliferating fraction and proportion of a cancer cell population that continues proliferating for more than 96 hours after the irradiation of 9 Gy. Experimental data was provided for various time points up to 96 hours. We initially assume that, within 96 hours after irradiation, full effects of cancer treatments, i.e., the arrest of the transition rates and cell death, can be detected. The flow cytometry profile data of human melanoma cell lines has been provided. These data include flow cytometry profiles of unperturbed cancer cell lines, cancer cell lines treated by paclitaxel at a concentration of 200 nM, cancer cell lines treated by 9 Gy strength irradiation, and a combined treatment of paclitaxel and 9 Gy irradiation. We cannot extract enough information from radiation data alone; thus, paclitaxel and the combined treatment flow cytometry profiles are vital. Flow cytometry data of cell lines treated with paclitaxel, in addition to that of radiation, are used to provide the uniqueness of the calculated values of arrested transition rates.

In Basse *et al.* (2010), theoretical profiles generated by the mathematical model are compared with the experimental flow cytometry profiles at various time points. Flow cytometry profiles of irradiated cell lines and irradiated cell lines with applied paclitaxel are used to determine if arrest occurs in the G_1 or G_2 phase. Authors of paper Basse *et al.* (2010) concluded that apoptosis does not occur after irradiation of the cell lines.

In this chapter, we estimate the proportion of the cancer cell population in each of the cell cycle phases (G_1, S, and combined G_2M) from flow cytometry profiles and then use this estimate as input data for our optimization routine. Since the flow cytometry method cannot distinguish the difference between the G_2 and M phases (due to the fact that DNA contents in both phases are twice that of the S-phase), we used a combined G_2M-phase in our mathematical model. We have assumed that cancer

cells can respond to radiation by cell cycle arrest, senescence, and cell death. There is evidence that radiation at lower doses produces damage that can lead to cell death but it can also be fairly rapidly repaired, while higher doses produce damage that is irreparable, and cells go into long-term cell cycle arrest Pawlik & Keyormarsi (2004). After radiation, some cells are lost by cell death (which makes no contribution to the flow cytometry profiles) and some by senescence (which contributes to the flow cytometry profiles), while others proliferate. We aim to estimate the proportion of proliferating cells. It is known that a small fraction of the initial population (0.1-10%, depending on the cell line) survives radiation (also called the surviving fraction) and that this fraction is the population that grows in a surviving colony assay Baguley (2011). Ultimately, we expect that our model will provide similar arrest values, as in Basse *et al.* (2010), if the cell loss (death) rate is not included. Moreover, in advance to Basse *et al.* (2010), we estimate the proportion of proliferating cells after the irradiation dose of 9 Gy. The main difference between the model presented in this chapter and the one examined in Basse *et al.* (2010) is that in our model does not require experimentally estimated transition rate values, apoptosis rates and doubling times as input variables. We used a DAE system as oppose to the ODE/PDE system used in Basse *et al.* (2010). Furthermore, we have estimated the surviving fraction of the population exposed to a single dose of irradiation and the transition rates between the consecutive phases.

This chapter presents several mathematical models that were constructed to utilise the experimental data of a cancer cell population that was first, unperturbed by any treatment, second, perturbed by 200 nM paclitaxel, third, perturbed by a combined treatment of 200 nM of paclitaxel and 9 Gy irradiation, and, four, perturbed by the irradiation of 9 Gy. Derivation of the mathematical model of radiation effects on cancer cell population dynamics is shown by introducing a general model with modifications made to fit the provided experimental data.

4.2 Mathematical model of cycling population. Cancer cell population dynamics after radiotherapy.

The following model is constructed to track the proliferating proportion of the cell population after radiation therapy. It describes temporary varying proportions observed after the irradiation of cancer cell lines.

4.2.1 Age-distribution system

Our mathematical model, presented in this chapter, shows the response to ionising radiation treatment (senescence, arrest, and cell death) by including the arrest and senescence phases that branch from G_1 and G_2M phases and the cell loss rate arising from the G_2M - phase, as depicted in Figure 4.1, where Sen_k with $k \in \{1, 2\}$ represents the senescence phase and A_k defines the arrest state for the appropriate cell cycle phase. The transition rates between phases are described in Table 4.1.

We proceed with defining the partial differential equation (PDE) system for our model. Later, we simplify it in order to apply the experimental data from flow cytometry profiles. Flow cytometry profiles illustrate the proportion of the cell population in each of the G_1, S, and combined G_2M phases. An example of a flow cytometry profile can be seen in Figure 1.3.

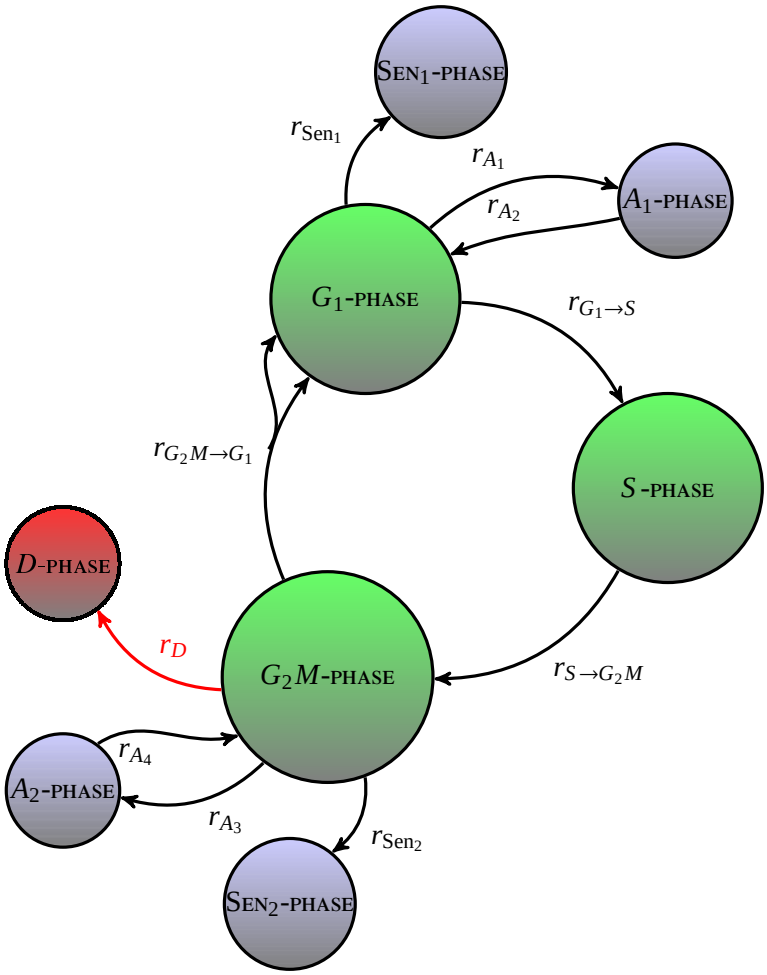

Figure 4.1: Diagram of the cell-cycle control of *in vitro* tumour cells perturbed by radiation. Transition rates are explained in Table 4.1.

We define a general age-structured model as follows:

$$\frac{\partial n_{G_1}(t,\tau)}{\partial t} + \frac{\partial n_{G_1}(t,\tau)}{\partial \tau} = -[r_{G_1\to S}(t,\tau) + r_{A_1}(t,\tau) + r_{Sen_1}(t,\tau)]n_{G_1}(t,\tau) + r_{A_2}(t,\tau)n_{A_1}(t,\tau), \quad (4.2.1a)$$

$$\frac{\partial n_S(t,\tau)}{\partial t} + \frac{\partial n_S(t,\tau)}{\partial \tau} = -r_{S\to G_2M}(\tau)n_S(t,\tau), \quad (4.2.1b)$$

$$\frac{\partial n_{G_2M}(t,\tau)}{\partial t} + \frac{\partial n_{G_2M}(t,\tau)}{\partial \tau} = -[r_{G_2M\to G_1}(t,\tau) + r_{A_3}(t,\tau) + r_{Sen_2}(t,\tau) + r_D(t,\tau)]n_{G_2M}(t,\tau) + r_{A_4}(t,\tau)n_{A_2}(t,\tau), \quad (4.2.1c)$$

$$\frac{\partial n_{A_1}(t,\tau)}{\partial t} = r_{A_1}(t,\tau)n_{G_1}(t,\tau) - r_{A_2}(t,\tau)n_{A_1}(t,\tau), \quad (4.2.1d)$$

$$\frac{\partial n_{Sen_1}(t,\tau)}{\partial t} = r_{Sen_1}(t,\tau)n_{G_1}(t,\tau), \quad (4.2.1e)$$

$$\frac{\partial n_{A_2}(t,\tau)}{\partial t} = r_{A_3}(t,\tau)n_{G_2M}(t,\tau) - r_{A_4}(t,\tau)n_{A_2}(t,\tau), \quad (4.2.1f)$$

$$\frac{\partial n_{Sen_2}(t,\tau)}{\partial t} = r_{Sen_2}(t,\tau)n_{G_2M}(t,\tau), \quad (4.2.1g)$$

with the renewal distribution conditions:

$$n_{G_1}(t,\tau=0) = 2\int_0^\infty r_{G_2M\to G_1}(t,\tau)n_{G_2M}(t,\tau)\,d\tau, \tag{4.2.2a}$$

$$n_S(t,\tau=0) = \int_0^\infty r_{G_1\to S}(t,\tau)n_{G_1}(t,\tau)\,d\tau, \tag{4.2.2b}$$

$$n_{G_2M}(t,\tau=0) = \int_0^\infty r_{S\to G_2M}(\tau)n_S(t,\tau)\,d\tau, \tag{4.2.2c}$$

and the initial age distribution:

$$n_{G_1}(t=0,\tau) = n^0_{G_1}(\tau), \tag{4.2.3a}$$

$$n_S(t=0,\tau) = n^0_S(\tau), \tag{4.2.3b}$$

$$n_{G_2M}(t=0,\tau) = n^0_{G_2M}(\tau), \tag{4.2.3c}$$

$$n_{A_1}(t=0,\tau) = n^0_{A_1}(\tau), \tag{4.2.3d}$$

$$n_{Sen_1}(t=0,\tau) = n^0_{\mathrm{Sen}_1}(\tau), \tag{4.2.3e}$$

$$n_{A_2}(t=0,\tau) = n^0_{A_2}(\tau), \tag{4.2.3f}$$

$$n_{Sen_2}(t=0,\tau) = n^0_{\mathrm{Sen}_1}(\tau), \tag{4.2.3g}$$

where n_m with $m \in \{G_1, S, G_2M, A_1, A_2, \mathrm{Sen}_1, \mathrm{Sen}_2\}$ represents the number density function at age τ at time t in a respective phase. Transition rates are shown in Table 4.1. Throughout this chapter, it is assumed that the maximum cell age $T \to \infty$. We have taken into account that cells in the senescent phase do not age; this assumption has also been made for cells in the arrest phase. Our model keeps track of the proportion of cells lost due to apoptosis, because system (4.2.1) expresses the dynamics of the cell population with a removal class (or cell death rate r_D). Flow cytometry profiles do not track the proportion of cells lost due to treatment; thus, one advantage of our model is that we estimate cell loss via mathematical means. Observe that the number two on the right-hand-side of the renewal equation (4.2.2a) is due to the fact that two daughter cells are produced after mitosis is complete.

We have defined problem (4.2.1)-(4.2.3) for a broad range of parameters that may vary with time and age. Although, in biological terms, this definition is a more realistic option, it is not simple enough for numerical calculations with the experimental data provided. Thus, as a first step, we make all transition rates between phases independent of age τ. While each cell has to age (grow) biologically within the G_1-phase before moving to the S-phase that also applies for S and G_2M phases, we neglect it in our model. This neglect is due to the lack of experimental estimates that would be needed to include a minimum time that each cell, on average, spends in a phase before leaving it. However, transition rates dependent on time t are necessary due to the effects of irradiation. Without any loss of generality, we impose that all transition rates after the treatment are piecewise linear functions with respect to time t. The total number of cells in a phase m, $N_m(t)$, was previously defined in Chapter 2 as follows:

$$N_m(t) = \int_0^\infty n_m(t,\tau)\,d\tau, \tag{4.2.4}$$

where $m \in \{G_1, S, G_2M, A_1, A_2, \mathrm{Sen}_1, \mathrm{Sen}_2\}$. The total number of cells in all of the phases $N_{tot}(t)$ is defined as follows:

$$N_{tot}(t) = \sum_m N_m(t). \tag{4.2.5}$$

parameter	description	units
$r_{G_1 \to S}$	rate transition G_1 to S-phase	hours^{-1}
$r_{S \to G_2 M}$	rate transition S to G_2M-phase	hours^{-1}
$r_{G_2 M \to G_1}$	rate transition G_2M to G_1-phase	hours^{-1}
r_{A_1}	arrest rate G_1 to A_1-phase	hours^{-1}
r_{A_2}	rate transition A_1 to G_1-phase	hours^{-1}
r_{Sen_1}	senescence rate G_1 to Sen$_1$-phase	hours^{-1}
r_{A_3}	arrest rate G_2M to A_2-phase	hours^{-1}
r_{A_4}	rate transition A_2 to G_2M-phase	hours^{-1}
r_{Sen_2}	senescence rate G_2M to Sen$_2$-phase	hours^{-1}
r_D	apoptosis rate from G_2M-phase	hours^{-1}

Table 4.1: Radiation model parameters with descriptions and units.

In addition, we derive formulae for a change in the total number of cells in phase p at time t using equations (4.2.1)-(4.2.2), identity (4.2.4), and expression $\lim_{\tau\to\infty} n_m(t,\tau) = 0$. For the G_1-phase, the formula can be written as follows:

$$\begin{aligned}
\frac{dN_{G_1}(t)}{dt} &= \int_0^\infty \frac{\partial n_{G_1}(t,\tau)}{\partial t}\, d\tau, \\
&= \int_0^\infty \Big(- \frac{\partial n_{G_1}(t,\tau)}{\partial \tau} - [r_{G_1\to S}(t) + r_{A_1}(t) + r_{Sen_1}(t)] n_{G_1}(t,\tau) + r_{A_2}(t) n_{A_1}(t,\tau)\Big) d\tau, \\
&= n(t,\tau=0) - [r_{G_1\to S}(t) + r_{A_1}(t) + r_{Sen_1}(t)] \int_0^\infty n_{G_1}(t,\tau) d\tau + r_{A_2}(t) \int_0^\infty n_{A_1}(t,\tau) d\tau, \\
&= 2 r_{G_2M\to G_1}(t) N_{G_2M}(t) - [r_{G_1\to S}(t) + r_{A_1}(t) + r_{Sen_1}(t)] N_{G_1}(t) + r_{A_2}(t) N_{A_1}(t). \qquad (4.2.6)
\end{aligned}$$

Similar ordinary differential equations (*ODE*) can be derived for the rest of the phases. An additional equation needs to be derived for the next section. The equation representing the change of the total number of cells over time, i.e., a time-dependent growth rate for the total number of cells, is defined as follows:

$$\frac{dN_{tot}(t)}{dt} = \sum_m \frac{dN_m(t)}{dt} = [r_{G_2M\to G_1}(t) - r_D(t)] N_{G_2M}(t). \qquad (4.2.7)$$

4.2.2 Probability density system

We have to normalise the age-distribution system in order to use irradiated cancer cell population flow cytometry data at different time points. We previously defined the probability density function of cells in Chapter 2 and express it here again for a phase m as:

$$\pi_m(t,\tau) = \frac{n_m(t,\tau)}{N_{tot}(t)}. \tag{4.2.8}$$

Implying the probability of finding the random variable in n_m at time t between τ and $\tau + d\tau$ is $\pi_m\, d\tau$. Therefore, the proportion of cells in phase m at a given time is $\Pi_m(t)$ and is defined as follows:

$$\Pi_m(t) = \int_0^T \pi_m(t,\tau)d\tau = \frac{N_m(t)}{N_{tot}(t)}. \tag{4.2.9}$$

We can then transform problem (4.2.1)-(4.2.3) to a probability density system, given that:

$$\frac{\partial \pi_m(t,\tau)}{\partial t} = \frac{\partial}{\partial t}\frac{n_m(t,\tau)}{N_{tot}(t)} = \frac{1}{N_{tot}(t)}\frac{\partial\, n_m(t,\tau)}{\partial t} - \pi_m(t,\tau)\frac{N'_{tot}(t)}{N_{tot}(t)}. \tag{4.2.10}$$

We can replace the first term on the right-hand-side of equation (4.2.10), namely, term $\frac{\partial}{\partial t}n_m(t,\tau)$, by using system (4.2.1) and then, by taking into account that transition rates are independent of age τ, we can write the probability density equation system as follows:

$$\frac{\partial \pi_{G_1}(t,\tau)}{\partial t} + \frac{\partial \pi_{G_1}(t,\tau)}{\partial \tau} = -[r_{G_1\to S}(t) + r_{A_1}(t) + r_{Sen_1}(t)]\pi_{G_1}(t,\tau) + r_{A_2}(t)\pi_{A_1}(t,\tau) - \pi_{G_1}(t,\tau)\frac{N'_{tot}(t)}{N_{tot}(t)}, \tag{4.2.11a}$$

$$\frac{\partial \pi_S(t,\tau)}{\partial t} + \frac{\partial \pi_S(t,\tau)}{\partial \tau} = -r_{S\to G_2M}\pi_S(t,\tau) - \pi_S(t,\tau)\frac{N'_{tot}(t)}{N_{tot}(t)}, \tag{4.2.11b}$$

$$\frac{\partial \pi_{G_2M}(t,\tau)}{\partial t} + \frac{\partial \pi_{G_2M}(t,\tau)}{\partial \tau} = -[r_{G_2M\to G_1}(t) + r_{A_3}(t) + r_{Sen_2}(t) + r_D(t)]\pi_{G_2M}(t,\tau) + r_{A_4}(t)\pi_{A_2}(t,\tau) - \pi_{G_2M}(t,\tau)\frac{N'_{tot}(t)}{N_{tot}(t)}, \tag{4.2.11c}$$

$$\frac{\partial \pi_{A_1}(t,\tau)}{\partial t} = r_{A_1}(t)\pi_{G_1}(t,\tau) - r_{A_2}(t)\pi_{A_1}(t,\tau) - \pi_{A_1}(t,\tau)\frac{N'_{tot}(t)}{N_{tot}(t)}, \tag{4.2.11d}$$

$$\frac{\partial \pi_{Sen_1}(t,\tau)}{\partial t} = r_{Sen_1}(t)\pi_{G_1}(t,\tau) - \pi_{Sen_1}(t,\tau)\frac{N'_{tot}(t)}{N_{tot}(t)}, \tag{4.2.11e}$$

$$\frac{\partial \pi_{A_2}(t,\tau)}{\partial t} = r_{A_3}(t)\pi_{G_2M}(t,\tau) - r_{A_4}(t)\pi_{A_2}(t,\tau) - \pi_{A_2}(t,\tau)\frac{N'_{tot}(t)}{N_{tot}(t)}, \tag{4.2.11f}$$

$$\frac{\partial \pi_{Sen_2}(t,\tau)}{\partial t} = r_{Sen_2}(t)\pi_{G_2M}(t,\tau) - \pi_{Sen_2}(t,\tau)\frac{N'_{tot}(t)}{N_{tot}(t)}, \tag{4.2.11g}$$

with the renewal distribution conditions as:

$$\pi_{G_1}(t,\tau=0) = 2\int_0^\infty r_{G_2M\to G_1}(t,\tau)\pi_{G_2M}(t,\tau)d\tau, \tag{4.2.12a}$$

$$\pi_S(t,\tau=0) = \int_0^\infty r_{G_1\to S}(t,\tau)\pi_{G_1}(t,\tau)d\tau, \tag{4.2.12b}$$

$$\pi_{G_2M}(t,\tau=0) = \int_0^\infty r_{S\to G_2M}(\tau)\pi_S(t,\tau)d\tau, \tag{4.2.12c}$$

and the initial age distribution as:

$$\pi_{G_1}(t=0,\tau) = \pi^0_{G_1}(\tau), \tag{4.2.13a}$$

$$\pi_S(t=0,\tau) = \pi^0_S(\tau), \tag{4.2.13b}$$

$$\pi_{G_2M}(t=0,\tau) = \pi^0_{G_2M}(\tau), \tag{4.2.13c}$$

$$\pi_{A_1}(t=0,\tau) = \pi^0_{A_1}(\tau), \tag{4.2.13d}$$

$$\pi_{Sen_1}(t=0,\tau) = \pi^0_{\mathrm{Sen}_1}(\tau), \tag{4.2.13e}$$

$$\pi_{A_2}(t=0,\tau) = \pi^0_{A_2}(\tau), \tag{4.2.13f}$$

$$\pi_{Sen_2}(t=0,\tau) = \pi^0_{\mathrm{Sen}_2}(\tau). \tag{4.2.13g}$$

Using equations (4.2.7) and (4.2.9), we define the growth rate function $\lambda(t)$ as:

$$\lambda(t) = \frac{N'_{tot}(t)}{N_{tot}(t)} = [r_{G_2M\to G_1}(t) - r_D(t)]\Pi_{G_2M}(t). \tag{4.2.14}$$

We observe that $\lambda(t)$ is the time-dependent growth function and the total population grows as:

$$N_{tot}(t) = N_{tot}(0)e^{\int_0^t \lambda(s)ds}. \tag{4.2.15}$$

This equation is an important parameter in our population model.
By using similar techniques as in equation (4.2.6), we can reduce the *PDE* system (4.2.11) to an *ODE* system as the transition rates are independent of age, τ,. Thus, the cell population proportion system

is as follows:

$$\frac{d\Pi_{G_1}(t)}{dt} = 2r_{G_2M\to G_1}(t)\Pi_{G_2M}(t) - [r_{G_1\to S}(t) + r_{A_1}(t) + r_{Sen_1}(t)]\Pi_{G_1}(t) + r_{A_2}(t)\Pi_{A_1}(t) - \lambda(t)\Pi_{G_1}(t), \tag{4.2.16a}$$

$$\frac{d\Pi_S(t)}{dt} = r_{G_1\to S}(t)\Pi_{G_1}(t) - r_{S\to G_2M}\Pi_S(t) - \lambda(t)\Pi_S(t), \tag{4.2.16b}$$

$$\frac{d\Pi_{G_2M}(t)}{dt} = r_{S\to G_2M}\Pi_S(t) - [r_{G_2M\to G_1}(t) + r_{A_3}(t) + r_{Sen_2}(t) + r_D(t)]\Pi_{G_2M}(t) + r_{A_4}(t)\Pi_{A_2}(t) - \lambda(t)\Pi_{G_2M}(t), \tag{4.2.16c}$$

$$\frac{d\Pi_{A_1}(t)}{dt} = r_{A_1}(t)\Pi_{G_1}(t) - r_{A_2}(t)\Pi_{A_1}(t) - \lambda(t)\Pi_{A_1}(t), \tag{4.2.16d}$$

$$\frac{d\Pi_{Sen_1}(t)}{dt} = r_{Sen_1}(t)\Pi_{G_1}(t) - \lambda(t)\Pi_{Sen_1}(t), \tag{4.2.16e}$$

$$\frac{d\Pi_{A_2}(t)}{dt} = r_{A_3}(t)\Pi_{G_2M}(t) - r_{A_4}(t)\Pi_{A_2}(t) - \lambda(t)\Pi_{A_2}(t), \tag{4.2.16f}$$

$$\frac{d\Pi_{Sen_2}(t)}{dt} = r_{Sen_2}(t)\Pi_{G_2M}(t) - \lambda(t)\Pi_{Sen_2}(t), \tag{4.2.16g}$$

with the following initial conditions:

$$\Pi_{G_1}(t=0) = \Pi^0_{G_1}, \tag{4.2.17a}$$

$$\Pi_S(t=0) = \Pi^0_S, \tag{4.2.17b}$$

$$\Pi_{G_2M}(t=0) = \Pi^0_{G_2M}, \tag{4.2.17c}$$

$$\Pi_{A_1}(t=0) = \Pi^0_{A_1}, \tag{4.2.17d}$$

$$\Pi_{Sen_1}(t=0) = \Pi^0_{\mathrm{Sen}_1}, \tag{4.2.17e}$$

$$\Pi_{A_2}(t=0) = \Pi^0_{A_2}, \tag{4.2.17f}$$

$$\Pi_{Sen_2}(t) = \Pi^0_{\mathrm{Sen}_2}. \tag{4.2.17g}$$

Equations (4.2.5) and (4.2.9) let us derive the following algebraic expression:

$$\sum_m \Pi_m(t) = 1, \quad \forall t \geq 0, \tag{4.2.18}$$

where $m \in \{G_1, S, G_2M, A_1, A_2, \mathrm{Sen}_1, \mathrm{Sen}_2\}$. Thus, a cell cycle dynamics problem expressed with an ODE system (4.2.16) with respective initial conditions (4.2.17) and a constraint equation (4.2.18) becomes a *DAE* system. Equation (4.2.18) is a constraint expression that has to be satisfied for all t greater or equal to zero, i.e., the proportions in each phase of the cell cycle add up to a value of one at any time. We remind here that ODE system (4.2.16) does not include the proportion of cells dying due to the treatment because flow cytometry method does not track cell loss.

4.2.3 DAE system for experimental data

For the purposes of the analysis involved in the next section, and in order to formulate the use of the experimental data, we rearrange system (4.2.16) by combining the proliferating and non-proliferating cells (arrested and senescent cells) into one phase (as would be seen in the flow cytometry profiles). We add together the proliferating and non-proliferating fractions of the cell population in G_1 and G_2M

phases and denote this variable as P_p with $p \in \{G_1, S, G_2M\}$:

$$P_{G_1}(t) = \Pi_{G_1}(t) + \Pi_{A_1}(t) + \Pi_{Sen_1}(t),$$
$$P_{G_2M}(t) = \Pi_{G_2M}(t) + \Pi_{A_2}(t) + \Pi_{Sen_2}(t),$$

where we see the non-proliferating proportions of G_1 and G_2M phases as the fractions $\Pi_{A_1}(t)+\Pi_{Sen_1}(t)$ and $\Pi_{A_2}(t) + \Pi_{Sen_2}(t)$, respectively. Although subdivision in proliferating and non-proliferating cell subpopulations is desirable, our experimental data do not differentiate between proliferating and non-proliferating subpopulations. We note that the whole proportion of the cell population in S-phase detected in flow cytometry is considered to be proliferating, thus $\Pi_S = P_S$. Thus, system (4.2.16) becomes, through the addition of appropriate equations, as follows:

$$\frac{dP_{G_1}(t)}{dt} = 2r_{G_2M\to G_1}(t)\Pi_{G_2M}(t) - r_{G_1\to S}(t)\Pi_{G_1}(t) - \lambda(t)P_{G_1}(t), \tag{4.2.19a}$$
$$\frac{dP_S(t)}{dt} = r_{G_1\to S}(t)\Pi_{G_1}(t) - r_{S\to G_2M}P_S(t) - \lambda(t)P_S(t), \tag{4.2.19b}$$
$$\frac{dP_{G_2M}(t)}{dt} = r_{S\to G_2M}P_S(t) - [r_{G_2M\to G_1}(t) + r_D(t)]\Pi_{G_2M}(t) - \lambda(t)P_{G_2M}(t), \tag{4.2.19c}$$

with initial conditions provided from the flow cytometry profiles of the unperturbed cancer cell line populations:

$$P_{G_1}(t=0) = P^0_{G_1}, \tag{4.2.20a}$$
$$P_S(t=0) = P^0_S, \tag{4.2.20b}$$
$$P_{G_2M}(t=0) = P^0_{G_2M}, \tag{4.2.20c}$$

where new proportions combining the proliferating and non-proliferating populations are defined as follows:

$$P_{G_1}(t) = \Pi_{G_1}(t) + \Pi_{A_1}(t) + \Pi_{Sen_1}(t), \tag{4.2.21a}$$
$$P_S(t) = \Pi_S(t), \tag{4.2.21b}$$
$$P_{G_2M}(t) = \Pi_{G_2M}(t) + \Pi_{A_2}(t) + \Pi_{Sen_2}(t). \tag{4.2.21c}$$

This system still incorporates knowledge of the proliferating proportions: $\Pi_{G_1}(t)$ and $\Pi_{G_2M}(t)$. The constraint (4.2.18) arising in cancer cell population proportion dynamics can be rewritten as follows:

$$\sum_p P_p(t) = 1, \quad \forall t \geq 0, \tag{4.2.22}$$

where $p \in \{G_1, S, G_2M\}$. From equations (4.2.21), we can introduce the following identities:

$$\Pi_{G_1}(t) = \alpha(t)P_{G_1}(t), \tag{4.2.23a}$$
$$\Pi_{G_2M}(t) = \beta(t)P_{G_2M}(t), \tag{4.2.23b}$$

with $\alpha(t), \beta(t) \in [0,1]$ for all $t \geq 0$. We then substitute equations (4.2.23) into the system (4.2.19) as follows:

$$\frac{dP_{G_1}(t)}{dt} = 2r_{G_2M\to G_1}(t)\beta(t)P_{G_2M}(t) - r_{G_1\to S}(t)\alpha(t)P_{G_1}(t) - \lambda(t)P_{G_1}(t), \tag{4.2.24a}$$

$$\frac{dP_S(t)}{dt} = r_{G_1\to S}(t)\alpha(t)P_{G_1}(t) - r_{S\to G_2M}P_S(t) - \lambda(t)P_S(t), \tag{4.2.24b}$$

$$\frac{dP_{G_2M}(t)}{dt} = r_{S\to G_2M}P_S(t) - [r_{G_2M\to G_1}(t) + r_D(t)]\beta(t)P_{G_2M}(t) - \lambda(t)P_{G_2M}(t), \tag{4.2.24c}$$

where the population growth rate $\lambda(t)$ (note that cancer cell population after irradiation or any cancer treatment does not exhibit BEG) from equation (4.2.14) can be rewritten as follows:

$$\lambda(t) = [r_{G_2M\to G_1}(t) - r_D(t)]\Pi_{G_2M}(t) = [r_{G_2M\to G_1}(t) - r_D(t)]\beta(t)P_{G_2M}(t). \tag{4.2.25}$$

We then introduce new transition rates:

$$r^*_{G_1\to S}(t) = \alpha(t)r_{G_1\to S}(t), \tag{4.2.26a}$$

$$r^*_{G_2M\to G_1}(t) = \beta(t)r_{G_2M\to G_1}(t), \tag{4.2.26b}$$

$$r^*_D(t) = \beta(t)r_D(t). \tag{4.2.26c}$$

This means the transition rates $r^*_{G_1\to S}(t)$, $r^*_{G_2M\to G_1}(t)$ and $r^*_D(t)$ have been modified from those of Table 4.1 and an asterisk in superscript * has been added to highlight the difference. From equations (4.2.23) and (4.2.26), the following three identities, linking subdivided (namely, Π_m) and not subdivided (P_p) proliferating subpopulations in G_1 and G_2M phases, arise:

$$r^*_{G_1\to S}(t)P_{G_1}(t) = r_{G_1\to S}(t)\Pi_{G_1}(t), \tag{4.2.27a}$$

$$r^*_{G_2M\to G_1}(t)P_{G_2M}(t) = r_{G_2M\to G_1}(t)\Pi_{G_2M}(t), \tag{4.2.27b}$$

$$r^*_D(t)P_{G_2M}(t) = r_D(t)\Pi_{G_2M}(t). \tag{4.2.27c}$$

We subsequently can express the *DAE* system that is used for numerical calculations as shown in the next section.

4.2.4 DAE for calculations

We consider a model involving combined proliferating and non-proliferating proportions, as shown in Figure 4.2. Transition rates that have not been affected by the treatment are notified with tilde above the transition rate symbol. We have assumed that transition probability rate from the S-phase to the G_2M-phase has not been affected by irradiation, thus $r_{S\to G_2M} = \widetilde{r}_{S\to G_2M}$. Using equations (4.2.24), (4.2.25), and (4.2.26), we can present the *DAE* system that is then used for our numerical simulations, as follows:

$$\frac{dP_{G_1}(t)}{dt} = 2r^*_{G_2M\to G_1}(t)P_{G_2M}(t) - r^*_{G_1\to S}(t)P_{G_1}(t) - \lambda(t)P_{G_1}(t), \tag{4.2.28a}$$

$$\frac{dP_S(t)}{dt} = r^*_{G_1\to S}(t)P_{G_1}(t) - \widetilde{r}_{S\to G_2M}P_S(t) - \lambda(t)P_S(t), \tag{4.2.28b}$$

$$\frac{dP_{G_2M}(t)}{dt} = \widetilde{r}_{S\to G_2M}P_S(t) - [r^*_{G_2M\to G_1}(t) + r^*_D(t)]P_{G_2M}(t) - \lambda(t)P_{G_2M}(t), \tag{4.2.28c}$$

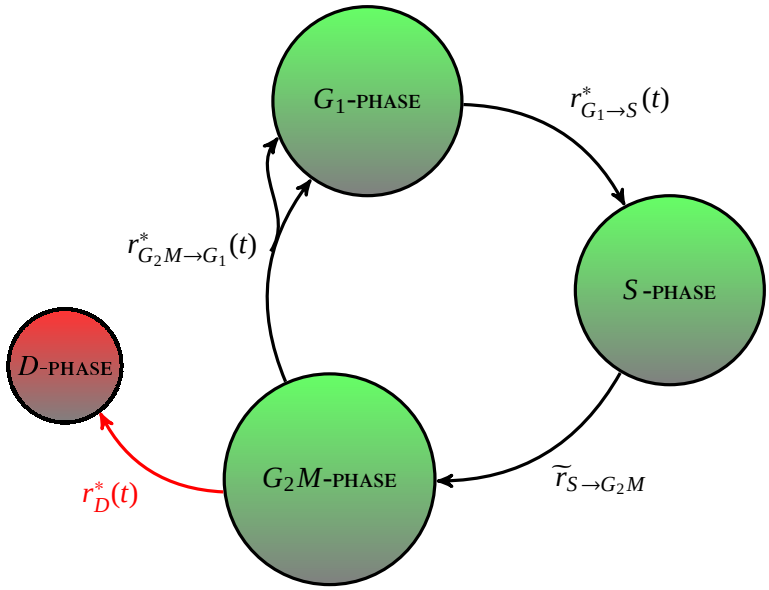

Figure 4.2: Diagram of the cell-cycle control of *in vitro* tumour cells perturbed by radiation, showing the proportions in each phase. This diagram is compatible with flow cytometry data. We note that flow cytometry profiles do not track cell loss/death proportion.

with the following constraint equation:

$$1 = P_{G_1}(t) + P_S(t) + P_{G_2M}(t), \quad t \geq 0. \tag{4.2.29}$$

From equation (4.2.25), we can see that the cancer cell population after irradiation grows at rate $\lambda(t) = [r^*_{G_2M\to G_1}(t) - r^*_D(t)]P_{G_2M}(t)$, with the initial population distributed among phases as follows:

$$P_{G_1}(t=0) = P^0_{G_1}, \tag{4.2.30a}$$
$$P_S(t=0) = P^0_S, \tag{4.2.30b}$$
$$P_{G_2M}(t=0) = P^0_{G_2M}. \tag{4.2.30c}$$

The model investigates the *DAE* system rather than an *ODE* one because constraint equation (4.2.29) must be satisfied at every internal calculation point. In our calculation, we use system (4.2.28) with side conditions (4.2.29) and (4.2.30) and the methods shown in Section 4.3 to estimate transition rates $r^*_{G_1\to S}(t)$, $r^*_{G_2M\to G_1}(t)$, and $r^*_D(t)$. Since cell death cannot be estimated successfully after radiotherapy via experimental means, we use a mathematical model describing the effects of the combined treatment of radiotherapy and paclitaxel to determine cell loss. In subsequent sections, we replace the estimation of transition rate $r^*_D(t)$ with cell death rate $\lambda_R(t) = -r^*_D(t)P_{G_2M}(t)$, as explained in Section 4.3.

It should be noted here that we simplified system (4.2.16) in order to be able to use the experimental data. We aim with our model, which contains a removal class, to recreate results from paper Basse *et al.* (2010); moreover, we aim to estimate the proportion of cells that keeps proliferating after irradiation.

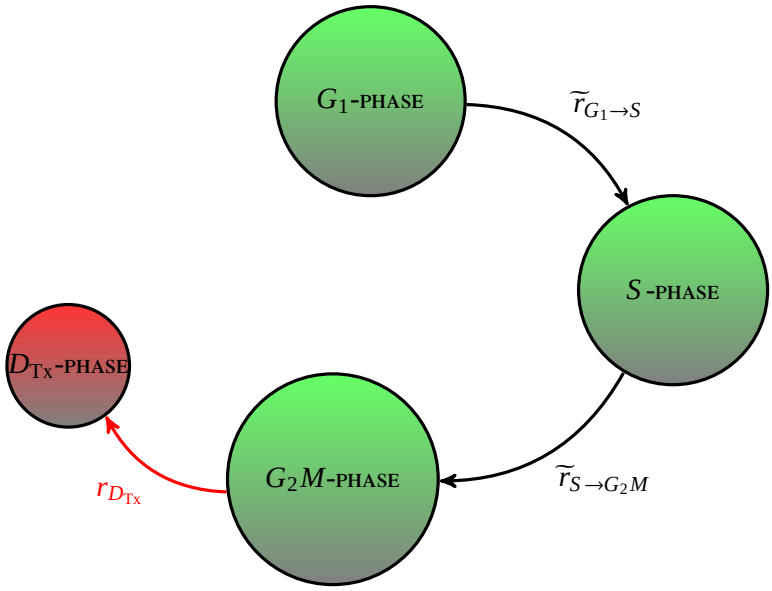

Figure 4.3: Diagram of the cell-cycle control of *in vitro* tumour cells perturbed by paclitaxel.

4.3 Non-cycling population models. Estimating arrested transition rate $r^*_{G_1\to S}(t)$ and cell loss due to paclitaxel and radiation treatments

The following models are introduced for the purposes of applying the experimental data of the cancer cell population treated by paclitaxel and a combination of the paclitaxel and irradiation that are schematically depicted in Figures 4.3 and 4.4, respectively. We observe that the experimental data of the cancer cell population's response to irradiation alone is not sufficient to ensure the uniqueness of problem (4.2.28) - (4.2.30) parameters, namely transition rates $r^*_{G_1\to S}(t)$, $r^*_{G_2M\to G_1}(t)$, and death rate $\lambda_R(t)$. Therefore, the experimental data of the cancer cell population perturbed by paclitaxel and paclitaxel with radiation is used. Since, in subsequent sections, we compare the proportion in the G_1-phase for different treatments, we will use superscripts Tx for paclitaxel, TxR for the combined treatment of paclitaxel and radiotherapy, and R for radiotherapy, e.g., $\Pi^{\mathrm{TxR}}_{G_1}(t)$ depicts the proliferating proportion in G_1-phase after a combined radiation and paclitaxel treatment at time t. The relationship between notions Π and P for each phase are shown in equation (4.2.21).

4.3.1 The paclitaxel model

The response of the cancer cell population to paclitaxel was analysed in Chapter 3. Here, we introduce a *DAE* system describing the dynamics of proportions of the cancer cell population after treatment with paclitaxel. The aim of the paclitaxel treatment response mathematical model is to estimate the death rate of the cancer population after exposure to paclitaxel. We start by introducing a conservation system that includes a death phase D_{Tx}. Terms $\breve{P}_w$ with $w \in \{G_1, S, G_2M, D_{\mathrm{Tx}}\}$ represent the proportion distribution of the population among the phases and can be expressed as $\breve{P}_w(t) = \breve{N}_w(t)/\breve{N}_T(t)$, where $\breve{N}_w(t)$ is a number of cells in w phase and $\breve{N}_T(t) = \sum_w \breve{N}_w(t)$. Cell loss proportion of population $\breve{P}_{D_{\mathrm{Tx}}}$ is considered to be a part of the total population, thus the growth (or death in the case of non-cycling population) rate $\lambda(t)$ is equal to zero at all times. Transition rates $\widetilde{r}_{G_1\to S}$ and $\widetilde{r}_{S\to G_2M}$ notify

the transition probability rate between the respective phases of the population that is unperturbed by any treatment. Paclitaxel interferes with the normal breakdown of microtubules during cell division, cells in mitosis are arrested and prevented from dividing; therefore, this effect is incorporated into our model by setting the transition rate from the G_2M-phase to the G_1-phase to zero. So the resulting conservation system, schematically depicted in Figure 4.3, is as follows:

$$\frac{d\breve{P}_{G_1}(t)}{dt} = -\widetilde{r}_{G_1\to S}\breve{P}_{G_1}(t), \tag{4.3.1a}$$

$$\frac{d\breve{P}_{S}(t)}{dt} = \widetilde{r}_{G_1\to S}\breve{P}_{G_1}(t) - \widetilde{r}_{S\to G_2M}\breve{P}_{S}(t), \tag{4.3.1b}$$

$$\frac{d\breve{P}_{G_2M}(t)}{dt} = \widetilde{r}_{S\to G_2M}\breve{P}_{S}(t) - r_{D_{\mathrm{Tx}}}(t)\breve{P}_{G_2M}(t), \tag{4.3.1c}$$

$$\frac{d\breve{P}_{D_{\mathrm{Tx}}}(t)}{dt} = r_{D_{\mathrm{Tx}}}(t)\breve{P}_{G_2M}(t), \tag{4.3.1d}$$

with a constraint equation:

$$1 = \breve{P}_{G_1}(t) + \breve{P}_{S}(t) + \breve{P}_{G_2M}(t) + \breve{P}_{D_{\mathrm{Tx}}}(t), \quad t \geq 0. \tag{4.3.2}$$

The initial conditions are:

$$\breve{P}_{G_1}(t=0) = P^0_{G_1}, \tag{4.3.3a}$$

$$\breve{P}_{S}(t=0) = P^0_{S}, \tag{4.3.3b}$$

$$\breve{P}_{G_2M}(t=0) = P^0_{G_2M}, \tag{4.3.3c}$$

$$\breve{P}_{D_{\mathrm{Tx}}}(t=0) = 0. \tag{4.3.3d}$$

Since, in the case of a conservation system approach, we require experimental estimates of cell loss proportion, but experimental estimates of cell loss after exposure to paclitaxel are not reliable, so we have to use a *DAE* system with a removal class similar to problem (4.2.28) - (4.2.30). From equations (4.2.5) and (4.2.9), we can express proportions in G_1, S, and G_2M phases (namely, $P_p(t)$ with $p \in \{G_1, S, G_2M\}$) for the case in which the cell loss phase is not included in the sum of the total cell number as $P_p(t) = N_p(t)/N_{tot}(t)$. Notions of the number of cells in phases $N_p(t)$ and $\breve{N}_w(t)$ are interchangeable with those of phases - G_1, S, and G_2M. We can then express proportion $\breve{P}_p(t)$ in p phase with $p \in \{G_1, S, G_2M\}$, in the case of a conservation system approach, or with the proportion $P_p(t)$ in the case of a system with a removal class, as follows:

$$\breve{P}_p(t) = P_p(t)[1 - \breve{P}_{D_{\mathrm{Tx}}}(t)], \quad \text{where} \quad p \in \{G_1, S, G_2M\}. \tag{4.3.4}$$

Equation (4.3.4) is substituted, using the appropriate phase index, into problem (4.3.1) - (4.3.3) and the following result is derived:

$$\frac{dP_{G_1}(t)}{dt} = -\widetilde{r}_{G_1\to S}P_{G_1}(t) - \lambda_{\mathrm{Tx}}(t)P_{G_1}(t), \tag{4.3.5a}$$

$$\frac{dP_S(t)}{dt} = \widetilde{r}_{G_1\to S}P_{G_1}(t) - \widetilde{r}_{S\to G_2M}P_S(t) - \lambda_{\mathrm{Tx}}(t)P_S(t), \tag{4.3.5b}$$

$$\frac{dP_{G_2M}(t)}{dt} = \widetilde{r}_{S\to G_2M}P_S(t) - r_{D_{\mathrm{Tx}}}(t)P_{G_2M}(t) - \lambda_{\mathrm{Tx}}(t)P_{G_2M}(t), \tag{4.3.5c}$$

$$1 = P_{G_1}(t) + P_S(t) + P_{G_2M}(t), \quad t \geq 0. \tag{4.3.5d}$$

Here, $\lambda_{\mathrm{Tx}}(t) = -r_{D_{\mathrm{Tx}}}(t)P_{G_2M}(t)$, with the following initial conditions:

$$P_{G_1}(0) = P^0_{G_1}, \tag{4.3.6a}$$

$$P_S(0) = P^0_S, \tag{4.3.6b}$$

$$P_{G_2M}(0) = P^0_{G_2M}. \tag{4.3.6c}$$

The initial conditions are provided by the proportion distribution of the unperturbed population obtained from flow cytometry profiles. We note that solution of problem (4.3.5)-(4.3.6) will be marked as $P^{\mathrm{Tx}}_p(t)$ to notify paclitaxel treatment. We can see from system (4.3.5) that the proportion of the G_1-phase after paclitaxel exposure can be written as follows:

$$P^{\mathrm{Tx}}_{G_1}(t) = P_{G_1}(0)e^{-\int_0^t [\widetilde{r}_{G_1\to S} + \lambda_{\mathrm{Tx}}(s)]ds}. \tag{4.3.7}$$

We impose that the death rate, $\lambda_{\mathrm{Tx}}(t)$, is a piecewise constant function. In our numerical simulations, we utilise the paclitaxel treatment response data to estimate the cell death from this treatment. The proportion of the initial cancer cell number that undergoes apoptosis after paclitaxel treatment can be evaluated using equations (4.3.1d), (4.3.4) and taking into account that $\lambda_{\mathrm{Tx}}(t) = -r_{D_{\mathrm{Tx}}}(t)P^{\mathrm{Tx}}_{G_2M}(t)$. Thus, we rewrite equation (4.3.1d) as follows:

$$\frac{d\check{P}_{D_{Tx}}(t)}{dt} = r_{D_{\mathrm{Tx}}}(t)P_{G_2M}(t)[1 - \check{P}_{D_{Tx}}(t)], \tag{4.3.8}$$

$$= -\lambda_{\mathrm{Tx}}(t)[1 - \check{P}_{D_{Tx}}(t)]. \tag{4.3.9}$$

By integrating the ODE above with the initial condition (4.3.3d), we get the following expression:

$$\check{P}_{D_{Tx}}(t) = 1 - e^{\int_0^t \lambda_{\mathrm{Tx}}(s)ds}, \tag{4.3.10}$$

where $\lambda_{\mathrm{Tx}}(t) = -r_{D_{\mathrm{Tx}}}(t)P^{\mathrm{Tx}}_{G_2M}(t)$. We observe that, since the cell population after paclitaxel treatment does not undergo arrest and is considered to be proliferating, notions $P^{\mathrm{Tx}}_{G_1}(t)$ and $\Pi^{\mathrm{Tx}}_{G_1}(t)$ are interchangeable, i.e., all cells in G_1-phase are proliferating.

4.3.2 Radiation with the paclitaxel model

Cancer cell population growth perturbed by a combined paclitaxel and radiation treatment is depicted in Figure 4.4. A combined treatment model has been constructed for the purposes of estimating transition rate $r^*_{G_1\to S}(t)$ and death rate after combined treatment. The effects of radiotherapy alone on cells in G_1-phase, i.e., $r^*_{G_1\to S}(t)$ can be derived from the combined treatment. We use problem

(4.2.16)-(4.2.18) as a base for the following combined treatment model. Since paclitaxel interferes with the mitosis stage of the cell cycle, we incorporate this into our model by setting $r_{G_2M\to G_1} = 0$. We assume that for the combined treatments of paclitaxel and radiation all cells in the population have stopped cell division, namely $r_{G_2M\to G_1} = 0$. Observe that the population growth rate $\lambda(t)$ have changed. In combined treatment model, we refer to growth rate as λ_{TxR}. Then we can rewrite problem (4.2.16)-(4.2.18) as follows:

$$\frac{d\Pi_{G_1}(t)}{dt} = -[r_{G_1\to S}(t) + r_{A_1}(t) + r_{Sen_1}(t)]\Pi_{G_1}(t) + r_{A_2}(t)\Pi_{A_1}(t) - \lambda_{\text{TxR}}(t)\Pi_{G_1}(t), \tag{4.3.11a}$$

$$\frac{d\Pi_S(t)}{dt} = r_{G_1\to S}(t)\Pi_{G_1}(t) - r_{S\to G_2M}\Pi_S(t) - \lambda_{\text{TxR}}(t)\Pi_S(t), \tag{4.3.11b}$$

$$\frac{d\Pi_{G_2M}(t)}{dt} = r_{S\to G_2M}\Pi_S(t) - [r_{A_3}(t) + r_{Sen_2}(t) + r_{D_1}(t) + r_D(t)]\Pi_{G_2M}(t) + r_{A_4}(t)\Pi_{A_2}(t) - \lambda_{\text{TxR}}(t)\Pi_{G_2M}(t), \tag{4.3.11c}$$

$$\frac{d\Pi_{A_1}(t)}{dt} = r_{A_1}(t)\Pi_{G_1}(t) - r_{A_2}(t)\Pi_{A_1}(t) - \lambda_{\text{TxR}}(t)\Pi_{A_1}(t), \tag{4.3.11d}$$

$$\frac{d\Pi_{Sen_1}(t)}{dt} = r_{Sen_1}(t)\Pi_{G_1}(t) - \lambda_{\text{TxR}}(t)\Pi_{Sen_1}(t), \tag{4.3.11e}$$

$$\frac{d\Pi_{A_2}(t)}{dt} = r_{A_3}(t)\Pi_{G_2M}(t) - r_{A_4}(t)\Pi_{A_2}(t) - \lambda_{\text{TxR}}(t)\Pi_{A_2}(t), \tag{4.3.11f}$$

$$\frac{d\Pi_{Sen_2}(t)}{dt} = r_{Sen_2}(t)\Pi_{G_2M}(t) - \lambda_{\text{TxR}}(t)\Pi_{Sen_2}(t). \tag{4.3.11g}$$

Furthermore, we express the death probability rate in two parts $r_{D_1}(t)$ and $r_D(t)$ to show the potential effects of each treatment separately. We note that system (4.3.11) is a conservation system, so adding the seven equations yields $\lambda_{\text{TxR}}(t) = -[r_{D_1}(t) + r_D(t)]\Pi_{G_2M}(t)$. The proportion dynamics of cancer cell population depicted in ODE system (4.3.11) has the following constraint equation :

$$\sum_m \Pi_m(t) = 1, \quad \forall t \geq 0, \tag{4.3.12}$$

where $m \in \{G_1, S, G_2M, A_1, A_2, \text{Sen}_1, \text{Sen}_2\}$. The respective initial conditions are as follows:

$$\Pi_{G_1}(t=0) = \Pi^0_{G_1}, \tag{4.3.13a}$$

$$\Pi_S(t=0) = \Pi^0_S, \tag{4.3.13b}$$

$$\Pi_{G_2M}(t=0) = \Pi^0_{G_2M}, \tag{4.3.13c}$$

$$\Pi_{A_1}(t=0) = \Pi^0_{A_1}, \tag{4.3.13d}$$

$$\Pi_{Sen_1}(t=0) = \Pi^0_{\text{Sen}_1}, \tag{4.3.13e}$$

$$\Pi_{A_2}(t=0) = \Pi^0_{A_2}, \tag{4.3.13f}$$

$$\Pi_{Sen_2}(t) = \Pi^0_{\text{Sen}_2}. \tag{4.3.13g}$$

Solution of problem (4.3.11)-(4.3.13) is denoted as $\Pi^{\text{TxR}}_m(t)$. We now examine the growth rates N'_{tot}/N_{tot}. The death rate of the population treated with a combination of paclitaxel and irradiation, namely $\lambda_{\text{TxR}}(t)$, is assumed to be a piecewise constant function. Now, if we consider model for radiotherapy without the paclitaxel, the population dynamic equations are as system (4.2.28) but the death rate is now $\lambda_R(t)$. Death rate $\lambda_R(t)$ is incorporated in the growth rate N'_{tot}/N_{tot}, denoted as $\lambda(t)$ in

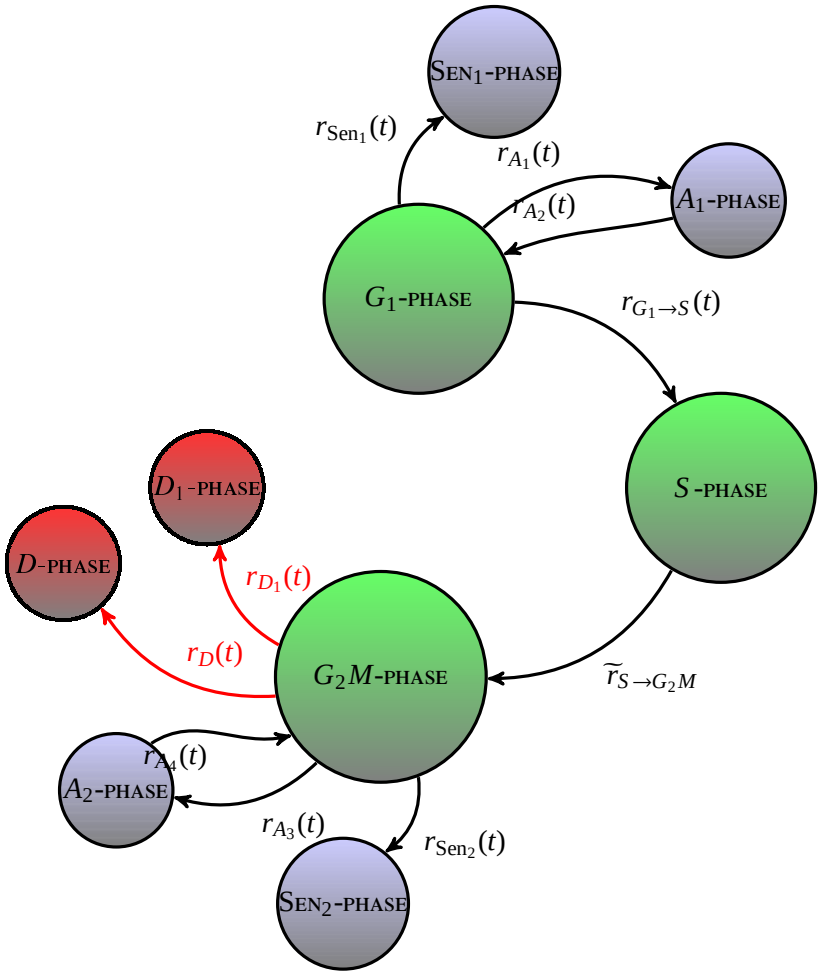

Figure 4.4: Diagram of the cell-cycle control of *in vitro* tumour cells perturbed by paclitaxel and radiation, with proliferating and non-proliferating cancer cell population subdivision.

system (4.2.28). Again, we impose that the death rate of the population affected by an irradiation dose alone is a piecewise constant function, namely $\lambda_R(t)$. We have assumed that cell death rate $\lambda_{\mathrm{Tx}}(t)$ from the paclitaxel treatment is unaffected by irradiation and has the same value as the one for the paclitaxel treatment alone. Therefore, the growth (death) rate $\lambda_{\mathrm{TxR}}(t)$ of the population treated by paclitaxel and irradiation can be presumed to be:

$$\lambda_{\mathrm{TxR}}(t) = \lambda_{\mathrm{Tx}}(t) + \lambda_R(t), \tag{4.3.14}$$

where $\lambda_{\mathrm{Tx}}(t) = -r_{D_1}(t)\Pi_{G_2M}(t)$ and $\lambda_R(t) = -r_D(t)\Pi_{G_2M}(t)$. Thus, the following statement is true:

$$|\lambda_{\mathrm{TxR}}(t)| \geq |\lambda_{\mathrm{Tx}}(t)| \quad for \quad t \geq 0. \tag{4.3.15}$$

Next, we proceed with the derivation of the relationship between transition rates of unperturbed and perturbed by treatment population. Term 'unperturbed' refers to a cell population that has not been affected by any treatment and 'perturbed' to a population that has been exposed to cancer treatment.

For the simplicity of further analysis, we introduce a new variable, $r_{Q_1}(t)$, a transition rate indicating the probability of a proliferating cell in the G_1-phase to enter a non-proliferating state. We replace terms $-[r_{A_1}(t) + r_{Sen_1}(t)]\Pi_{G_1}(t) + r_{A_2}(t)\Pi_{A_1}(t)$ in equation (4.3.11a) with a new notion $r_{Q_1}(t)\Pi_{G_1}(t)$ as follows:

$$\frac{d\Pi_{G_1}(t)}{dt} = -[r_{G_1\to S}(t) + r_{Q_1}(t)]\Pi_{G_1}(t) - \lambda_{\mathrm{TxR}}(t)\Pi_{G_1}(t). \tag{4.3.16}$$

We assume that $r_{Q_1}(t)$ is non-negative, and define it as follows:

$$r_{Q_1}(t) = r_{A_1}(t) + r_{Sen_1}(t) - r_{A_2}(t)\frac{\Pi_{A_1}(t)}{\Pi_{G_1}(t)}. \tag{4.3.17}$$

We then solve equation (4.3.16) using the initial condition (4.3.13a) and show that the proliferating proportion of the G_1-phase after the combined radiation and paclitaxel treatment can be expressed as follows:

$$\Pi^{\mathrm{TxR}}_{G_1}(t) = \Pi^0_{G_1} e^{-\int_0^t [r_{G_1\to S}(s) + r_{Q_1}(s) + \lambda_{\mathrm{TxR}}(s)]ds}. \tag{4.3.18}$$

We have assumed that the proportion of the proliferating cells in the G_1-phase after the combined treatment (namely, $\Pi^{\mathrm{TxR}}_{G_1}(t)$) is equal to the proliferating cell proportion in the G_1-phase after paclitaxel treatment $\Pi^{\mathrm{Tx}}_{G_1}(t)$ that has been scaled down by cell loss from radiotherapy with death rate $\lambda_R(t)$, and can be expressed as:

$$\Pi^{\mathrm{Tx}}_{G_1}(t)e^{\lambda_R(t)t} = \Pi^{\mathrm{TxR}}_{G_1}(t). \tag{4.3.19}$$

Thus, from equations (4.3.7), (4.3.18), and (4.3.19), we can see that the following is true:

$$\widetilde{r}_{G_1\to S} \geq r_{G_1\to S}(t) \quad for \quad t \geq 0. \tag{4.3.20}$$

A similar inequality can be derived for the transition rate: $\widetilde{r}_{G_2M\to G_1}$. A different therapeutic agent such as carboplatin, which interferes with DNA replication without affecting mitosis, can be used to derive the following inequality:

$$\widetilde{r}_{G_2M\to G_1} \geq r_{G_2M\to G_1}(t) \quad for \quad t \geq 0. \tag{4.3.21}$$

We proceed to derive a DAE system that is used in the numerical simulations for transition rate $r^*_{G_1\to S}(t)$ and death rate λ_{TxR} estimation. Since flow cytometry profiles do not distinguish between proliferating and non-proliferating cells within a particular phase, we rearrange problem (4.3.11) - (4.3.13) by using techniques from Section 4.2.3, to the following problem and use it for the numerical simulations discussed in Section 4.4.4:

$$\frac{dP_{G_1}(t)}{dt} = -r^*_{G_1\to S}(t)P_{G_1}(t) - \lambda_{\mathrm{TxR}}(t)P_{G_1}(t), \tag{4.3.22a}$$

$$\frac{dP_S(t)}{dt} = r^*_{G_1\to S}(t)P_{G_1}(t) - \widetilde{r}_{S\to G_2M}P_S(t) - \lambda_{\mathrm{TxR}}(t)P_S(t), \tag{4.3.22b}$$

$$\frac{dP_{G_2M}(t)}{dt} = \widetilde{r}_{S\to G_2M}P_S(t) - [r_{D_{\mathrm{Tx}}}(t) + r^*_D(t)]P_{G_2M}(t) - \lambda_{\mathrm{TxR}}(t)P_{G_2M}(t), \tag{4.3.22c}$$

$$1 = P_{G_1}(t) + P_S(t) + P_{G_2M}(t), \quad t \geq 0, \tag{4.3.22d}$$

where $\lambda_{\mathrm{TxR}}(t) = -[r_{D_{\mathrm{Tx}}}(t) + r_D^*(t)]P_{G_2M}(t)$ and with the initial conditions:

$$P_{G_1}(0) = P_{G_1}^0, \tag{4.3.23a}$$
$$P_S(0) = P_S^0, \tag{4.3.23b}$$
$$P_{G_2M}(0) = P_{G_2M}^0. \tag{4.3.23c}$$

Similar identities to equations (4.2.27) can be derived from systems (4.3.11) and (4.3.22):

$$r_{D_{\mathrm{Tx}}}(t)P_{G_2M}(t) = r_{D_1}(t)\Pi_{G_2M}(t), \tag{4.3.24a}$$
$$r_D^*(t)P_{G_2M}(t) = r_D(t)\Pi_{G_2M}(t). \tag{4.3.24b}$$

The proportion of the cell population that underwent apoptosis after paclitaxel and radiation treatment (similarly derivable as equation (4.3.10)) can be calculated by the following expression:

$$P_{D_{\mathrm{TxR}}}(t) = 1 - e^{\int_0^t \lambda_{\mathrm{TxR}}(s)ds}, \tag{4.3.25}$$

where the death rate $\lambda_{\mathrm{TxR}}(t) = -[r_{D_{\mathrm{Tx}}}(t) + r_D^*(t)]P_{G_2M}(t)$.

4.4 Experimental data and calculations

We have five different types of experimental data available. These terms will be explained in the following subsections:

1. for the flow cytometry data of unperturbed cell lines, see subsection 4.4.2;
2. for the plateau logarithmic reduction values for each cell line, see subsection 4.4.2;
3. for the flow cytometry data of cell lines perturbed by paclitaxel, see subsection 4.4.3;
4. for the flow cytometry data of cell lines perturbed by paclitaxel and then irradiated, see subsection 4.4.4;
5. for the flow cytometry data of cell lines perturbed by radiation, see subsection 4.4.5.

In order to track the proliferating proportion of the cell population after treatment with radiotherapy, we have to monitor the proportion of the cell population that enters the G_1-phase (hence, having undergone mitosis). We cannot extract sufficient information from the flow cytometry profiles of the irradiated population alone; therefore, we need extra information from the rest of the data provided. The flow cytometry profiles are analysed using the Cylchred software program provided by Cytonet, UK, and we obtain estimates of the population proportions subdivided between phases G_1, S, and G_2M at time points - $0, 18, 48, 72$, and 96 hours for each cell line for every treatment.

4.4.1 Experimental data extracted from flow cytometry profiles

The flow cytometry profiles were analysed using Cylchred software provided by Cytonet, UK. We have extracted estimates of population proportions in each phase from the flow cytometry profiles (an example of a flow cytometry profile is shown in Figure 1.3) for all provided treatments and cell lines. An example of such data collected for cell line $NZM3$ can be seen in Table 4.2 that shows variations of percentages in the G_1, S and G_2M phases for every treatment at experimental time points from 0 up

treatment	hours	$\%G_1$	$\%S$	$\%G_2M$
Paclitaxel 200 nM	0	52.25	29.69	18.06
	18	4.9546	28.2548	66.7906
	48	4.5587	21.8494	73.5919
	72	5.3123	36.7733	57.9144
	96	5.1227	42.0292	52.8481
Radiation 9 Gy and paclitaxel 200 nM	0	52.25	29.69	18.06
	18	16.8273	27.6499	55.5228
	48	7.235	21.497	71.268
	72	5.9558	37.4681	56.5761
	96	7.1407	36.3593	56.5
Radiation 9 Gy	0	52.25	29.69	18.06
	18	19.05	31.34	49.61
	48	30.79	38.91	30.3
	72	45.09	32.97	21.94
	96	45.42	26.93	27.65

Table 4.2: Data extracted from the flow cytometry profiles of cell line $NZM3$. In paper Basse *et al.* (2010), the transition rate from the G_1-phase to the S-phase for the unperturbed cell lines is not estimated from mathematical model but rather provided by experimentalists ($r_{G_1 \to S} = 0.051$). The first column shows the treatment used. The second column represents the hours at which flow cytometry profiles were generated for each treatment. Last three columns show the percentages in G_1, S, and G_2M phases for every experimental hour for every treatment.

to 96 hours after treatment applications. Percentages in each phase of the $NZM3$ cell line unperturbed by any treatment (i.e., in BEG state) are shown in Table 4.2 at hour zero for every treatment.

4.4.2 Unperturbed data and plateau log reduction value

The flow cytometry data of unperturbed cell lines gives us information about the proportion of the cell population in each phase (G_1, S, and the combined G_2M). Unperturbed data refers to a cell population that has not been affected by any treatment. In Daukste *et al.* (2012), we have shown that having estimates of the proportions in each phase at BEG state and a plateau log reduction value allow us to calculate unique constant transition rate values between phases ($\widetilde{r}_{G_1 \to S}$, $\widetilde{r}_{S \to G_2M}$ and $\widetilde{r}_{G_2M \to G_1}$) and the growth rate of the population ($\widetilde{\lambda}$). We can then express population doubling time T_d, from Chapter 2, $T_d = ln(2)/\widetilde{\lambda}$. For more information on the plateau log reduction value method, see Chapter 3. Observe we use a tilde to denote the unperturbed transition values and the growth rate. **Calculations:** A system of four nonlinear algebraic equations is solved using damped Newton's method (as showed in Chapter 3).
Estimated variables thus far are transition rates $\widetilde{r}_{G_1 \to S}$, $\widetilde{r}_{S \to G_2M}$, $\widetilde{r}_{G_2M \to G_1}$, and the growth rate of the unperturbed population $\widetilde{\lambda}$.

4.4.3 Paclitaxel data

Paclitaxel is a mitotic inhibitor chemotherapy drug. The changes in flow cytometry data in the proportion of the G_1-phase are used to determine the cell loss due to the treatment (noted as our variable $\lambda_{\text{Tx}}(t)$, introduced in Section 4.3). Since we have estimated the $\widetilde{r}_{G_1\to S}$ value as shown in Section 4.4.2, we use the equation (4.3.10) showed in Section 4.3 to determine the proportion of cells lost after exposure to paclitaxel.
Calculations: Exponential equation (4.3.7) is solved to acquire the estimate of cell loss shown in Section 4.3.
Estimated variables from Section 4.4.2 are the transition rates $\widetilde{r}_{G_1\to S}$, $\widetilde{r}_{S\to G_2M}$, $\widetilde{r}_{G_2M\to G_1}$, and the growth rate of the unperturbed population $\widetilde{\lambda}$. Paclitaxel data provides an estimate of the death rate $\lambda_{\text{Tx}}(t)$.

4.4.4 Radiation with paclitaxel data

A response of cell lines to radiation results in senescence, arrest, and apoptosis in both the G_1 and G_2M phases. Furthermore, a cell line subsequently exposed to paclitaxel stops dividing, i.e., $r_{G_2M\to G_1}(t) = 0$ for $t \geq 0$.
Calculations: Built-in MatLab functions *ode15s* and *fmincon* are used to solve the DAE problem (4.3.22) - (4.3.23). Optimization function *fmincon* determines transition rate $r^*_{G_1\to S}(t)$. There are four inputs for the optimization function. The first is derived from the proportions in each phase at the two consecutive time points. Second is transition rate $\widetilde{r}_{S\to G_2M}$, where we assume that the transition rate from the S-phase to G_2M-phase is unaffected by paclitaxel or radiation treatment and has been determined from the unperturbed data and the plateau log reduction value, as discussed in Section 4.4.2. Third is that the cell death from the paclitaxel treatment $\lambda_{\text{Tx}}(t)$ is unaffected by irradiation and has the same value as for the paclitaxel treatment alone. We assume that paclitaxel treatment has not affected the transition rate from the G_1-phase to S-phase, but irradiation has. We impose that $r^*_{G_1\to S}(t)$, if reduced after the irradiation dose, is expected to recover piecewise linearly, as shown in Figure 4.5(a). The solution converges quickly to the optimal value.
Known variables so far are the transition rates $\widetilde{r}_{G_1\to S}$, $\widetilde{r}_{S\to G_2M}$, $\widetilde{r}_{G_2M\to G_1}$, and cell death from the paclitaxel treatment $\lambda_{\text{Tx}}(t)$. Thus, we can estimate the transition rate $r^*_{G_1\to S}(t)$ and the cell death from irradiation $\lambda_R(t)$ (this variable has been introduced in Section 4.3) from the provided data.

4.4.5 Radiation data

A response of cell lines to radiation results in respective senescence, arrest and apoptosis in the G_1 and G_2M phases.
Calculations: Built-in MatLab functions *ode15s* and *fmincon* are used to solve the DAE problem (4.2.28) - (4.2.30). Optimization routine *fmincon* determines transition rate $r^*_{G_2M\to G_1}(t)$. There are four inputs for the optimization function. The first is derived from the proportions in each phase at the two consecutive time points. Second is transition rate $r^*_{G_1\to S}(t)$, which has been determined from the data of the cell population treated through a combination of paclitaxel and irradiation, as discussed in Section 4.4.4. Third is the cell death $\lambda_R(t)$ from irradiation, as determined in Section 4.4.4. Fourth is transition rate $\widetilde{r}_{S\to G_2M}$, where we assume that the transition rate from the S-phase to the G_2M-phase is unaffected by the paclitaxel or radiation treatment and has been determined from the unperturbed data and the plateau log reduction value, as discussed in Section 4.4.2. We also assume that the transition rate from the G_2M-phase to the G_1-phase, if reduced in value after the irradiation dose, is expected to recover piecewise linearly, as shown in Figure 4.5(b). The solution converges quickly to the optimal

value.
Known variables are transition rates $\widetilde{r}_{G_1\to S}, \widetilde{r}_{S\to G_2M}, \widetilde{r}_{G_2M\to G_1}, r^*_{G_1\to S}(t)$, and $\lambda_R(t)$. From the provided radiotherapy data, we estimate the transition rate: $r^*_{G_2M\to G_1}(t)$.

4.5 Estimating the initial proliferating fraction

The aim of this model is to estimate the initial proliferating fraction of the cancer cell population after a one-time irradiation dose of 9 Gy of five cell lines.

It is known that a small fraction of the initial population (0.1-10%, depending on the cell line) survives radiation (called a surviving fraction in biological terminology), and that this is the population that grows into a surviving colony assay. Just where these surviving cells come from is unclear, but it is thought that they will sustain DNA damage and move ultimately to the G_2-phase until DNA repair is complete, whereupon they will divide and re-enter the cell cycle. This re-entry will be asynchronous, so the surviving population will be distributed through all cycle phases.

4.5.1 Initial proliferating fraction interval

Our model has limitations in estimating the initial proliferating fraction. We can only calculate an interval where such fraction is located. We introduce a variable Φ_{init} and refer to it throughout this chapter as the initial proliferating fraction. We define initial proliferating fraction Φ_{init} as a sum of proliferating proportions in G_1, S and G_2M phases at time 0 as follows:

$$\Phi_{init} = \Pi_{G_1}(0) + \Pi_S(0) + \Pi_{G_2M}(0). \tag{4.5.1}$$

When calculating the initial proliferating fraction, we assume that cells in the S-phase at hour zero are all proliferating; therefore, the initial proportion of the cell population in S-phase (as mentioned before, notions $\Pi_S(0)$ and P^0_S are interchangeable) is added to the proliferating fraction. We assume that the proportion of the cell population after combined radiation and paclitaxel treatment in the G_1-phase that has moved from the G_1-phase to the S-phase within the first 18 hours is the proliferating fraction of the population in the G_1-phase. Since there is radiation induced apoptosis present, we calculate the proliferating fraction in the G_1-phase as follows:

$$\Pi_{G_1}(0) = [P^{\mathrm{TxR}}_{G1}(0) - P^{\mathrm{TxR}}_{G_1}(18)]e^{\lambda_R 18}. \tag{4.5.2}$$

The initial proliferating fraction in the G_2M-phase (namely, $\Pi_{G_2M}(0)$) is not detectable without different chemotherapeutic agents that interfere with DNA replication without affecting mitosis. Thus, from equations (4.2.27b) and (4.3.21), we can express only the following inequality:

$$\Pi_{G_2M}(t) = \frac{r^*_{G_2M\to G_1}(t)}{r_{G_2M\to G_1}(t)} P_{G_2M}(t) \geq \frac{r^*_{G_2M\to G_1}(t)}{\widetilde{r}_{G_2M\to G_1}} P_{G_2M}(t), \quad \forall t \geq 0. \tag{4.5.3}$$

Therefore, we can estimate only an interval of the proliferating fraction in the G_2M-phase, denoted by F_{G_2M}, as follows:

$$F_{G_2M} \in \left[\frac{r^*_{G_2M\to G_1}(0)}{\widetilde{r}_{G_2M\to G_1}} P_{G_2M}(0), \quad P_{G_2M}(0)\right], \tag{4.5.4}$$

where the initial arrest of the division rate $r^*_{G_2M\to G_1}(0)$ and the unperturbed value $\widetilde{r}_{G_2M\to G_1}$ have been shown in Figures 4.5-4.9. We observe that for cell lines $NZM3$, $NZM4$ and $NZM13$ cell division has

briefly stopped $r^*_{G_2M\to G_1}(0) = 0$. Using our model, we estimate the initial proliferating fraction of the population treated with radiotherapy as follows:

$$\Phi_{init} \in [\Pi_{G_1}(0) + \Pi_S(0) + F_{G_2M}]. \tag{4.5.5}$$

Intervals of initial proliferating fraction estimates of five cancer cell lines are shown in Table 4.3 in column two.

4.5.2 Proliferating fraction interval 96 hours post irradiation

In this section, we estimate the proliferating fraction, named Φ_{end}, of the cancer cell population at the final experimental observation time ($t_{end} = 96$ hours). We define proliferating fraction Φ_{end} as a sum of proliferating proportions in the G_1, S, and G_2M phases at time t_{end} as follows:

$$\Phi_{end} = \Pi_{G_1}(t_{end}) + \Pi_S(t_{end}) + \Pi_{G_2M}(t_{end}). \tag{4.5.6}$$

As discussed in Section 4.5.1, our model is limited to estimating intervals of proliferating proportions for each cell line. The lower bound, denoted by LB, of the proliferating population proportion after 96 hours post the irradiation enables us to say that at least LB per cent of the population is proliferating. It follows that our mathematical model supports that the effect of the irradiation dose is the arrest of the transition rates, i.e., a decrease in their numerical values.

Taking into account equations (4.2.27), we can rewrite (4.5.6) as:

$$\Phi_{end} = \frac{r^*_{G_1\to S}(t_{end})}{r_{G_1\to S}(t_{end})} P_{G_1}(t_{end}) + P_S(t_{end}) + \frac{r^*_{G_2M\to G_1}(t_{end})}{r_{G_2M\to G_1}(t_{end})} P_{G_2M}(t_{end}), \tag{4.5.7}$$

where $t_{end} = 96$ hours. Measurement of the transition rates, $r_{G_1\to S}(t_{end})$ and $r_{G_2M\to G_1}(t_{end})$, is not possible. Thus, we can only provide the lower bound of the proliferating proportion of the population after irradiation. Using equations (4.3.20) and (4.3.21), we rewrite equation (4.5.7) as:

$$\Phi_{end} \geq \frac{r^*_{G_1\to S}(t_{end})}{\widetilde{r}_{G_1\to S}} P_{G_1}(t_{end}) + P_S(t_{end}) + \frac{r^*_{G_2M\to G_1}(t_{end})}{\widetilde{r}_{G_2M\to G_1}} P_{G_2M}(t_{end}) = LB, \tag{4.5.8}$$

where $t_{end} = 96$ hours, and the right-hand-side of inequality (4.5.8) is referred to as our variable LB.

Our model estimates the interval of the proportion that continues proliferating after 96 hours post radiotherapy as:

$$\Phi_{end} \in [LB, \ 1]. \tag{4.5.9}$$

Intervals of the proliferating fraction 96 hours post radiotherapy of five cancer cell lines are shown in Table 4.3 in column three.

4.6 Results: transition rate arrest and proliferating fractions

We impose that transition rates $r^*_{G_1\to S}(t)$ and $r^*_{G_2M\to G_1}(t)$, if reduced in value after irradiation, will recover piecewise linearly. Radiotherapy effects on the transition rates are shown in Figures 4.5 - 4.9.

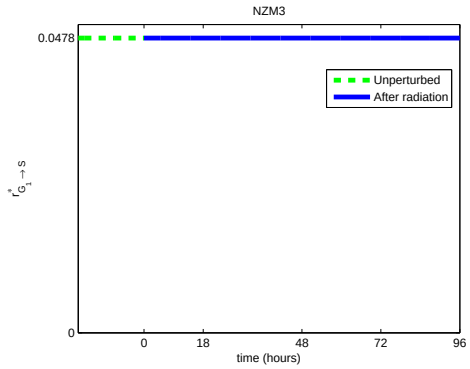

(a) The arrest of transition rate $r^*_{G_1 \to S}$ for cell line $NZM3$. The dashed line represents the value of transition rate $\widetilde{r}_{G_1 \to S}$ of an unperturbed population. The solid line shows the arrested value of $r^*_{G_1 \to S}(t)$.

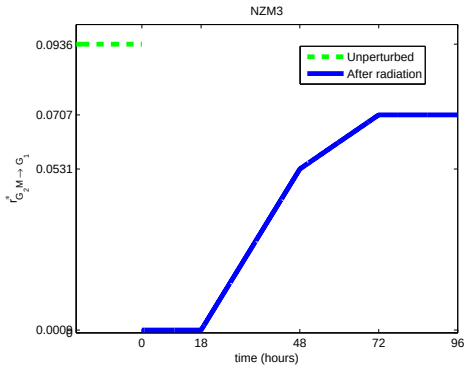

(b) The arrest of transition rate $r^*_{G_2M \to G_1}(t)$ for cell line $NZM3$. The dashed line represents the value of transition rate $\widetilde{r}_{G_2M \to G_1}$ of an unperturbed population. The solid line shows the arrested value of $r^*_{G_2M \to G_1}(t)$.

Figure 4.5: Arrest of the transition rates after the irradiation of cell line $NZM3$. The mathematical optimization function discussed in Section 4.4 produced piecewise linear functions for the transition rates: $r^*_{G_1 \to S}(t)$ and $r^*_{G_2M \to G_1}(t)$, shown in subfigures (a) and (b), respectively.

4.6.1 NZM3 cell line

From our model, we estimated that after the irradiation cancer cell population taken from cell line $NZM3$ initially stopped cell division for 18 hours, as can be seen in Figure 4.5(b), but recovered within 96 hours to 75% of its unperturbed value. Radiotherapy had no impact on the cell population transition probability from the G_1 - phase to S - phase, as can be seen in Figure 4.5(a). Apoptosis induced by irradiation was close to 1%. An experimental estimate for the recovering fraction of 6%. We present the initial proliferating interval calculated via our model in Table 4.3.

4.6.2 NZM4 cell line

Our model predicted an initial decrease in transition rate $r^*_{G_1 \to S}(t)$ to 63% of its unperturbed value and full recovery to its unperturbed value within 48 hours after irradiation, as shown in Figure 4.6(a). The cell division rate was estimated to drop to zero abut started to recover immediately and reached its unperturbed value over 96 hours after irradiation, as shown in Figure 4.6(b). The death rate induced by irradiation was close to zero.

4.6.3 NZM5 cell line

Irradiation had not stopped cell division for the $NZM5$ cell line, as shown in Figure 4.7(b). It initially reduced transition rate $r^*_{G_2M \to G_1}(t)$ to 31% of its unperturbed value and 49% of its unperturbed value after 96 hours. Transition rate $r^*_{G_1 \to S}(t)$ was not affected, as can be seen in Figure 4.7(a). Apoptosis induced by irradiation was estimated at 4%.

4.6.4 NZM6 cell line

Numerical simulations proposed an initial drop in the value of transition rate $r^*_{G_1 \to S}(t)$ to 57% of its unperturbed value with full recovery within 72 hours, as shown in Figure 4.8(a). Cell division rate

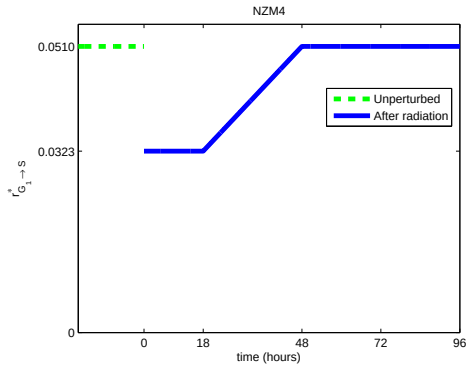

(a) The arrest of transition rate $r^*_{G_1 \to S}$ for cell line $NZM4$. The dashed line represents the value of transition rate $\widetilde{r}_{G_1 \to S}$ of an unperturbed population. The solid line shows the arrested value of $r^*_{G_1 \to S}(t)$.

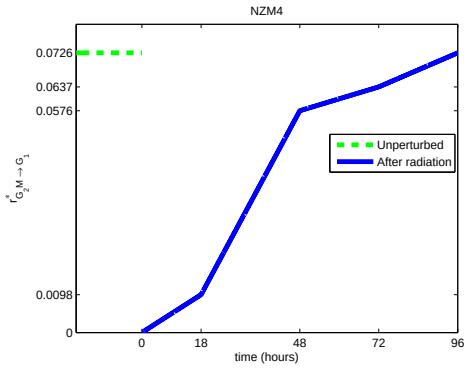

(b) The arrest of transition rate $r^*_{G_2M \to G_1}(t)$ for cell line $NZM4$. The dashed line represents the value of transition rate $\widetilde{r}_{G_2M \to G_1}$ of an unperturbed population. The solid line shows the arrested value of $r^*_{G_2M \to G_1}(t)$.

Figure 4.6: Arrest of the transition rates after the irradiation of cell line $NZM4$. The mathematical optimization function discussed in Section 4.4 produced piecewise linear functions for the transition rates: $r^*_{G_1 \to S}(t)$ and $r^*_{G_2M \to G_1}(t)$, shown in subfigures (a) and (b), respectively.

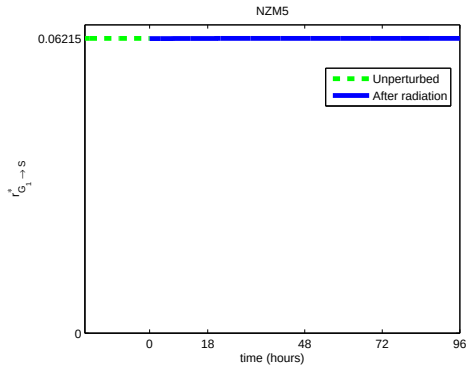

(a) The arrest of transition rate $r^*_{G_1 \to S}$ for cell line $NZM5$. The dashed line represents the value of transition rate $\widetilde{r}_{G_1 \to S}$ of an unperturbed population. The solid line shows the arrested value of $r^*_{G_1 \to S}(t)$.

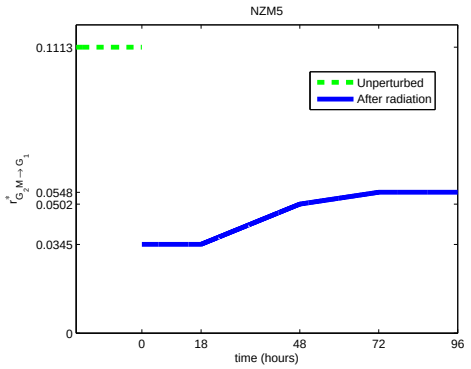

(b) The arrest of transition rate $r^*_{G_2M \to G_1}(t)$ for cell line $NZM5$. The dashed line represents the value of transition rate $\widetilde{r}_{G_2M \to G_1}$ of an unperturbed population. The solid line shows the arrested value of $r^*_{G_2M \to G_1}(t)$.

Figure 4.7: Arrest of the transition rates after the irradiation of cell line $NZM5$. The mathematical optimization function discussed in Section 4.4 produced piecewise linear functions for the transition rates: $r^*_{G_1 \to S}(t)$ and $r^*_{G_2M \to G_1}(t)$, shown in subfigures (a) and (b), respectively.

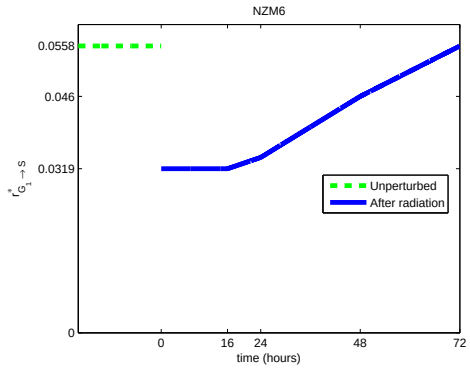

(a) The arrest of transition rate $r^*_{G_1\to S}$ for cell line $NZM6$. The dashed line represents the value of transition rate $\widetilde{r}_{G_1\to S}$ of an unperturbed population. The solid line shows the arrested value of $r^*_{G_1\to S}(t)$.

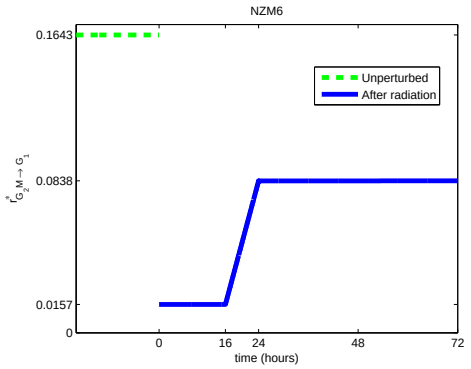

(b) The arrest of transition rate $r^*_{G_2M\to G_1}(t)$ for cell line $NZM6$. The dashed line represents the value of transition rate $\widetilde{r}_{G_2M\to G_1}$ of an unperturbed population. The solid line shows the arrested value of $r^*_{G_2M\to G_1}(t)$.

Figure 4.8: Arrest of the transition rates after the irradiation of cell line $NZM6$. The mathematical optimization function discussed in Section 4.4 produced piecewise linear functions for the transition rates: $r^*_{G_1\to S}(t)$ and $r^*_{G_2M\to G_1}(t)$, shown in subfigures (a) and (b), respectively.

$r^*_{G_2M\to G_1}(t)$ initially underwent arrest to 9% of its unperturbed value and reached a new plateau value at 51% of the unperturbed rate within 24 hours after irradiation. Apoptosis caused by the treatment was close to 1%.

4.6.5 NZM13 cell line

Our model suggests that cell division $r^*_{G_2M\to G_1}(t)$ was initially stopped due to irradiation, with immediate recovery reaching 44% of the unperturbed value, as shown in Figure 4.9(b). We remark that it a new plateau value has not been reached during 96 hours as can be seen for other cell lines. Transition rate $r^*_{G_1\to S}(t)$ initially dropped to 19% of the unperturbed value and recovered to 86% of the unperturbed value but also seems not have reached a new plateau value, as shown in Figure 4.9(a). We note that population doubling time T_d has been experimentally estimated as 76.8 hours (see Table 4.4). This cell line's T_d is longer compared to the other four cell line population doubling times. This suggests that the transition rate recovery duration is correlated to the population doubling time. Our model suggests that cell death due to irradiation was close to 1%. Cell number measured 96 hours after radiation at 9 Gy was 75% of that expected, and our model suggests that it is 68%, due solely to cell cycle arrest and not cell death, see Table 4.4.

4.6.6 Proliferating cell population proportions

We present the proliferating proportion interval for each cell line in Table 4.3. For example, the proliferating proportion of cell culture Φ_{end} taken from cell line $NZM3$ can be calculated with equation (4.5.8) as follows: firstly, estimate ratios $r^*_{G_1\to S}(t_{end})/\widetilde{r}_{G_1\to S}$ and $r^*_{G_2M\to G_1}(t_{end})/\widetilde{r}_{G_2M\to G_1}$ from Figure 4.5 and, secondly, use Table 4.2, which contains the values of the proportions of populations in each phase after 96 hours post-irradiation. From Table 4.3, we can see that following 96 hours after exposure to the radiation of 9 Gy, the cell population of the $NZM3$ cell line culture will be composed of at least 93.2% of proliferating cells.

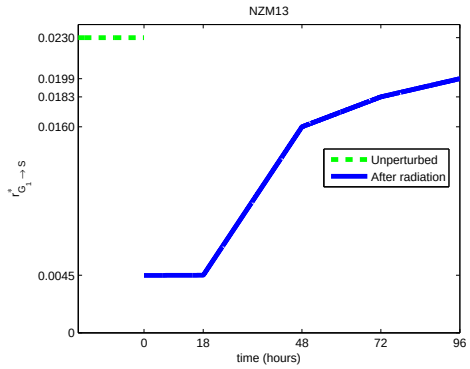

(a) The arrest of transition rate $r^*_{G_1\to S}$ for cell line $NZM13$. The dashed line represents the value of transition rate $\widetilde{r}_{G_1\to S}$ of an unperturbed population. The solid line shows the arrested value of $r^*_{G_1\to S}(t)$.

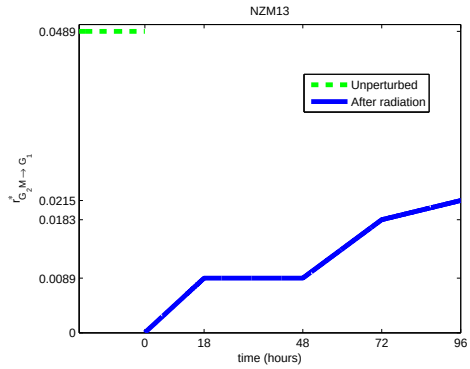

(b) The arrest of transition rate $r^*_{G_2M\to G_1}(t)$ for cell line $NZM13$. The dashed line represents the value of transition rate $\widetilde{r}_{G_2M\to G_1}$ of an unperturbed population. The solid line shows the arrested value of $r^*_{G_2M\to G_1}(t)$.

Figure 4.9: Arrest of the transition rates after the irradiation of cell line $NZM13$. The mathematical optimization function discussed in Section 4.4 produced piecewise linear functions for the transition rates: $r^*_{G_1\to S}(t)$ and $r^*_{G_2M\to G_1}(t)$, shown in subfigures (a) and (b), respectively.

The recovering survival fraction, denoted by $\Phi_{experim}$, was experimentally measured for every cell line. It is an estimate of colonies counted after 1-3 weeks over the initial number of cells seeded.

We have shown in Table 4.3 the proliferating proportion intervals of the cancer cell populations taken from five cell lines. The second column, Φ_{init}, shows the interval of the initial proliferating fraction after a one-time irradiation dose (at $t = 0$) for each cell line estimated by our model. The third column, Φ_{end}, presents the interval of the proliferating cell proportion of each cell line after 96 hours following irradiation. Column four, $\Phi_{experim}$, shows the experimental estimates of the proliferating fraction for each cell line.

4.6.7 Cell loss and expected number of cells

Table 4.4 shows the parameters of cell cycle dynamics for five cell lines. We have calculated the population doubling times using the plateau log reduction method (discussed in Chapter 3) for cell lines $NZM5$ and $NZM6$. For the rest of the cell lines, we used the experimental estimates of the population doubling times, which were obtained by constructing a growth curve. The transition rates between respective phases, calculated with methods described in Section 4.4.2, have been shown in columns three to five in Table 4.4. We have estimated from equation (4.3.10) the initial proportion of the population lost within 18 hours following the paclitaxel treatment application for each cell line from. We refer to it as $TxLoss$ and present in column six. By utilising the arrested rates $r^*_{G_1\to S}(t)$ and $r^*_{G_2M\to G_1}(t)$ in Figures 4.5 - 4.9, we have calculated from system (4.2.28) the proportion of cell number expected after 96 hours, e.g., cell line $NZM13$ has 68% of the expected number of cells after 96 hours following irradiation; and refer to as E_{Mod}. Column eight in Table 4.4, $E_{Experim}$, shows the experimental estimate of the expected proportion of cell number measured 96 hours after irradiation at 9Gy.

Cell line	Φ_{init}	Φ_{end}	$\Phi_{experim}$
$NZM3$	[0.67, 0.85]	[0.93, 1]	0.06
$NZM4$	[0.55, 0.76]	[1, 1]	0.20
$NZM5$	[0.23, 0.32]	[0.83, 1]	0.20
$NZM6$	[0.32, 0.44]	[0.82, 1]	0.02
$NZM13$	[0.35, 0.51]	[0.75, 1]	0.08

Table 4.3: Proliferating proportion intervals of the cancer cell population taken from five cell lines. The second column, Φ_{init}, shows the interval of the proliferating fraction after a one-time irradiation dose (at $t = 0$) for each cell line estimated by our model. The third column, Φ_{end}, indicates the interval of the proliferating cell proportion of each cell line after 96 hours following irradiation. Column four, $\Phi_{experim}$, shows the experimental estimates of the proliferating fraction for each cell line.

4.7 Discussion

We used optimization methods in order to estimate the initial proliferating fraction and the proliferating proportion of the population after 96 hours following a one-time irradiation dose.

We analysed five cell lines, identical to the ones in paper Basse *et al.* (2010), and our mathematical model results agreed with the model presented in paper Basse *et al.* (2010), i.e., cancer cell population growth undergoing arrest and little cell death occurring due to irradiation. We imposed that the transition rates from the G_1-phase to the S-phase and from the G_2M-phase to the G_1-phase, if decreased in value, would recover in a piecewise linear mode after radiotherapy.

A significant difference between our mathematical model and that in Basse *et al.* (2010) is in estimation of transition rates. We estimated the unperturbed population transition rates (namely, $\widetilde{r}_{G_1\to S}$, $\widetilde{r}_{S\to G_2M}$ and $\widetilde{r}_{G_2M\to G_1}$) by applying a mathematical model rather than using values provided by experimentalists. We used the plateau log reduction value (discussed in Chapter 3) to calculate all transition rates of the unperturbed cancer cell population; therefore, our numerical values differed from those given in Basse *et al.* (2010).

After an irradiation dose, the cell division rates (i.e., the transition rate from the G_2M - phase to the G_1 - phase) for cell lines $NZM3$, $NZM5$, and $NZM6$ plateaued at a lower value than they did in the unperturbed state. The cancer cell population taken from cell line $NZM4$ recovered from radiation within the 96 hours after treatment and reached the original unperturbed BEG state. A one-time irradiation dose of 9 Gy for some cell lines did not induce a long-term cell cycle arrest, as we can see in Table 4.3, the proliferating proportion Φ_{end} after 96 hours post-irradiation is equal to 1. For cancer cell line $NZM13$, transition rates did not plateau within 96 hours. From Figures 4.5 - 4.9 and Table 4.4, we can see that the transition rate speed of recovery is related to the doubling time: the shorter the doubling time, the faster the recovery to the unperturbed value or a new plateau value.

Cell loss induced by irradiation is approximately 1% for every cell line apart from $NZM5$, which produced a 4% cell loss within 96 or 72 hours. Our mathematical model estimates of the proportion of cells expected after 96 hours (E_{Mod}) are shown in the seventh column of Table 4.2. An experimental

Cell Line	T_d (hours)	$\widetilde{r}_{G_1 \to S}$ ($hours^{-1}$)	$\widetilde{r}_{S \to G_2M}$ ($hours^{-1}$)	$\widetilde{r}_{G_2M \to G_1}$ ($hours^{-1}$)	Tx Loss	E_{Mod}	$E_{Experim}$
$NZM3$	41*	0.04781	0.06723	0.09361	0	1	*n.a.*
$NZM4$	46*	0.05105	0.05406	0.07258	0	1	*n.a.*
$NZM5$	31.2	0.06215	0.09782	0.11129	0.32	0.54	*n.a.*
$NZM6$	27.5	0.05583	0.12967	0.16426	0.18	0.75	*n.a.*
$NZM13$	76.8*	0.02297	0.04254	0.04889	0.12	0.68	0.75

Table 4.4: Parameters of cell cycle dynamics for five cell lines. Column two, T_d, shows the population doubling time of each cell line: asterisks indicate the doubling times that are experimentally estimated; T_d values with no asterisks show that the doubling time is calculated from the plateau logarithmic reduction value. Columns three to five show the transition rate values from respective phases of the unperturbed cancer cell population calculated with the methods discussed in Section 4.4.2. Column six shows the calculated value of the proportion of the initial population number lost within 18 hours after the paclitaxel treatment application of each cell line, which are the methods discussed in Section 4.4.3. Column seven, E_{Mod}, indicates the proportion of cell number expected after 96 hours. Column eight, $E_{Experim}$, shows the experimental estimate of the expected proportion of cell number measured 96 hours after irradiation at 9 Gy; *n.a.* indicates that this data is not available.

observation for that, which was expected for cell line $NZM13$ is shown in 75%. In comparison, our mathematical model derived the expected cell number at 68% of that initial. No experimental data was available for the other cell lines. Thus, our mathematical estimate was very good for the observed data point.

Loss of clonogenical survival was experimentally estimated for every cell line and was in a range of 90 – 99%: this percentage of population has lost capability to reproduce indefinitely. We argue that within 96 hours following irradiation flow cytometry method cannot detect this loss. The initial proliferating fractions Φ_{init} and the proliferating proportions of the cell population Φ_{end} for five cell lines are shown in Table 4.3. The initial proliferating fraction interval estimated via our mathematical model is much higher in value than experimentally estimated ones, because, after irradiation, some cells do divide once or twice before dying. These cells have lost the capability to reproduce indefinitely and are considered dead in biological terminology but not in our mathematical approach. Experimental observations stopped at 96 hours for cells lines $NZM3$, $NZM4$, $NZM5$, and $NZM13$, and at 72 hours for cell line $NZM6$. These times are at most the length of three average cell cycles times for some cell lines (we presumed here that the average cell-cycle time is similar to that of population doubling, see Chapter 2). A proportion of the population that is not a part of the survival fraction divides once or twice or more before undergoing apoptosis; thus, our model cannot estimate the surviving fraction successfully, as experimental observations stop too soon. Our model results do not agrees with the following statement from Basse *et al.* (2010): "the long-term cell cycle arrest, rather than apoptosis, accounts for much of the loss of viability observed in clonogenicity assays". This statement implies that flow cytometry profiles could differentiate what proportion of arrested cell

population would eventually undergo apoptosis, which is not the case.

The flow cytometry profiles of cell populations perturbed by paclitaxel and paclitaxel in combination with irradiation were very noisy after certain experimental observation points, and measurements with Cylchred method seemed very inaccurate.

We note that our data readings, i.e., slight variations in the plateau log reduction value or in estimates of proportions in each phase from flow cytometry profiles via different methods (Cylchred or others), affect the result of the unperturbed population transition rates that then affect the results of the optimization routine. However, it does not affect the conclusions derived from our model that the transition rates undergo arrest, little cell death occurs within 96 hours, and that the initial proliferating proportion is much larger in value than the surviving fraction due to the fact that more cells die after 96 hour observation point.

Since little apoptosis is detected via our mathematical model, and the one presented in Basse *et al.* (2010) during the first 96 hours after radiotherapy and the entire initial proportion in the S-phase after irradiation is assumed to be proliferating, the instant result is the proliferating fraction calculated with our model to be larger than the experimental estimates of the initial surviving fraction.

For successful estimation of the surviving fraction via mathematical modelling, we require experimental data beyond the observation point of 96 hours. With our mathematical model, we could then estimate cell loss that occurs beyond 96 hours, thus leading us to more precise calculation of the surviving fraction of the cancer cell population after the one-time irradiation dose.

Chapter 5

Application of the Two-Population Model

There is increasing evidence that the growth of human tumours is driven by a small proportion of tumour stem cells with self-renewal properties. Multiplication of these cells leads to loss of self-renewal and after division for a finite number of times the cells undergo programmed cell death. Cell-cycle times of human cancers have been measured *in vivo* and shown to vary in the range from two days and several weeks, depending on the individual. Cells cultured directly from tumours removed at surgery initially grow at a rate comparable to the *in vivo* rate but continued culture leads to the generation of cell lines that have shorter cycle times (1-3 days). It has been postulated that the more rapidly growing sub-population exhibits some of the properties of tumour stem cells and are the precursors of a slower growing sub-population that comprise the bulk of the tumour. We have previously developed a mathematical model to describe the behaviour of cell lines and we extend this model here to describe the behaviour of a system with two cell populations with different kinetic characteristics and a precursor-product relationship. The aim is to provide a framework for understanding the behaviour of cancer tissue that is sustained by a minor population of proliferating stem cells.

5.1 Introduction

Stem cells for normal tissues in the human body are thought to act as a reservoir of self renewing cells and are supported within a spatially constrained microenvironment called a niche Moore & Lemischka (2006); Watt & Hogan (2000). It is hypothesised that proliferation, apoptosis, senescence, and differentiation of stem cells are inhibited within the niche, but that once stem cells leave the niche they are able to proliferate (via a controlled number of cell divisions), migrate to surrounding tissue and differentiate, constituting the bulk of normal tissue (as illustrated in Figure 5.1). There is increasing evidence that the growth of human tumours is also driven by a population of tumour stem cells that have the property of self-renewal and are located in a spatially constrained niche microenvironment Dittmat & Zanker (2009); Lindeman & Visvader (1999); Schatton & Frank (2007); Sole *et al.* (2008) but with unlimited proliferation potential, giving rise to progeny outside the niche that are not spatially constrained but have limited proliferation potential. While retaining the property of self-renewal in the niche, tumour stem cells have in many cases lost the ability to respond to niche signals and therefore continue to proliferate Baguley (2006). When these cells leave the niche, they (i) lose self-renewal capacity, (ii) continue to proliferate, (iii) fail to differentiate properly and (iv) undergo programmed cell death after a finite number of cell divisions. These cells form the majority of the tumour tissue. Their average cell-cycle time can be measured *in vivo* and various studies have shown cycle times to vary in the range from two days to several weeks, depending on the individual Wilson *et al.* (1988).

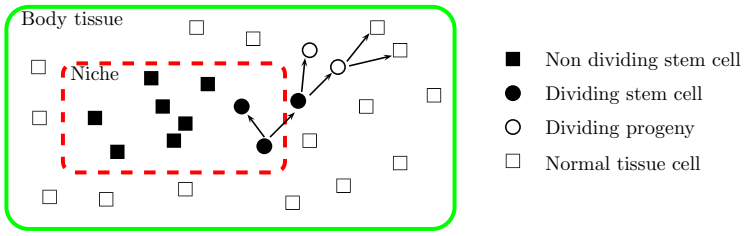

Figure 5.1: Schematic diagram of a niche in a human tissue. Stem cells, located in a spatially constrained niche microenvironment but with unlimited proliferation potential, normally divide asymmetrically with one daughter cell remaining in the niche and one, once triggered by demand, migrating from the niche to surrounding tissue. Stem cell progenies proliferate in surrounding body tissue and eventually (after proliferation ceases) differentiate to become normal tissue cells.

Tumour tissue removed at surgery can be grown in culture and measurements of primary culture cycle time show a range of 3 days to several weeks, which is similar to that observed *in vivo* Baguley & Marshall (2004); Furneaux *et al.* (2008). Continued culture of clinical tumour material results in death of the majority of the cells but in the emergence after several months of stably growing cells called cell lines, as shown by the scheme in Figure 5.2. These lines have shorter cell-cycle times than those of the primary cultures with a range, depending on the individual, of 1-3 days. Notably, the cell-cycle times of cell lines are correlated to the cell-cycle times of the primary cultures from which they were initially derived and it has been postulated that cell lines exhibit some of the properties of tumour stem cells Baguley & Marshall (2008).

Mathematical models describing the kinetic behaviour of cell lines, both under steady state behaviour and following perturbation with radiation and cytotoxic drugs can be found in the literature Basse & Ubezio (2007); Basse *et al.* (2003, 2005); Begg (2007). In Johnston *et al.* (2006), a mathematical model is used to describe stem and semi-differentiated cells in the colonic crypt. In this chapter, we have combined aspects of these models with our model in Chapter 2 to describe the behaviour of the tumour tissue in terms of the above stem cell model, where the tumour comprises two sub-populations with different kinetic properties. One small sub-population of recently migrated stem cells from the niche exhibits rapid growth (we term this sub-population the 'rapid sub-population cells') and the other slower growing sub-population of partially differentiated stem cell progeny making up the bulk of the tumour (termed the 'slow sub-population cells'). Cell-cycle times and percentages in each phase of the cell cycle have been determined experimentally in cell lines as described in Section 5.2 and these measurements are used to establish estimates of model parameters. It should be noted here that the term growth refers to the number of cells in the population or sub-population increasing and not to the actual size of individual cells.

When tumour cells from a surgical sample are placed into culture, the niche structure is destroyed so that no new stem cells migrate from the niche. The more slowly growing, partially differentiated

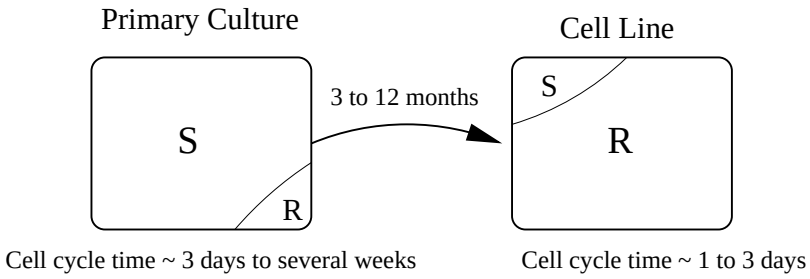

Figure 5.2: Schematic diagram of a primary culture of tumour tissue (left), comprising mainly of relatively slowly growing sub-population of cells (cycle times of 3 days to several weeks) and a small sub-population with the potential for more rapid growth (cell-cycle times of 1 to 3 days). With continued culture of the primary culture for several months, the more slowly growing sub-population cells die and are replaced by more rapidly growing sub-population cells, termed a cell line.

progeny tumour cells, which form the majority of the population, continue to proliferate and to undergo apoptosis. However, the small population of rapidly growing tumour 'ex stem' cells continues to proliferate and is resistant to apoptosis, such that with continuing culture, the proportion of slowly growing sub-population of cells decreases while that of the more rapidly growing sub-population increases. Eventually, the proportion of slowly growing sub-population of cells is negligible and virtually the entire population is composed of more rapidly growing sub-population of cells and may be termed a cell line (Figure 5.2).

The aim of this communication is to construct a mathematical model that reproduces the main elements of this scheme for tumour cells in primary cultures and established cell lines, and apply this to *in vivo* tumour growth. In Section 5.2, we describe the experimental procedure for measuring cell-cycle times and cell cycle phase percentages of cell lines. Section 5.3 outlines the mathematical model for the two sub-populations of growing cells and also shows the equilibrium result of the switch from a high percentage of 'slow sub-population cells' (the primary culture case) to a high percentage of 'rapid sub-population cells' (the cell line case). Cell death via time dependent apoptosis is added to the model in Section 5.4. Section 5.5 describes two applications of the model. The first compares model results to experimental cell-cycle times of primary cultures and established cell lines. The second looks at *in vivo* tumour cell population growth where a population of slow sub-population cells is maintained by a fixed number of stem cells in a niche.

5.2 Experimental procedure

5.2.1 Derivation of cell lines from primary cultures

The derivation of the cell lines from melanoma specimens has been reported in several publications and two references are provided here Marshall *et al.* (1993); Parmar *et al.* (2000). More than 150 cell lines have now been derived from clinical samples, and of these, 31 have corresponding cell cycle data from primary cultures. It is from this set that the correlation between the cycle time of the primary culture and the corresponding cell lines has been obtained Baguley & Marshall (2004).

5.2.2 Determining cell-cycle times of established cell lines

This has been described in detail in other publications Baguley *et al.* (1995); Furneaux *et al.* (2008). Growth of cultured cells can be measured by direct counting, but direct measurement of clinical samples grown in primary culture is impossible because of the presence of host cells in the sample and the loss of tumour cells. However, it was found using tumour cell lines that the degree of incorporation of ^3H-thymidine into DNA at different times after addition of paclitaxel, an inhibitor of mitosis and cell division, was a function of the measured culture doubling time Baguley *et al.* (1995), as discussed in Chapter 3. It is assumed by biologists that culture doubling time was similar to culture cycle time for cell lines (i.e., that cell loss was negligible) and developed an empirical formula that related culture cycle time to the ^3H-thymidine incorporation data.

5.2.3 Determination of the percentage of cells in each phase of the cell division cycle

This was determined for established cell lines by fixing the cells, staining with the DNA stain propidium iodide, and measuring the frequencies of cells with differing DNA content using flow cytometry Holdaway *et al.* (1992).

5.3 A simple model for primary culture cell populations evolving into established cell lines

5.3.1 Two-population age-structured model: solution existence, BEG condition

In accordance with tumour tissue comprising newly arrived tumour stem cells and their progeny, it is assumed that primary culture cell populations are composed of both 'rapidly growing' (ex stem cells) and 'slowly growing' (progeny) sub-populations, and that both are further subdivided by cell cycle phase. We denote $n^{\mathcal{R}}_{G_1}(t,\tau)$ to be the number density of rapidly growing sub-population cells in the G_1 phase at time t and age τ and similarly $n^{\mathcal{R}}_{S}(t,\tau)$ and $n^{\mathcal{R}}_{G_2M}(t,\tau)$ are the number densities of rapidly growing sub-population cells in the S and combined G_2M phases, respectively. The G_2 and M-phases are combined here because they cannot be separated by flow cytometry as described in Section 1.5. Here we use the superscript $\mathcal{R}$ for the rapidly growing sub-population. Cells progress through the cell cycle by having a rate of transition probabilitys from one phase to the next according to Figure 5.3 where $r^{\mathcal{R}}_{G_1\to S}$ is that rate of transition from G_1-phase to S-phase and other rates have similar form as specified in Table 5.1. For the slow growing sub-population cells (superscript $\mathcal{S}$) we define $n^{\mathcal{S}}_{G_1}(t,\tau)$, $n^{\mathcal{S}}_{S}(t,\tau)$ and $n^{\mathcal{S}}_{G_2M}(t,\tau)$ to be the number densities of the slow growing sub-population cells in the G_1, S and G_2M phases, respectively. Cell death via apoptosis is achieved by removing cells at a rate $r^{\mathcal{S}}_{G_1\to A}$ per unit time from the slower growing sub-population G_1-phase compartment.

	parameter	description	units
	t	time	hours
	τ	age	hours
rapid growing cells	$r^{\mathcal{R}}_{G_1\to S}$	rate transition G_1 to S-phase	hours^{-1}
	$r^{\mathcal{R}}_{S\to G_2M}$	rate transition S to G_2M-phase	hours^{-1}
	$r^{\mathcal{R}}_{G_2M\to G_1}$	rate transition G_2M to G_1-phase	hours^{-1}
	ρ	differentiation rate	hours^{-1}
slowly growing cells	$r^{\mathcal{S}}_{G_1\to S}$	rate transition G_1 to S-phase	hours^{-1}
	$r^{\mathcal{S}}_{S\to G_2M}$	rate transition S to G_2M-phase	hours^{-1}
	$r^{\mathcal{S}}_{G_2M\to G_1}$	rate transition G_2M to G_1-phase	hours^{-1}
	$r^{\mathcal{S}}_{G_1\to A}$	apoptosis rate	hours^{-1}

Table 5.1: Model parameters with descriptions and units. The parameters for the slow growing cells are similar except the superscript $\mathcal{S}$ is added.

The rate of differentiation of the rapidly growing sub-population G_1-phase cells to the slower growing sub-population G_1-phase cells is denoted ρ per unit time.

It is assumed that primary culture cell populations are composed of both 'rapidly growing' (ex stem cells) and 'slowly growing' (progeny) sub-populations and that both are further subdivided by cell cycle phase. We denote $\mathbf{n}^{\mathcal{R}}(t,\tau)$ to be the number density vector of rapidly growing sub-population cells, thus $\mathbf{n}^{\mathcal{R}}(t,\tau) = [n^{\mathcal{R}}_{G_1}(t,\tau) \quad n^{\mathcal{R}}_{S}(t,\tau) \quad n^{\mathcal{R}}_{G_2M}(t,\tau)]^T$. The number densities of slow growing sub-population cells (superscript $\mathcal{S}$) we define by $\mathbf{n}^{\mathcal{S}}(t,\tau) = [n^{\mathcal{S}}_{G_1}(t,\tau) \quad n^{\mathcal{S}}_{S}(t,\tau) \quad n^{\mathcal{S}}_{G_2M}(t,\tau)]^T$. Similarly to the age-structure model for one population, as showed in Section 2.2, we define continuous function $\mathbf{n}(t,\tau)$ as:

$$\mathbf{n}(t,\tau) = [\mathbf{n}^{\mathcal{R}}(t,\tau) \quad \mathbf{n}^{\mathcal{S}}(t,\tau)], \tag{5.3.1}$$

where vector components are continuous functions on (t,τ) and transition rates are piecewise continuous functions of time t and age τ. The age-structured two-population growth model can be expressed (just like in Chapter 2) as:

$$\frac{\partial}{\partial t}\mathbf{n}(t,\tau) + \frac{\partial}{\partial \tau}\mathbf{n}(t,\tau) = -\mathbf{D}_{\text{out}}(t,\tau)\mathbf{n}(t,\tau), \quad 0 < t < \infty, \quad 0 < \tau < T, \tag{5.3.2}$$

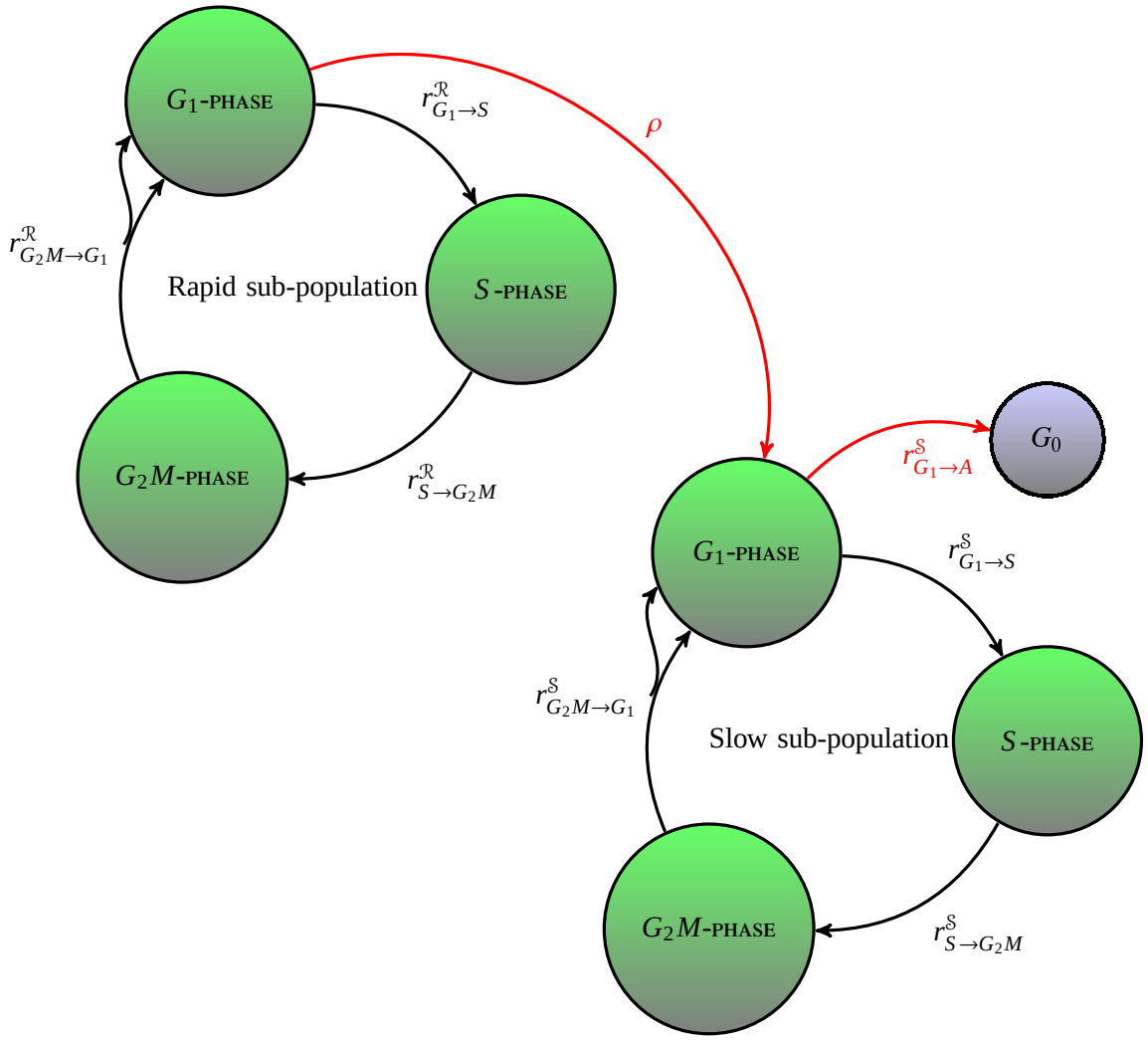

Figure 5.3: Scheme of cell-cycle control of a tumour cell population containing slow and rapidly growing sub-populations of cells. Each sub-population is further subdivided into G_1, S and G_2M-phases with the possibility that cells can transfer from one phase to the next according to a transition rate (see Table 5.1). Rapid sub-population cells differentiate to become slow sub-population cells at a rate of ρ per hour. Slow sub-population cells are mortal with apoptosis rate from G_1 phase denoted $r^{\mathcal{S}}_{G_1\to A}$ per unit time.

with respective side conditions defined as follows:

$$\mathbf{n}(t=0,\tau) = \mathbf{n}^0(\tau), \quad \text{initial age distribution,} \tag{5.3.3}$$

$$\mathbf{n}(t,\tau=0) = \int_0^T \mathbf{D}_{\text{in}}(t,\tau)\mathbf{n}(t,\tau)\,d\tau, \quad t>0, \quad \text{renewal distribution.} \tag{5.3.4}$$

The matrix $\mathbf{D}_{\text{out}}$ represents the loss of cells from the various phases via death and transfer to other

phases, and is defined as:

$$\mathbf{D}_{\text{out}} = \text{diagonal}\begin{bmatrix}\mathbf{D}^{\mathcal{R}}_{\text{out}}\\ \\ \mathbf{D}^{\mathcal{S}}_{\text{out}}\end{bmatrix}, \tag{5.3.5}$$

with the following transition rate matrices for rapid and slow compartments:

$$\mathbf{D}^{\mathcal{R}}_{\text{out}}(t,\tau) = \begin{bmatrix} r^{\mathcal{R}}_{G_1\to S} + \rho & 0 & 0\\ 0 & r^{\mathcal{R}}_{S\to G_2M} & 0\\ 0 & 0 & r^{\mathcal{R}}_{G_2M\to G_1}\end{bmatrix}(t,\tau), \tag{5.3.6}$$

and

$$\mathbf{D}^{\mathcal{S}}_{\text{out}}(t,\tau) = \begin{bmatrix} r^{\mathcal{S}}_{G_1\to S} + r^{\mathcal{S}}_{G_1\to A} & 0 & 0\\ 0 & r^{\mathcal{S}}_{S\to G_2M} & 0\\ 0 & 0 & r^{\mathcal{S}}_{G_2M\to G_1}\end{bmatrix}(t,\tau). \tag{5.3.7}$$

The renewal matrix $\mathbf{D}_{\text{in}}$ represents the gain of cells at age $\tau = 0$ in each phase and is caused by transfer from other phases. $\mathbf{D}_{\text{in}}$ is defined as:

$$\mathbf{D}_{\text{in}} = \begin{bmatrix}\mathbf{D}^{\mathcal{R}}_{\text{in}} & \mathbf{0}\\ \mathbb{C} & \mathbf{D}^{\mathcal{S}}_{\text{in}}\end{bmatrix}, \tag{5.3.8}$$

where

$$\mathbf{D}^{\mathcal{R}}_{\text{in}}(t,\tau) = \begin{bmatrix} 0 & 0 & 2r^{\mathcal{R}}_{G_2M\to G_1}\\ r^{\mathcal{R}}_{G_1\to S} & 0 & 0\\ 0 & r^{\mathcal{R}}_{S\to G_2M} & 0\end{bmatrix}(t,\tau), \tag{5.3.9}$$

and

$$\mathbf{D}^{\mathcal{S}}_{\text{in}}(t,\tau) = \begin{bmatrix} 0 & 0 & 2r^{\mathcal{S}}_{G_2M\to G_1}\\ r^{\mathcal{S}}_{G_1\to S} & 0 & 0\\ 0 & r^{\mathcal{S}}_{S\to G_2M} & 0\end{bmatrix}(t,\tau), \tag{5.3.10}$$

with

$$\mathbb{C} = \begin{bmatrix}\rho & 0 & 0\\ 0 & 0 & 0\\ 0 & 0 & 0\end{bmatrix}. \tag{5.3.11}$$

The solution of the system (5.3.2)-(5.3.4) is still of the form of equation (2.2.21) from Chapter 2. When solution (2.2.21) is substituted into the renewal condition (5.3.4), the Volterra integral equation of second kind is as in equation (2.3.1) from Chapter 2, we rewrite it here as:

$$\mathbf{n}(t,0) = \mathcal{F}(t) + \int_0^t K(t,s)\mathbf{n}(s,0)\,ds, \tag{5.3.12}$$

where

$$\mathcal{F}(t) = \int_t^T \mathbf{D}_{\text{in}}(t,\tau)\exp\left(-\int_{\tau-t}^{\tau}\mathbf{D}_{\text{out}}(s+t-\tau,s)\,ds\right)\mathbf{n_0}(\tau-t)\,d\tau, \tag{5.3.13}$$

and kernel of integro-equation for rapidly growing sub-population is defined as follows:

$$K(t,s) = \mathbf{D}^{\mathcal{R}}_{\text{in}}(t,t-s)\exp\left(-\int_0^{t-s}\mathbf{D}^{\mathcal{R}}_{\text{out}}(\xi+s,\xi)\,d\xi\right), \tag{5.3.14}$$

The existence and uniqueness of the solution is given by Theorem 2.3.1 from Chapter 2 with the

appropriate interpretations for each compartment.

We continue with the proof of BEG existence for the two-population model with transition rates now only dependent on age τ and the derivation of the characteristic equation for each compartment. We assume that cell population composed of two sub-populations with different kinetic properties grows exponentially as follows:

$$\mathbf{n}(t,\tau) = e^{\lambda t}\widehat{\mathbf{n}}(\tau), \tag{5.3.15}$$

same assumption was made for one-compartment model in Section 2.4. When the ansatz (5.3.15) is substituted into equation (5.3.12), just like in Chapter 2, we obtain the following nonlinear eigenproblem:

$$\Big[\mathbb{A}(\lambda) - \mathbb{I}\Lambda\Big]\widehat{\mathbf{n}}(0) = 0, \tag{5.3.16}$$

now $\mathbb{I}$ is the 6-dimensional unit matrix, $\widehat{\mathbf{n}}$ is the 6-dimensional vector of number density functions, where the matrix $\mathbb{A}$ is as follows:

$$\mathbb{A} = \begin{bmatrix} \mathbb{A}^{\mathcal{R}} & \mathbf{0} \\ \nu\mathbb{C} & \mathbb{A}^{\mathcal{S}} \end{bmatrix}, \tag{5.3.17}$$

with $\mathbb{A}^{\mathcal{R}}$ and $\mathbb{A}^{\mathcal{S}}$ given by

$$\mathbb{A}^{p2} = \int_0^T \mathbf{D}_{\text{in}}^{p2}(s)\exp\Big(-\int_0^s [\mathbf{D}_{\text{out}}^{p2}(s') + \mathbb{I}\lambda]\,ds'\Big)ds, \quad \text{with} \quad p2 \in \{\mathcal{R},\mathcal{S}\}, \tag{5.3.18}$$

and

$$\nu = \int_0^T \rho(s)\exp\Big(-\int_0^s [r_{G_1\to S}^{\mathcal{R}}(\xi) + \lambda]\,d\xi\Big)ds. \tag{5.3.19}$$

The structure of matrices $\mathbb{A}^{\mathcal{R}}$ and $\mathbb{A}^{\mathcal{S}}$ is as follows:

$$\mathbb{A}^{p2} = \begin{bmatrix} 0 & 0 & \kappa_{G_2M}^{p2} \\ \kappa_{G_1}^{p2} & 0 & 0 \\ 0 & \kappa_S^{p2} & 0 \end{bmatrix}, \tag{5.3.20}$$

for $p2 \in \{\mathcal{R},\mathcal{S}\}$, where κ_p with $p \in \{G_1, S, G_2M\}$ is a positive element and has been defined in equation (2.4.5) in Chapter 2 with two-population model specific transition rates.

The matrix $\mathbb{A}$ is now reducible, as its connected graph shows in Figure 5.4, slow sub-population makes no contribution to any stage of rapid sub-population, see Appendix for more on reducible matrices. So previous approach from Chapter 2 is not applicable. However, it can be seen that when $\rho = 0$, we have two decoupled algebraic systems. Matrices $\mathbb{A}^{\mathcal{R}}$ and $\mathbb{A}^{\mathcal{S}}$ are irreducible and imprimitive. Hence, Theorem 2.4.1 applies to each of the sub-populations individually. This means, there exists a $\Lambda = 1$ and both, the rapid and slow sub-populations, have one positive eigenvalue each, denoted as λ_0^R and λ_0^S, respectively. These solve the characteristic equations (2.4.6) and (2.4.8), derived in Chapter 2, with the appropriate two-population model transition probability rates.

So now let us consider the coupled system again. As stated above, equation (5.3.16) is reducible, and is of the form

$$\Big[\mathbb{A}^{\mathcal{R}}(\lambda) - \mathbb{I}\Lambda\Big]\widehat{\mathbf{n}}^{\mathcal{R}}(0) = \mathbf{0}, \tag{5.3.21}$$

$$\mathbb{C}\widehat{\mathbf{n}}^{\mathcal{R}}(0) + \Big[\mathbb{A}^{\mathcal{S}}(\lambda) - \mathbb{I}\Lambda\Big]\widehat{\mathbf{n}}^{\mathcal{S}}(0) = 0, \tag{5.3.22}$$

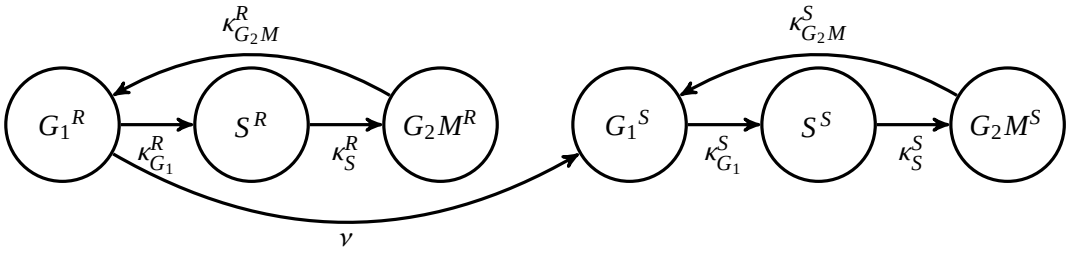

Figure 5.4: Reducible matrix $\mathbb{A}$ diagram.

then Theorem 2.4.1 applies to the rapid sub-population; therefore, there exists a λ_0^R, hence $\Lambda = 1$ such that $\widehat{\mathbf{n}}^{\mathcal{R}}(0) > 0$ (proven with the Perron-Frobenius theorem presented in Section 2.4). Furthermore, if $\lambda \neq \lambda_0^S$, then $\left[\mathbb{A}^{\mathcal{S}}(\lambda) - \mathbb{I}\Lambda\right]$ is not singular, and

$$\widehat{\mathbf{n}}^{\mathcal{S}}(0) = -\left[\mathbb{A}^{\mathcal{S}}(\lambda) - \mathbb{I}\Lambda\right]^{-1} \mathbb{C}\widehat{\mathbf{n}}^{\mathcal{R}}(0). \tag{5.3.23}$$

If $\lambda = \lambda_0^S$, then the Fredholm Alternative theorem applies and $\mathbb{C}\widehat{\mathbf{n}}^{\mathcal{R}}(0)$ must be orthogonal kernel of $\left[\mathbb{A}^{\mathcal{S}}(\lambda) - \mathbb{I}\Lambda\right]$ for a solution to exist, see Kantorovich & Akilov (1982). The solution is then a combination of the eigenvectors $\widehat{\mathbf{n}}^{\mathcal{R}}(0)$ and $\widehat{\mathbf{n}}^{\mathcal{S}}(0)$ of the uncoupled system.

5.3.2 Two-population model ODE

Two-population age-structured model can be reduced to the ODE system, as shown in Section 2.6. Number of cells in G_1-phase for rapid-subpopulation is denoted with variable $N^{\mathcal{R}}_{G_1}$, where $N^{\mathcal{R}}_{G_1}(t) = \int_0^T n^{\mathcal{R}}_{G_1}(t,\tau)\,d\tau$, and similar notions have been derived for the rest of the phases. Thus, two-population dynamics can be modelled by six ordinary differential equations, one for each phase, namely:

$$\frac{dN^{\mathcal{R}}_{G_1}}{dt} = 2r^{\mathcal{R}}_{G_2M\to G_1}N^{\mathcal{R}}_{G_2M} - r^{\mathcal{R}}_{G_1\to S}N^{\mathcal{R}}_{G_1} - \rho N^{\mathcal{R}}_{G_1}, \tag{5.3.24}$$

$$\frac{dN^{\mathcal{R}}_{S}}{dt} = r^{\mathcal{R}}_{G_1\to S}N^{\mathcal{R}}_{G_1} - r^{\mathcal{R}}_{S\to G_2M}N^{\mathcal{R}}_{S}, \tag{5.3.25}$$

$$\frac{dN^{\mathcal{R}}_{G_2M}}{dt} = r^{\mathcal{R}}_{S\to G_2M}N^{\mathcal{R}}_{S} - r^{\mathcal{R}}_{G_2M\to G_1}N^{\mathcal{R}}_{G_2M}, \tag{5.3.26}$$

for the rapidly growing sub-population cells and

$$\frac{dN^{\mathcal{S}}_{G_1}}{dt} = \rho N^{\mathcal{R}}_{G_1} + 2r^{\mathcal{S}}_{G_2M\to G_1}N^{\mathcal{S}}_{G_2M} - (r^{\mathcal{S}}_{G_1\to S} + r^{\mathcal{S}}_{G_1\to A})N^{\mathcal{S}}_{G_1}, \tag{5.3.27}$$

$$\frac{dN^{\mathcal{S}}_{S}}{dt} = r^{\mathcal{S}}_{G_1\to S}N^{\mathcal{S}}_{G_1} - r^{\mathcal{S}}_{S\to G_2M}N^{\mathcal{S}}_{S}, \tag{5.3.28}$$

$$\frac{dN^{\mathcal{S}}_{G_2M}}{dt} = r^{\mathcal{S}}_{S\to G_2M}N^{\mathcal{S}}_{S} - r^{\mathcal{S}}_{G_2M\to G_1}N^{\mathcal{S}}_{G_2M}, \tag{5.3.29}$$

$\rho < r^{\mathcal{R}}_{G_1\to S}$ $(\lambda_{\mathcal{R}} > 0)$	$r^{\mathcal{S}}_{G_1\to A} < r^{\mathcal{S}}_{G_1\to S}$ $(\lambda_{\mathcal{S}} > 0)$	$\mathbf{N}(t) \to c_R\mathbf{v}_{\mathcal{R}}e^{\lambda_{\mathcal{R}}t} + c_S\mathbf{v}_{\mathcal{S}}e^{\lambda_{\mathcal{S}}t}$
$\rho < r^{\mathcal{R}}_{G_1\to S}$ $(\lambda_{\mathcal{R}} > 0)$	$r^{\mathcal{S}}_{G_1\to A} > r^{\mathcal{S}}_{G_1\to S}$ $(\lambda_{\mathcal{S}} < 0)$	$\mathbf{N}(t) \to c_R\mathbf{v}_{\mathcal{R}}e^{\lambda_{\mathcal{R}}t}$
$\rho > r^{\mathcal{R}}_{G_1\to S}$ $(\lambda_{\mathcal{R}} < 0)$	$r^{\mathcal{S}}_{G_1\to A} < r^{\mathcal{S}}_{G_1\to S}$ $(\lambda_{\mathcal{S}} > 0)$	$\mathbf{N}(t) \to c_S\mathbf{v}_{\mathcal{S}}e^{\lambda_{\mathcal{S}}t}$
$\rho > r^{\mathcal{R}}_{G_1\to S}$ $(\lambda_{\mathcal{R}} < 0)$	$r^{\mathcal{S}}_{G_1\to A} > r^{\mathcal{S}}_{G_1\to S}$ $(\lambda_{\mathcal{S}} < 0)$	$\mathbf{N}(t) \to 0$

Table 5.2: Long term behaviour of the solution $\mathbf{N}(t)$ (with $t \geq 0$) to equations (5.3.24) - (5.3.29) will depend on the sign of the eigenvalues ($\lambda_{\mathcal{S}}$ and $\lambda_{\mathcal{R}}$) of the system.

for the slower growing sub-population cells. These equations are defined on $t > 0$ with initial conditions specified at $t = 0$.

If the transition rates between compartments are assumed to be positive constants then it can be shown that there are at most two positive real eigenvalues to this system that can be found by solving the characteristic equation for the rapid sub-population:

$$F_{\mathcal{R}}(\lambda) = \frac{(r^{\mathcal{R}}_{G_2M\to G_1} + \lambda)(r^{\mathcal{R}}_{S\to G_2M} + \lambda)(r^{\mathcal{R}}_{G_1\to S} + \rho + \lambda)}{2r^{\mathcal{R}}_{G_1\to S}r^{\mathcal{R}}_{S\to G_2M}r^{\mathcal{R}}_{G_2M\to G_1}}, \tag{5.3.30}$$

where $F_{\mathcal{R}}(\lambda) = 1$. The function $F_{\mathcal{R}}(\lambda)$ is a positive cubic and has dominant positive real solution, as shown in Section 5.3.1, which we call $\lambda_{\mathcal{R}}$.
Similarly, the characteristic equation for the slow sub-population is expressed as

$$F_{\mathcal{S}}(\lambda) = \frac{(r^{\mathcal{S}}_{G_2M\to G_1} + \lambda)(r^{\mathcal{S}}_{S\to G_2M} + \lambda)(r^{\mathcal{S}}_{G_1\to S} + r^{\mathcal{S}}_{G_1\to A} + \lambda)}{2r^{\mathcal{S}}_{G_1\to S}r^{\mathcal{S}}_{S\to G_2M}r^{\mathcal{S}}_{G_2M\to G_1}}. \tag{5.3.31}$$

The equation $F_{\mathcal{S}}(\lambda) = 1$ has only one positive real solution, which we call $\lambda_{\mathcal{S}}$.

The asymptotic analytical solution of this system is described in Table 5.2. This solution depends on the conditions above and can be written in vector form in terms of the positive eigenvalues ($\lambda_{\mathcal{R}}$ and $\lambda_{\mathcal{S}}$) and their corresponding eigenvectors (which we may call $\mathbf{v}_{\mathcal{R}}$ and $\mathbf{v}_{\mathcal{S}}$ respectively) and the constants c_R and c_S obtained via the initial conditions. The long term proportions in the phases depend on the eigenvectors $\mathbf{v}_{\mathcal{R}}$ and $\mathbf{v}_{\mathcal{S}}$ and the time it takes to reach this asymptotic state will depend on the transition rates and the initial conditions. The initial state at $t = 0$ represents the primary culture and the asymptotic solution represents the established cell line. Experimentally rapid sub-population cells dominate a cell line so we proceed by running simulations corresponding to parameters chosen in rows one and two of Table 5.2 where $\lambda_{\mathcal{R}} > 0$.

In Figure 5.5(a), we see a numerical solution of the system obtained using Runge-Kutta methods supplied by the *ode45* function in *MatLab*. The parameter values are summarized in the caption. The rates of the transition between phases were chosen based on the transition rates obtained for unperturbed cell lines in Basse *et al.* (2005). The remaining have been chosen arbitrarily according

to the second row of Table 5.2 so that ρ, the differentiation rate, is smaller than $r^{\mathcal{R}}_{G_1\to S}$, the transition rate from G_1-phase to S-phase for the rapid sub-population cells. Thus $\lambda_{\mathcal{R}}$ is positive and the rapid sub-population of cells increase. In addition the rate to apoptosis in the slow sub-population of cells ($r^{\mathcal{S}}_{G_1\to A}$) is bigger than the G_1 to S-phase transition rate ($r^{\mathcal{S}}_{G_1\to S}$) so $\lambda_{\mathcal{S}}$ is negative. However this does not mean that the slow sub-population cells disappear because there are non-zero slow sub-population cell components in the eigenvector $\mathbf{v}_{\mathcal{R}}$ corresponding to $\lambda_{\mathcal{R}}$. Initially, for the primary culture, we have assumed that the number of slower sub-population cells is higher than the number of rapid sub-population cells, i.e., 99% of slow sub-population cells, 1% of rapid sub-population cells. In Figure 5.5(a), we see the number of slow sub-population cells first decreasing and then increasing again. The growth rate of the slow sub-population cells, after a time delay, is eventually the same as the rapid sub-population cells. This can be explained by looking at row 2 of Table 5.2 where asymptotically the solution behaves like $e^{\lambda_{\mathcal{R}}t}$. Eventually the proportion of rapidly growing sub-population cells is much higher than the proportion of slow growing sub-population cells but the slow growing sub-population cells are still there, that is the slow growing population does not disappear (Figure 5.5(b)). This is theoretically the established cell line.

For our theoretical established cell line, because the proportion of slow sub-population cells to rapid sub-population cells is negligible, we may consider the rapid sub-population cells alone. That is, we set our differentiation rate $\rho = 0$ and investigate equations (5.3.24) - (5.3.26). We can easily calculate the proportions in each phase that become asymptotically constant. Constant proportions in the phases are obtained experimentally in cell lines, in equations (3.2.10). Let $\Pi^{\mathcal{R}}_{G_1}$ be the proportion of rapidly growing cells in the G_1-phase and similar notation for the other phases then we can show:

$$\frac{\Pi^{\mathcal{R}}_{S}}{\Pi^{\mathcal{R}}_{G_1}} = \frac{r^{\mathcal{R}}_{G_1\to S}}{r^{\mathcal{R}}_{S\to G_2M} + \lambda_{\mathcal{R}}}, \tag{5.3.32}$$

$$\frac{\Pi^{\mathcal{R}}_{G_2M}}{\Pi^{\mathcal{R}}_{S}} = \frac{r^{\mathcal{R}}_{S\to G_2M}}{r^{\mathcal{R}}_{G_2M\to G_1} + \lambda_{\mathcal{R}}}, \tag{5.3.33}$$

$$\Pi^{\mathcal{R}}_{G_1} + \Pi^{\mathcal{R}}_{S} + \Pi^{\mathcal{R}}_{G_2M} = 1. \tag{5.3.34}$$

We can compute the average cell age in each phase from equations (2.5.42) in Chapter 2 (by taking aging times $\tau_p \to 0$, for $p \in \{G_1, S, G_2M\}$) as follows:

$$T^{\mathcal{R}}_{G_1} = \frac{\Pi^{\mathcal{R}}_{G_1}}{(r^{\mathcal{R}}_{G_1\to S} + \lambda_{\mathcal{R}})}, \tag{5.3.35}$$

$$T^{\mathcal{R}}_{S} = \frac{\Pi^{\mathcal{R}}_{S}}{(r^{\mathcal{R}}_{S\to G_2M} + \lambda_{\mathcal{R}})}, \tag{5.3.36}$$

$$T^{\mathcal{R}}_{G_2M} = \frac{\Pi^{\mathcal{R}}_{G_2M}}{(r^{\mathcal{R}}_{G_2M\to G_1} + \lambda_{\mathcal{R}})}, \tag{5.3.37}$$

for each of G_1, S and G_2M-phases, respectively.
The doubling time for the established cell line is related through the $\lambda_{\mathcal{R}}$ by

$$T^{\mathcal{R}}_{d} = \frac{ln2}{\lambda_{\mathcal{R}}}, \tag{5.3.38}$$

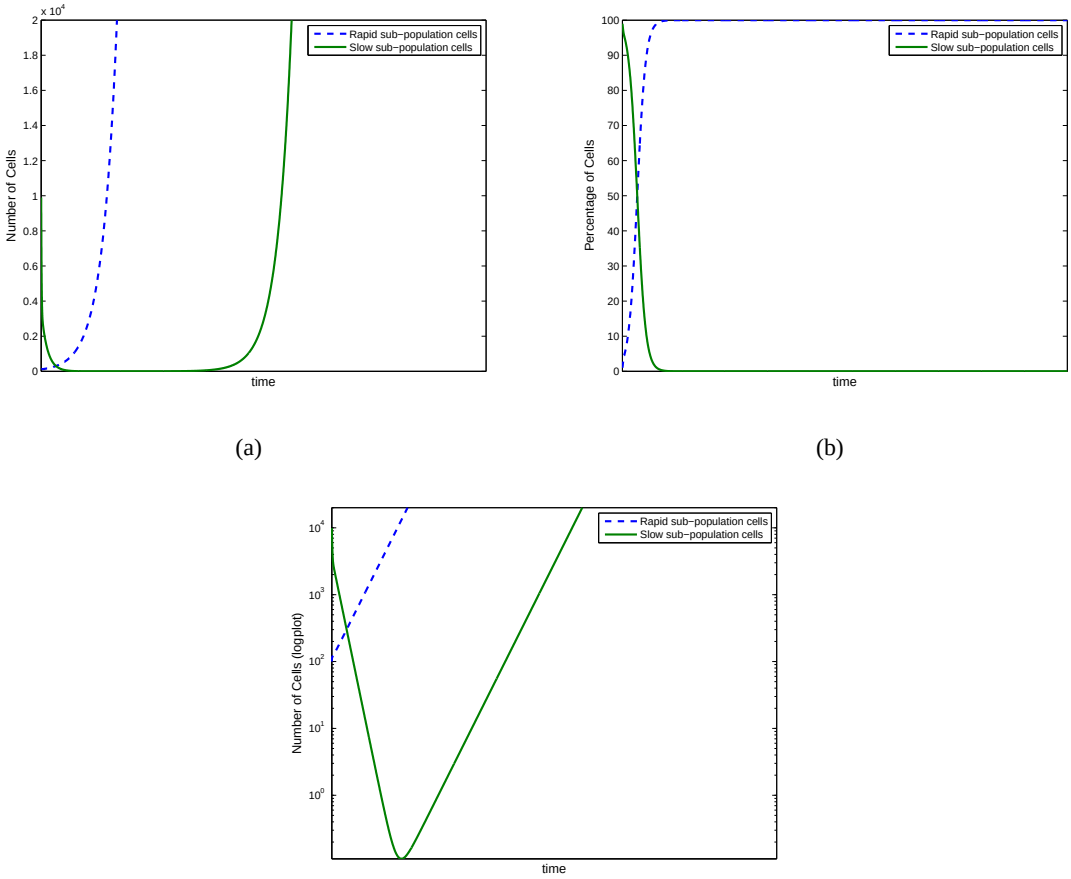

(a) (b)

(c)

Figure 5.5: Simulation of the solution to the system equations (5.3.24) - (5.3.29). Initially we assume there are 10000 cells with 99% slow sub-population cells and 1% rapid sub-population cells. The proportion of cells in each phase for both slow and rapid sub-populations is initially G_1-phase 53%, S-phase 31% and G_2M-phase 16%. The apoptosis rate is constant $r^{\mathcal{S}}_{G_1\to A} = 1$ per hour. Transition rates between the phases for the rapid sub-population cells are $r^{\mathcal{R}}_{G_1\to S} = 0.052729$, $r^{\mathcal{R}}_{S\to G_2M} = 0.052$ and $r^{\mathcal{R}}_{G_2M\to G_1} = 1.8$ per hour. For the slow sub-population cells, we chose the same transition rates as the rapid sub-population cells except for $r^{\mathcal{S}}_{G_1\to S}$ which is chosen to be 10% of $r^{\mathcal{R}}_{G_1\to S}$ ($\alpha = 0.1$) in equation (22). The differentiation rate from rapid sub-population cells to slow sub-population cells is $\rho = 0.00001$ per hour.

and an estimate of the corresponding average cell age is just the sum of the proportions in each phase

$$T^{\mathcal{R}}_a = \left[\frac{\Pi^{\mathcal{R}}_{G_1}}{(r^{\mathcal{R}}_{G_1\to S} + \lambda_{\mathcal{R}})} + \frac{\Pi^{\mathcal{R}}_{S}}{(r^{\mathcal{R}}_{S\to G_2} + \lambda_{\mathcal{R}})} + \frac{\Pi^{\mathcal{R}}_{G_2M}}{(r^{\mathcal{R}}_{G_2M\to G_1} + \lambda_{\mathcal{R}})}\right]. \tag{5.3.39}$$

Thus for an established cell line, we have a relationship between proportions in each phase, rate transitions between phases, population doubling time and cell-age time. Equations (5.3.32)-(5.3.34),

(5.3.38) and (5.3.39) specify these relationships where $\lambda_{\mathcal{R}}$ is determined by solving equation (5.3.30). Numerical explorations of these six equations using the damped Newton's method indicate that even with no cell loss the cell-age time is not equal to the doubling time, demonstrated before in Figure 2.6.

Experimentally, one can determine the proportions in each phase of an established cell line using flow cytometry and estimate cell-cycle times as described in Section 5.2. In the further calculations, we assume that experimentally estimated cell-cycle time is equal to what we refer to as the average cell-age time T_a. We remark here that if we assume that the experimental cell-cycle time is equal to the removal time, introduced in Section 2.5.6, then the qualitative results obtained by using the average cell-age time carry-over to the removal time notion. In this chapter, terms average cell-age and cell-cycle time are interchangeable. One can then obtain all the remaining model parameters using our equations.

5.4 Time dependent apoptosis

In the previous section, we have described a model of a primary culture cell population composed of mainly a slower growing sub-population of cells changing over time into an established cell line composed of mainly rapid sub-population cells and a correspondingly shorter cell-cycle time. We assumed that model parameters were constant, and now we investigate the case where the apoptosis of a progeny cell (slow sub-population cell) occurs after a number of successive cell divisions. This statement is inferred from the kinetics of *in vivo* human tumours, where the volume doubling time is much longer than the calculated average cell-cycle time of the individual tumour cells, implying extensive turnover and therefore death after a number of cell divisions Watson (1991). We do not track individual cells through successive cell divisions but we can incorporate this phenomenon into the model by having the apoptosis rate increasing with time. We chose a sigmoid function for the apoptosis rate

$$r^{\mathcal{S}}_{G_1\to A}(t) = \frac{\mu}{1+\beta_1 e^{-\beta_2 t}}, \tag{5.4.1}$$

as depicted in Figure 5.6.

We see in Figure 5.7(a) that the slower sub-population of cells initially keeps growing while $r^{\mathcal{S}}_{G_1\to A} < r^{\mathcal{S}}_{G_1\to S}$ as shown in the first row of Table 5.2. Since the apoptosis rate value is increasing above $r^{\mathcal{S}}_{G_1\to S}$, we move to the second row of Table 5.2, where the slow sub-population cells decrease. Rapid sub-population cells are resistant to apoptosis and they keep growing exponentially at any apoptosis rate.

5.5 Model applications

5.5.1 Comparing cell-cycle times of primary cultures and established cell lines

In the laboratory experiments, the cell-cycle times of primary cultures are longer than those of established cell lines. This can be seen clearly in Figure 5.8 where the experimental estimates of cell-cycle times (see Table 5.3) of 22 primary cultures and their corresponding cell lines have been plotted. Two studies, one in ovarian cancer and one in brain cancer, have shown that cell-cycle times are related to survival Baguley & Marshall (2004); Furneaux *et al.* (2008); therefore, it is important to understand the underlying dynamics that might cause this phenomenon. In particular, we ask whether our simple ODE model with the two - slow and rapid sub-populations of cells can recover the data in Figure 5.8.

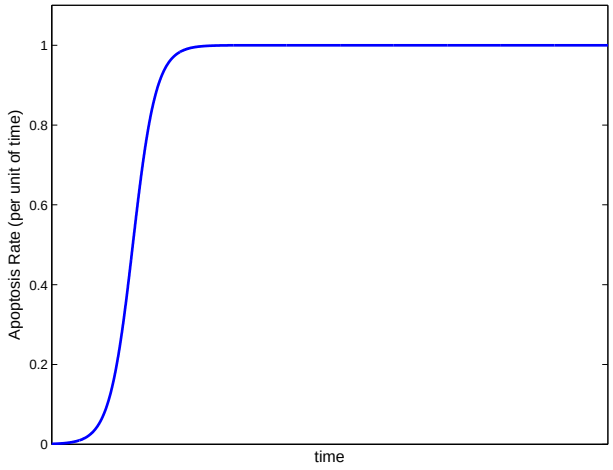

Figure 5.6: The apoptosis rate as a sigmoid function described in equation (5.4.1). Here $\mu = 1, \beta_1 = e^7$ and $\beta_2 = \frac{1}{30}$.

We proceed as follows. For each of 22 established cell lines, we note the experimentally calculated cell-cycle times and the proportions in each of the G_1, S and G_2M phases (see Table 5.3). We assume that the proportion of slow sub-population cells in the established cell line is small compared to the rapid sub-population cells and we use the six equations (5.3.32)-(5.3.34),(5.3.38), (5.3.39) and (5.3.30) to find the phase transition rates for the rapid sub-population cells. This in turn can give us a model estimate of the cell doubling time, $T_d^{\mathcal{R}}$, for the rapid sub-population cells. As an interesting aside we note that even in the absence of cell death the cell line doubling time is longer than the cell-cycle time for established cell lines, as depicted in Figure 5.9, where we have plotted the model estimate of the doubling time versus the model input of the experimentally obtained cell-cycle time for our 22 cell lines. The relationship between the two is described by the non-linear equations mentioned above but looks almost linear and a least squares regression line has been fitted.

We make the assumption that the difference in cell-cycle times between the slow sub-population cells and the rapid sub-population cells is caused by a longer G_1-phase transit time in the slow sub-population cells. Thus we set the transition probabilities for the slow sub-population cells to be the same as for the rapid sub-population cells with the exception of the rate transition from G_1-phase. We assume that the rate transition from G_1 to S-phase of the rapid sub-population cells is proportional to the rate transition from G_1 to S-phase of the slow sub-population cells, i.e.,

$$r^{\mathcal{S}}_{G_1 \to S} = \alpha r^{\mathcal{R}}_{G_1 \to S}, \tag{5.5.1}$$

where $\alpha \in [0, 1]$ is to be determined in such a way as to recover the cycle time of the primary culture. To obtain the doubling time $T_d^{\mathcal{S}}$ of the primary culture (slow sub-population cells) where

$$T_d^{\mathcal{S}} = \frac{ln2}{\lambda_{\mathcal{S}}}, \tag{5.5.2}$$

we use equation (5.3.31) and the same cell-cycle time formula for slow sub-population cells as for

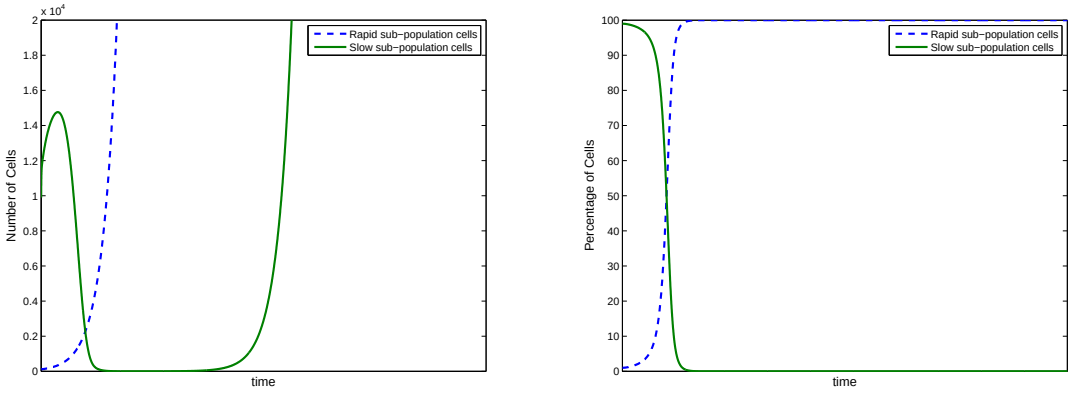

(a)

(b)

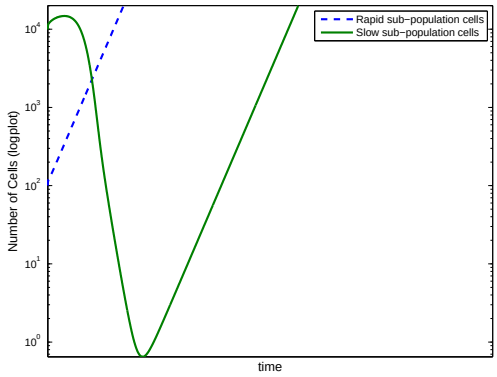

(c)

Figure 5.7: Simulation of the solution to the system equations (5.3.24) - (5.3.29) with parameter values and initial conditions the same as Figure 5.5 except death via apoptosis from G_1-phase of slowly growing sub-population cells is increasing until it reaches a constant value according to the sigmoid function of Figure 5.6.

rapid sub-population cells (equation (5.3.39)) with a change from $\mathcal{R}$ to $\mathcal{S}$ respectively. For the primary culture there was no experimental data for the proportional distribution among phases given. Proportions in each phase can be expressed through the rate transitions using equations (5.3.32)-(5.3.34).

The two unknown parameters α and $\lambda_{\mathcal{S}}$ can be obtained by solving the system of equations (5.3.31) and (5.3.39) with the damped Newton's method. Initial guesses of $\alpha = 0.1$ and $\lambda_{\mathcal{S}} = 0.005$ gave convergence to positive value parameters.

Using equation (5.5.2), we can now calculate doubling times for each of the 22 primary cultures as seen in Figure 5.10. We see from this figure and also Figure 5.9 that the model recovers the experimental data depicted in Figure 5.8.

Patient code	Primary culture T_c (hours)	Cell line T_c (hours)	Percentage G_1 phase	Percentage S phase
NZC01	60	24	57	30
NZEN1	100.8	60	86	8
NZM02	93.6	43.2	62	28
NZM03	93.6	40.8	44	38
NZM04	216	29.8	54	32
NZM09	156	45.6	56	30
NZM12	86.4	25.9	81	11
NZM13	312	76.8	69	16
NZM16	228	50.4	85	7
NZM17	79.2	43.2	66	11
NZM18	163.2	62.5	84	8
NZM19	177.6	63.1	86	10
NZM21	93.6	22.8	84	8
NZM22	213.6	81.4	77	13
NZM24	177.6	39.4	75	13
NZM25	177.6	37.1	80	14
NZM26	105.6	63.1	84	4
NZM28	139.2	38.4	72	24
NZM30	64.8	29.6	69	25
NZM33	132	62.4	64	17
NZM34	105.6	40.8	65	23
NZM56	67.2	33.6	87	12

Table 5.3: Experimentally obtained cell-cycle times (T_c) for 22 primary cultures and their corresponding cell line cell-cycle times. Column 4 and 5 contain data of experimentally obtained percentage distribution among phases for 22 cell lines. Patient codes starting with the NZM correspond to the melanoma cells, NZCO stands for the colorectal cancer cells, NZEN - endometrial.

5.5.2 *In vivo* tumours

A further application of the model is to consider an *in vivo* tumour, which is sustained by a number of (rapid sub-population cells) stem cells in a niche. In choosing parameters, we have assumed that the stem cell population (rapid sub-population cells) has the kinetic properties of the cell line and that the progeny cells (slow sub-population cells) have the kinetic properties of the corresponding primary tumour cultures. Because biologically the micro-environment of the niche has a given size, we set the parameters so that the number of rapid sub-population cells remains constant. This is done by using the threshold case, where $\rho = r^{\mathcal{R}}_{G_1 \to S}$. Deviations from the threshold condition will result in population exponential growth or decay according to Table 5.2. In reality, *in vivo* cell population dynamics are much more complicated. However, our simple linear model is used here to identify the essential population dynamics associated with stem cells and their progeny.

Starting with 100% of cells in the rapid sub-population compartment and 0% in the slower sub-population compartment the entire slow sub-population cell compartment (the tumour cells) is generated over time from rapid sub-population cell proliferation (the stem cells in the niche). The parame-

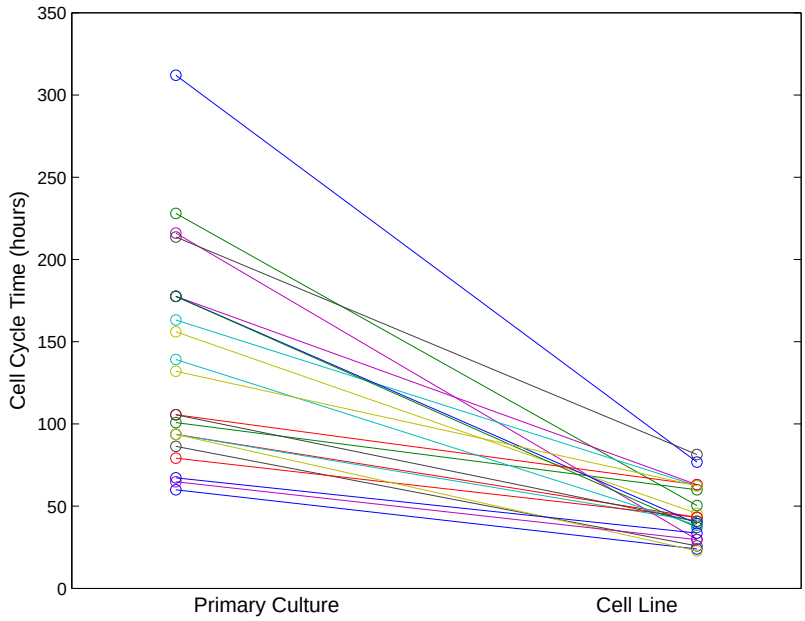

Figure 5.8: Cell-cycle times of 22 primary cultures and corresponding derived cell lines. Recreated from previously published experimental data Baguley & Marshall (2008).

ters of the sigmoid function for the apoptosis rate were chosen by trial and error so that the initial rate is small and the horizontal asymptote is approximately equal to $r^{S}_{G_1 \to S}$. Thus eventually the number of slow sub-population cells becomes constant, i.e., $r^{S}_{G_1 \to A} = r^{S}_{G_1 \to S}$ and $\lambda_S = 0$ (see Table 5.2). Then the total size of the slow sub-population with time resembles a sigmoid function as depicted in Figure 5.11. This is in accordance with experimental estimates of tumour growth being classified as sigmoid (including logistic or Gomperzian growth as described in Kozusko & Bourdeau (2007) and references therein).

The initial number of cells was chosen arbitrarily to be 1000 rapid sub-population cells (stem cells in the niche) and 0 slow sub-population cells (i.e., no tumour). The emphasis here is on the qualitative results where eventually the slow sub-population cells dominate showing that the niche sustains the tumour and results in a sigmoid shaped curve for the number of slow sub-population (tumour) cells. It is the parameter values and where they are chosen from Table 5.2 that dictate the 'long' term behaviour of the slow sub-population cells not the (non-zero) initial size of the stem cell population.

5.6 Discussion and conclusion

The transition from *in vivo* tumour to primary culture to established cell line is biologically complex and not fully understood. In this chapter, we have described a simplistic mathematical model, which does not address this degree of complexity but aims to capture the essential population dynamics of these transitions by considering theoretically interacting stem cell and progeny populations. We did this by formulating six differential equations for a cohort of cells comprising of two sub-populations.

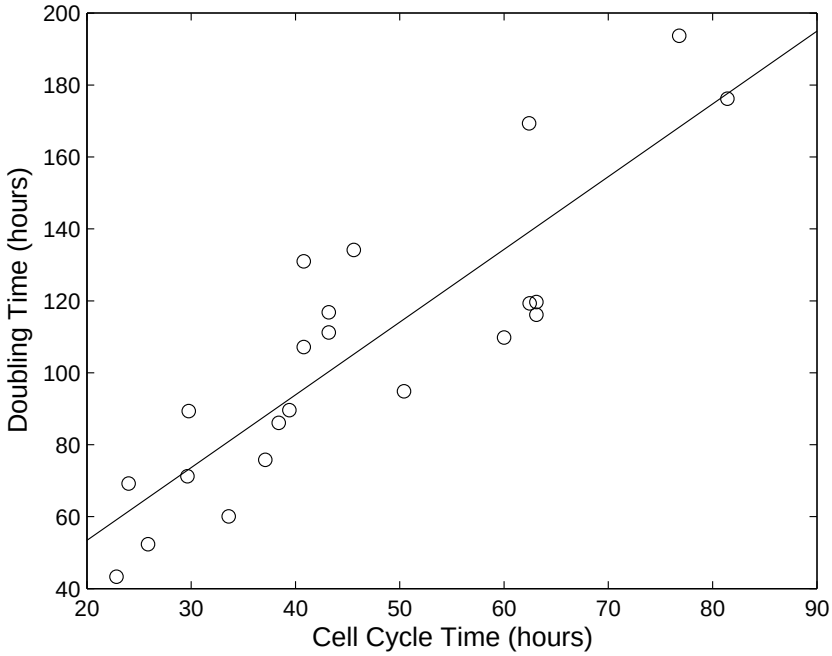

Figure 5.9: Cell line doubling time vs. cell line cycle time for 22 cell lines. Cell-cycle time on the horizontal axis are experimental data that are used in addition to experimentally obtained percentage distributions Π_{G_1}, Π_S in order to calculate cell line doubling time (vertical axis). Each dot represents a particular cell line. A least-squares line is fitted through the scatter plot (coefficient of determination $r^2 = 0.75$).

One exhibiting slow population growth (the 'slow sub-population cells') and the other having a faster population growth rate (the 'rapid sub-population cells'). Each sub-population is further divided corresponding to three distinct phases of the cell cycle (G_1, S and G_2M phase) with transition rates between phases. The slow sub-population cells are a mortal population with death via apoptosis from G_1-phase. The rapid sub-population cells can differentiate to become slow sub-population cells according to the differentiation rate ρ.

If transition rates are constant then the asymptotic solution of the corresponding differential equation system are summarised in Table 5.2. The initial condition ($t = 0$) is chosen to represent a primary culture and is composed of mainly slow sub-population cells. The asymptotic solution corresponds to an established cell line and comprises mainly rapid sub-population cells.

We considered the case of rapid sub-population cells alone, i.e., an established cell line. We found relationships (as described by equations (5.3.32)-(5.3.34), (5.3.38),(5.3.39) and (5.3.30)) between the proportions in each phase, the rate transitions between phases, the population doubling time and the average cell age. These relationships confirm that even with no cell loss the average cell age is not equal to the doubling time. The following simple example illustrates that as soon as synchrony is broken the average cell age will be different to the cell doubling time. Consider two cells in perfect synchrony starting the cell age at the same time and each having the same average cell-age. In this case, the average cell-age is equal to the population doubling time. If this synchrony is broken by each cell having its own average cell age T_a^1 and T_a^2, respectively, where say that T_a^1 is slightly smaller

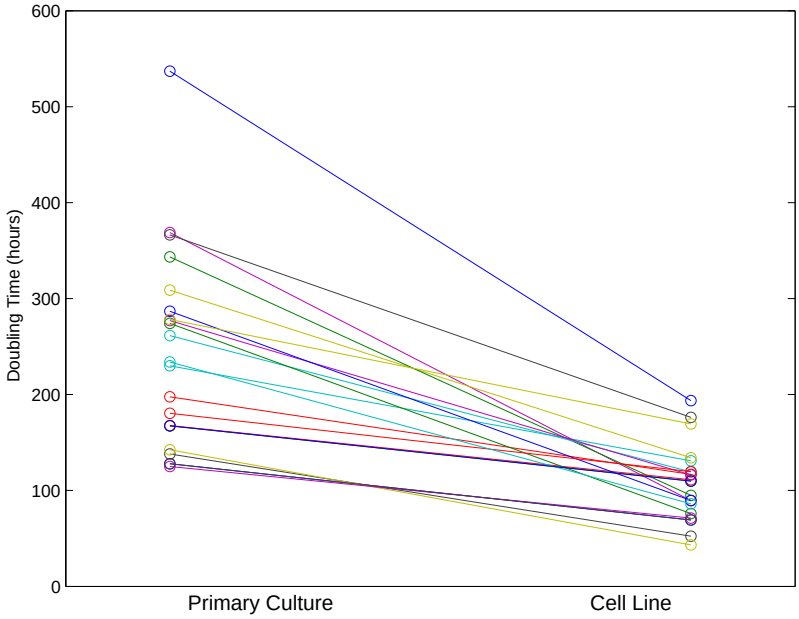

Figure 5.10: Cell doubling times of 22 primary cultures and corresponding derived cell lines. Doubling time of the cell lines was calculated using experimentally obtained cell-cycle times and proportions in each phase, for primary cultures this was achieved using experimental cell-cycle times and model derived rapid sub-population cell transition rates.

than T_a^2 then the population will double at time $T_d = T_a^2$ and the average cell-age will be $(T_a^1 + T_a^2)/2$ which will be smaller than the doubling time. Our data has resulted in doubling times being greater than average cell-age as depicted in Figure 5.9.

In calculations, we assumed that experimentally estimated cell-cycle time is equal to what we refer to as the average cell-age T_a. We remark here that if we assume that the experimental cell-cycle time is equal to the average removal time, introduced in Section 2.5.6, then the qualitative results of the average cell-age time carry-over to the average removal time notion. In this chapter, terms average cell-age and the experimental cell-cycle time are interchangeable. More importantly, if one has experimental estimates of the cell-cycle time (or doubling time) and the proportions in any two phases then one can use the mathematical model equations to estimate the population doubling time (or the average cell age of the population) for a particular cell line. This model can be easily extended for the mathematical estimation of the average removal times. We used the model to recover average cell age of primary cultures given the experimental cell-cycle times of established cell lines.

As a further application of the model we considered an *in vivo* case of a tumour being sustained by a niche of (a constant number of) stem cells. We assumed initially no slow sub-population cells but over time the rapid sub-population cells differentiated to become slow sub-population cells. The population of the slow sub-population cells was sigmoid that corresponds to empirical estimates of tumour growth.

The concept that the fraction of stem cells in tumour samples and cell lines is small has been reported in a number of papers. However, a recent publication has shown that when cells isolated

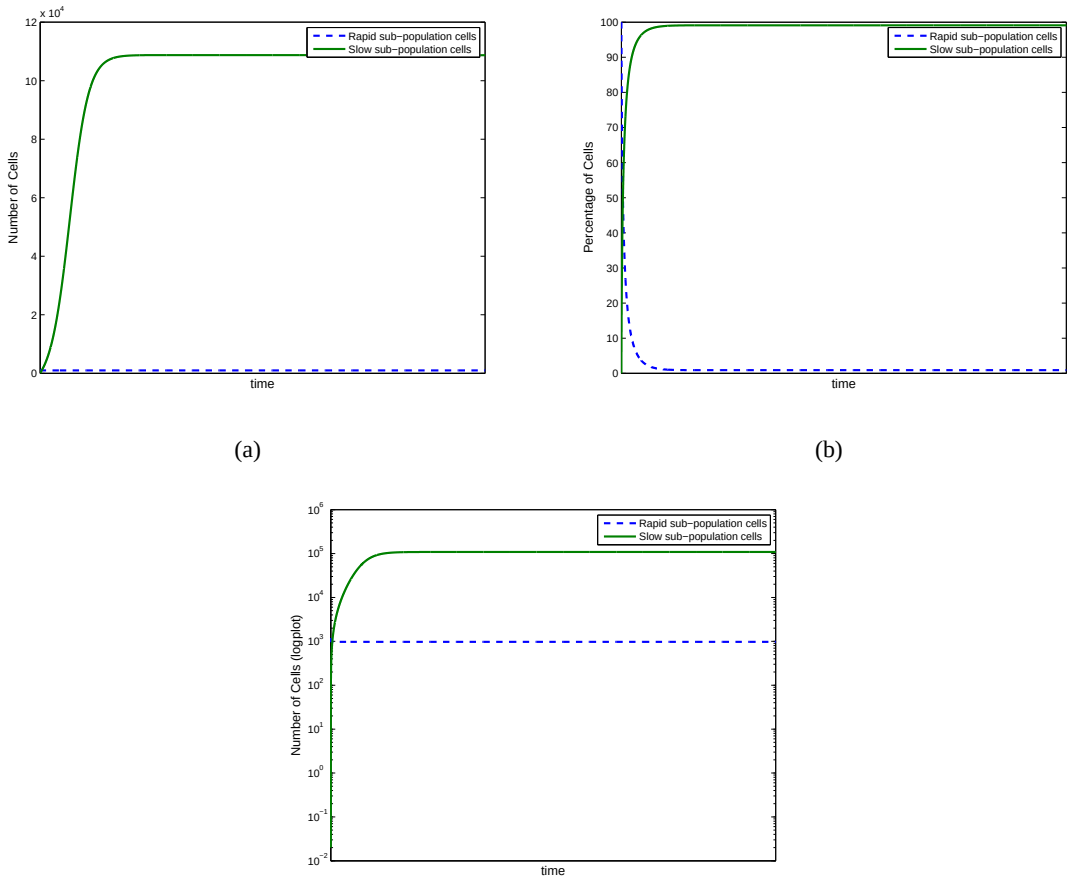

(a) (b)

(c)

Figure 5.11: Simulation of the solution to the system equations (5.3.24) - (5.3.29). Initially we assume there are 1000 cells with 0% slow sub-population cells and 100% rapid sub-population cells. The proportion of cells in each phase for rapid sub-populations is initially G_1-phase 53%, S-phase 31% and G_2M-phase 16%. Transition rates between the phases for the rapid sub-population cells are $r^{\mathcal{R}}_{G_1\to S} = 0.052729$, $r^{\mathcal{R}}_{S\to G_2M} = 0.052$ and $r^{\mathcal{R}}_{G_2M\to G_1} = 1.8$ per hour. For the slow sub-population cells we chose the same transition rates as the rapid sub-population cells except for $r^{\mathcal{S}}_{G_1\to S}$ which is chosen to be 10% of $r^{\mathcal{R}}_{G_1\to S}$. The differentiation rate from rapid sub-population cells to slow sub-population cells is $\rho = r^{\mathcal{R}}_{G_1\to S}$ per hour. $r^{\mathcal{S}}_{G_1\to A}$ is a sigmoid function, where $\mu = 0.005528$, $\beta_1 = e^{3.3}$ and $\beta_2 = \frac{1}{200}$.

from human melanomas are grown in host mice with a high degree of immunosuppression, up to 25% of cells are able to grow into tumours and should thus be defined as tumour stem cells Quintana *et al.* (2008).

Stem cells in normal tissue are normally slow growing but this slow growth is maintained by the niche microenvironment and in response to an appropriate stimulus (e.g. depletion of cells) stem cells can divide rapidly. The signalling pathways that maintain normal stem cells in a slow growing state may be defective in tumour stem cells, but definitive evidence is lacking because tumour stem cells cannot be identified in situ. The range of cycle times determined for the primary cultures is similar to

that for the bulk of tumour cells reported *in vivo*.

An understanding of the underlying kinetics of cell lines and the relationship with those of primary cultures is essential to understanding how human patients with *in vivo* tumours respond to cancer therapy. Cell-cycle times of cell lines are related to cell-cycle times of primary culture and our simple mathematical model goes some way towards explaining that. Since the cell-cycle time of a cell line is a measure of patient survival it is important to see how this relates back to the *in vivo* case.

Chapter 6

Conclusions and Suggestions for Further Work

In this thesis, investigation of the age-structured models has led to the derivation of biologically significant parameters describing the dynamics of an exponentially growing cancer cell population. We have shown the relationship between the average cell-cycle time (also called the average cell-removal time) and the population doubling time, where the cell-cycle time of the population is greater or equal to the population doubling time. This result is of great interest to biologists, as they generally assume that the cell-cycle time is always equal to the population doubling time.

In Chapter 2, we have proven the existence of the balanced exponential growth state for the age-structured model with piecewise continuous transition rates. For the case of piecewise constant transition rates, we have derived analytical formulae for the population distribution among the cell-cycle phases, the average cell age and the expected (average) removal time for the population in BEG. We note that the average age of the cells removed from all phases is the average cell-cycle time. Our expression for the average cell removal time can be found in the literature, where it has been referred to as the cell-cycle time of the population. However, the formulae in the literature has been assumed and then verified by using a discrete computational simulation, whereas, in this thesis, it has been derived from the age-structured model with piecewise constant transition rates. Furthermore, we have shown that a delay differential equation system can be obtained from the age-structured model with piecewise constant transition rates. We presented the reduction of the age-structure model to the ordinary differential equation model and thereafter applied it in the analysis of the cancer cell population response to various cancer treatments. A study of a case of piecewise linear transition rates, would provide a further generalisation of the model.

In Chapter 3, we have derived an analytical expression for the estimation of the population doubling time from a single experimental observation point using the stathmokinetic method. In the literature, this method has been proposed from empirical studies. Furthermore, our mathematical model has provided justification for the stathmokinetic method and presented simple analytical formulae that could be useful for biologists. A further extension of this model would involve: first, incorporating the necessary aging times of cells in each phase of the cell cycle to increase biological realism of the model; and second, deriving expressions to estimate the cell-cycle time from a single experimental observation of the plateau log reduction value, similar to the ones presented in Table 3.2 for the doubling time. We aim to elaborate on the model in Chapter 3 and publish this result.

In Chapter 4, we have analysed the effects of the radiotherapy on five melanoma cell lines via mathematical modelling. Our mathematical model was constructed with the objective of estimating

the proportion of cells that continue to proliferate after a one-time ionising radiation dose. Flow cytometry profiles of five melanoma cell lines exposed to three types of cancer treatment were utilised in the optimization routine. This provided the uniqueness of the numerical results. We have concluded that little apoptosis occurs initially after irradiation. However, this result contradicts the empirical estimates of the surviving fractions. Therefore, we have reasoned that our high magnitudes of the proliferating cell proportions in each phase at time zero post irradiation suggests that some cells, although sustaining DNA damage from irradiation, continue to divide several times before undergoing apoptosis. A further extension of this study would involve the application of our model to the experimental data for the same cell lines but with longer observation times, thus providing a better understanding of the numbers of cells undergoing apoptosis after dividing several times following irradiation.

In Chapter 5, we have proved the existence of the BEG state for the age-structured model depicting the growth of the cell population composed of two sub-populations with different kinetic parameters. Furthermore, the age-structured model was reduced to the ordinary differential equation model and applied to provide an insight into the transition from *in vivo* tumour to primary culture to established cell line. The linearity of our mathematical model does not cover the biological complexity of this problem. However, it provides a small insight into the hypothesis that a cancer tissue is sustained by a minor population of proliferating stem cells. The extension of the mathematical models presented in this thesis to describe the dynamics of cells in the primary culture may be of a great interest to biologists as its dynamics reflect the conditions of malignant tumour dynamics.

Appendix A

Appendix

A.1 The existence and uniqueness theorem from Linz (1985)

When the kernel is unbounded (or has some irregular behaviour) it is often convenient to rewrite linear second kind Volterra equation $f(t) = g(t) + \int_0^t k(t,s)f(s)\,ds$, as follows:

$$f(t) = g(t) + \int_0^t p(t,s)\,k(t,s)\,f(s)\,ds, \tag{A.1.1}$$

where $p(t,s)$ represents the part with the non-smooth behaviour.

Theorem A.1.1. *Assume that in equation A.1.1*

1. *$g(t)$ is continuous in $0 \le t \le T$,*
2. *$k(t,s)$ is continuous in $0 \le s \le t \le T$,*
3. *for each continuous function h and all $0 \le \tau_1 \le \tau_2 \le t$, the integrals*

$$\int_{\tau_1}^{\tau_2} p(t,s)\,k(t,s)\,h(s)\,ds \tag{A.1.2}$$

and

$$\int_0^t p(t,s)\,k(t,s)\,h(s)\,ds \tag{A.1.3}$$

are continuous functions of t,

4. *$p(t,s)$ is absolutely integrable with respect to s for all $0 \le t \le T$,*
5. *there exist points $0 = T_0 < T_1 < T_2 < \ldots < T_N = T$ such that with $t \ge T_i$*

$$\mathbb{K}\int_{T_i}^{\min(t,T_{i+1})} |p(t,s)|\,ds \le \alpha < 1, \tag{A.1.4}$$

where

$$\mathbb{K} = \max_{0\le s\le t\le T} |k(t,s)|, \tag{A.1.5}$$

6. *for every* $t \geq 0$

$$\lim_{\delta \to 0^+} \int_t^{t+\delta} |p(t+\delta, s)|\, ds \;=\; 0. \tag{A.1.6}$$

Then A.1.1 has a unique continuous solution in $0 \leq t \leq T$.

A.2 The Perron-Frobenius theorem

The Perron-Frobenius theorem describes the eigenvalues and eigenvectors of a nonnegative matrix A. Its most important conclusion is that there generally exists one eigenvalue that is greater than or equal to any of the others in magnitude. Without loss of generality, we can call this eigenvalue λ_1; it is called the dominant eigenvalue of A. The properties of nonnegative matrices have been subdivided into two cases: reducible and irreducible. Irreducible matrices have been further subdivided into primitive and imprimitive, Caswell (2001).

A.2.1 Irreducible but imprimitive matrices

A nonnegative matrix is irreducible if and only if its life cycle graph contains a path from every node to every other node. An imprimitive matrix is said to be cyclic and to have an index of imprimitivity d equal to the greatest common divisor of the loop lengths in the life cycle graph.

Theorem A.2.1. *If the matrix A is irreducible but imprimitive, with index of primitivity d, then there exists a real positive eigenvalue* λ_1*, which is a simple root of the characteristic equation. The associated right and left eigenvectors* w_1 *and* v_1 *are positive.*
The dominant eigenvalue λ_1 *is greater than or equal in magnitude to any of the other eigenvalues, i.e.,*

$$\lambda_1 \geq |\lambda_i|, \qquad i > 1, \tag{A.2.1}$$

but the spectrum of A contains d eigenvalues equal in magnitude to λ_1*. One* λ_1 *itself, and the others are the* $d - 1$ *complex eigenvalues:*

$$\lambda_1 \exp 2k\pi i/d \qquad k = 1, 2, \ldots d - 1. \tag{A.2.2}$$

A.2.2 Reducible matrices

Theorem A.2.2. *Is A is reducible, there exists a real eigenvalue* $\lambda_1 \geq 0$ *with corresponding right and left eigenvectors* $w_1 \geq 0$ *and* $v_1 \geq 0$*. This eigenvalue* $\lambda_1 \geq |\lambda_i|, \qquad i > 1.$

Appendix B

Appendix

B.1 Proof of Theorem 3.2.1 - nonlinear mapping properties

As discussed in Section 3.2.1 in Chapter 3 for an established cell line, we have a relationship between proportions in each phase, the rate transitions between phases, the population doubling time and this can be reduced to an implicit relationship involving $\mathbf{r} = \{\mathbf{r_{G_1 \to S}}, \mathbf{r_{S \to G_2 M}}, \mathbf{r_{G_2 M \to G_1}}\}$, and $\boldsymbol{\sigma} = \{\Pi_{G_1}, \Pi_S, \lambda\}$. So it can be shown that the system can be written

$$\mathbf{G}(\mathbf{r}, \boldsymbol{\sigma}) = \mathbf{G}(\mathbf{r_{G_1 \to S}}, \mathbf{r_{S \to G_2 M}}, \mathbf{r_{G_2 M \to G_1}}, \mathbf{\Pi_{G_1}}, \mathbf{\Pi_S}, \lambda) = \mathbf{0}. \tag{B.1.1}$$

The existence of functional relationships between the variables will be determined by the implicit function theorem and this is conditional on certain characterisations of the jacobian matrix of $\mathbf{G}$, which is given by

$$\begin{aligned} J_G &= \left[\begin{array}{cc|ccc} \frac{-\Pi_S}{\Pi_{G_1}^2} & \frac{1}{\Pi_{G_1}} & \frac{r_{G_1 \to S}}{(r_{S \to G_2 M}+\lambda)^2} & \frac{-1}{(r_{S \to G_2 M}+\lambda)} & \frac{r_{G_1 \to S}}{(r_{S \to G_2 M}+\lambda)^2} & 0 \\ \frac{-1}{\Pi_S} & \frac{-\Pi_{G_2 M}}{\Pi_S^2} & \frac{r_{S \to G_2 M}}{(r_{G_2 M \to G_1}+\lambda)^2} & 0 & \frac{-1}{(r_{G_2 M \to G_1}+\lambda)} & \frac{r_{S \to G_2 M}}{(r_{G_2 M \to G_1}+\lambda)^2} \\ 0 & 0 & \partial_\lambda F & \partial_{r_{G_1 \to S}} F & \partial_{r_{S \to G_2 M}} F & \partial_{r_{G_2 M \to G_1}} F \end{array}\right] \\ &= \left[\begin{array}{cc|c} J_{\boldsymbol{\sigma}} & | & J_{\mathbf{r}} \end{array}\right] \end{aligned}$$

Here

$$\begin{aligned} \partial_\lambda F &= \frac{1}{2 r_{G_1 \to S} r_{S \to G_2 M} r_{G_2 M \to G_1}} \left[(r_{S \to G_2 M} + \lambda)(r_{G_1 \to S} + \lambda) + \right. \\ &\qquad \left. (r_{G_2 M \to G_1} + r_A + \lambda)(r_{G_1 \to S} + \lambda) + (r_{G_2 M \to G_1} + r_A + \lambda)(r_{S \to G_2 M} + \lambda) \right], \end{aligned} \tag{B.1.2a}$$

$$\partial_{r_{G_1 \to S}} F = \frac{1}{2 r_{G_1 \to S} r_{S \to G_2 M} r_{G_2 M \to G_1}} \left[(r_{G_2 M \to G_1} + r_A + \lambda)(r_{S \to G_2 M} + \lambda) \right] - \frac{F(\lambda)}{r_{G_1 \to S}}, \tag{B.1.2b}$$

$$\partial_{r_{S \to G_2 M}} F = \frac{1}{2 r_{G_1 \to S} r_{S \to G_2 M} r_{G_2 M \to G_1}} \left[(r_{G_2 M \to G_1} + r_A + \lambda)(r_{G_1 \to S} + \lambda) \right] - \frac{F(\lambda)}{r_{S \to G_2 M}}, \tag{B.1.2c}$$

$$\partial_{r_{G_2 M \to G_1}} F = \frac{1}{2 r_{G_1 \to S} r_{S \to G_2 M} r_{G_2 M \to G_1}} \left[(r_{G_1 \to S} + \lambda)(r_{S \to G_2 M} + \lambda) \right] - \frac{F(\lambda)}{r_{G_2 M \to G_1}}, \tag{B.1.2d}$$

with F given by equation (3.2.6). We have partitioned J into the first three columns, and called this

square matrix $J_{\boldsymbol{\sigma}}$, with the remaining three columns called $J_{\mathbf{r}}$, and then the implicit function theorem assures us that the jacobian $J_{\mathbf{r}} = \frac{d\boldsymbol{\sigma}}{d\mathbf{r}}$ exists locally provided the jacobian J_σ is non singular, i.e.,

$$\det J_\sigma = \partial_\lambda F \left(\frac{\Pi_{G_2 M}}{\Pi_S \Pi_{G_1}} + \frac{1}{\Pi_S \Pi_{G_1}} \right) > 0. \tag{B.1.3}$$

This is true if $\partial_\lambda F > 0$ as the proportional of cells in each phase are positive. To see that the condition on F is true for the domain under consideration here, we note for exponential growth that $\lambda > 0$, and all the rates in equation (B.1.2a) are also positive, so that $\partial_\lambda F > 0$. Hence the map $\boldsymbol{\sigma} = R(\mathbf{r})$ is locally unique and determined.

To invert this mapping we must look into the singularity of J_r and this can be determined from

$$\det J_r = \frac{1}{(r_{S\to G_2 M} + \lambda)} \left(\frac{r_{S\to G_2 M} \partial_{r_{G_2 M \to G_1}} F}{(r_{G_2 M \to G_1} + \lambda)} + \frac{r_{S\to G_2 M} \partial_{r_{S\to G_2 M}} F}{(r_{G_2 M \to G_1} + \lambda)^2} \right) + \frac{\partial_{r_{G_1 \to S}} F r_{G_1 \to S} r_{S\to G_2 M}}{(r_{S\to G_2 M} + \lambda)(r_{G_2 M \to G_1} + \lambda)^2} > 0, \tag{B.1.4}$$

so that provided $\det J_r \neq 0$ anywhere, a local map $\mathbf{r}(\boldsymbol{\sigma})$ will exist almost everywhere.

To prove this, we first look at equation (B.1.2b) and see this can be written

$$\partial_{r_{G_1 \to S}} F = F(\lambda) \left[\frac{1}{(r_{G_1 \to S} + \lambda)} - \frac{1}{r_{G_1 \to S}} \right], \tag{B.1.5}$$

and in S', $F(\lambda) = 1$, with $\lambda > 0$ so

$$\partial_{r_{G_1 \to S}} F < 0. \tag{B.1.6}$$

A similar argument applies to the other two derivatives of F in equation (B.1.2). As in S' all the transition probabilities and λ are positive, it follows $\det J_r < 0$ and we have the result.

B.2 Approximate solution of $F(\lambda) - 1 = 0$

To enable this, we first look at the dependence of $F(\lambda) = 1$ on λ, example of $F(\lambda) = 1$ plot shown in Figure 2.4. So with the understanding of approximating the graph of $F(\lambda)$, we consider a quadratic that crosses the x-axis at $-\beta$, $-\alpha$ and the y-axis at γ and that is positive for large x. We also assume that $\beta < \alpha$. Then this quadratic is

$$y(x) = \frac{\gamma}{\alpha\beta}(x + \beta)(x + \alpha). \tag{B.2.1}$$

Again with consideration of equation (3.2.6), we consider the roots of the equation $y(x) = 1$, and these are given by

$$x = \frac{1}{2} \left[-(\beta + \alpha) \pm \sqrt{(\beta + \alpha)^2 + \frac{4\alpha\beta}{(\beta + \alpha)^2} (\frac{1}{\gamma} - 1)} \right]. \tag{B.2.2}$$

With the assumption $\frac{4\alpha\beta}{(\beta+\alpha)^2}(\frac{1}{\gamma} - 1) << 1$ the positive root is given by

$$\frac{\alpha\beta}{(\beta + \alpha)}(\frac{1}{\gamma} - 1). \tag{B.2.3}$$

When $\frac{\alpha}{(\beta+\alpha)} \approx 1$, which is true for $|\alpha|$ large. We then find an approximation to the positive root is

$$x \approx \beta(\frac{1}{\gamma} - 1) - \mathcal{O}(\frac{\beta}{\alpha}), \quad \beta < \alpha. \tag{B.2.4}$$

We observe that the root found to $y(x) = 1$ if a linear polynomial is fitted through the x-axis at $-\beta$, and the y-axis at γ, i.e., $y(0) = \gamma$ is equation (B.2.4) with no error term. So the degree of approximation is determined by how close $\frac{\alpha}{(\beta+\alpha)} \approx 1$. In conclusion, the linear approximation of λ in equation (3.2.6), when α, β are chosen from $r_{S\to G_2M}$, $r_{S\to G_2M}$ depending on which is larger, and the y-axis crossing is $1/2$, is given by equation (3.3.14). This is because

$$\alpha = \max\Big(|r_{G_1\to S}|, |r_{S\to G_2M}|\Big), \quad \beta = \min\Big(|r_{G_1\to S}|, |r_{S\to G_2M}|\Big), \tag{B.2.5}$$

and $\gamma = 2$.

B.3 Phase solutions with no division in Chapter 3

We consider the solution when the system is *not* exhibiting BEG. Solving equations (3.2.1), when the transition rates between compartments are assumed to be positive constants and $r_{G_2M\to G_1}$ is set to zero, gives us analytical formulas for the number of cells N_p, $p \in \{G_1, S, G_2M\}$, in each of the phases. We can subdivide the solution of the ODE system into two cases. Firstly, let $r_{G_1\to S} \neq r_{S\to G_2M}$, then the system of differential equations (3.2.1) can be solved analytically as follows:

$$N_{G_1}(t) = N_{G_1}(0)e^{-r_{G_1\to S}t}, \tag{B.3.1a}$$

$$N_S(t) = N_{G_1}(0)\frac{r_{G_1\to S}}{r_{S\to G_2M} - r_{G_1\to S}}\Big(e^{-r_{G_1\to S}t} - e^{-r_{S\to G_2M}t}\Big) + N_S(0)e^{-r_{S\to G_2M}t}, \tag{B.3.1b}$$

$$N_{G_2M}(t) = \Big(\frac{r_{G_1\to S}r_{S\to G_2M}}{(r_A - r_{G_1\to S})(r_A - r_{S\to G_2M})}N_{G_1}(0) + \frac{r_{S\to G_2M}}{r_{S\to G_2M} - r_A}N_S(0) + N_{G_2M}(0)\Big)e^{-r_At} \tag{B.3.1c}$$

$$+ \frac{r_{S\to G_2M}}{r_A - r_{S\to G_2M}}\Big(N_S(0) - \frac{r_{G_1\to S}}{r_{S\to G_2M} - r_{G_1\to S}}N_{G_1}(0)\Big)e^{-r_{S\to G_2M}t} \tag{B.3.1d}$$

$$+ \frac{r_{G_1\to S}r_{S\to G_2M}}{(r_{S\to G_2M} - r_{G_1\to S})(r_A - r_{G_1\to S})}N_{G_1}(0)e^{-r_{G_1\to S}t}. \tag{B.3.1e}$$

Secondly, when $r_{G_1\to S} = r_{S\to G_2M}$, the analytical solution of the system (3.2.1) is:

$$N_{G_1}(t) = N_{G_1}(0)e^{-r_{G_1\to S}t}, \tag{B.3.2a}$$

$$N_S(t) = [N_S(0) + tN_{G_1}(0)r_{G_1\to S}]e^{-r_{G_1\to S}t}, \tag{B.3.2b}$$

$$N_{G_2M}(t) = \Big(N_{G_2M}(0) - \frac{1}{r_A - r_{G_1\to S}}N_S(0)\Big)e^{-r_At} + \frac{1}{r_A - r_{G_1\to S}}\Big(N_S(0) + r_{G_1\to S}N_{G_1}(0)t\Big)e^{-r_{G_1\to S}t}. \tag{B.3.2c}$$

But solution (B.3.2) will occur with probability of zero when running a Monte Carlo simulation such as in Section 3.3.3 so it is not considered further.

References

Alberts, B., Bray, D., Lewis, J., Raff, M., Roberts, K. & Watson, J.D. (1994). *Molecular biology of the cell*. Garland Publishing , Inc. 1

Andrade, R., Crisol, L., Prado, R., Boyano, M.D., Arluzea, J. & Arechaga, J. (2010). Plasma membrane and nuclear envelope integrity during the blebbing stage of apoptosis: a time-lapse study. *Biology of the Cell*, **102**, 25–35. 36

Arino, O. (1995). A survey of structured cell population dynamics. *Acta Biotheoretica*, **43**, 3 – 25. 9

Baguley, B.C. (2006). Tumor stem cell niches: a new functional framework for the action of anticancer drugs. *Recent Patents on Anti-Cancer Drug Discovery*, **1**, 121 – 127. 85

Baguley, B.C. (2011). The paradox of cancer cell apoptosis. *Frontiers in Bioscience*, **16**, 1759 – 1767. 36, 57

Baguley, B.C. & Marshall, E.S. (2004). In vitro modelling of human tumour behaviour in drug discovery programmes. *European Journal of Cancer*, **40**, 794 – 801. 3, 11, 86, 88, 97

Baguley, B.C. & Marshall, E.S. (2008). The use of human tumour cell lines in the discovery of new cancer chemotherapeutic drugs. *Expert Opin. Drug Discov.*, **3**, 153 – 161. 3, 86, 101

Baguley, B.C., Marshall, E.S., Whittaker, J.R., Dotchin, M.C., Nixon, J. & McCrystal, M.R. (1995). Resistance mechanisms determining the in vitro sensitivity to paclitaxel of tumour cells cultured from patients with ovarian cancer. *European Journal of Cancer*, **31A**, 230 – 237. 36, 37, 41, 42, 43, 44, 46, 47, 48, 49, 51, 52, 53, 88

Baguley, B.C., Marshall, E.S. & Finlay, G.J. (1999). Short-term cultures of clinical tumor material: potential contributions to oncology research. *Oncology Research*, **11**, 115 – 124. 37, 41, 53

Baguley, B.C., Marshall, E.S. & Christmas, T.I. (2002). Cultures of surgical material from lung cancers. A kinetic approach. *Lung Cancer. Molecular Pathology Methods and Reviews.*, **1**, 527 – 544. 3

Barazzoul, L., Burnet, N., Jena, R., Jones, B., Jefferies, S. & Kirkby, N. (2010). A mathematical model of brain tumour response to radiotherapy and chemotherapy considering radiobiological aspects. *Journal of Theoretical Biology*, **262**, 553 – 565. 55

Barnes, J., Collins, B., Luft, C. & Allen, J. (2001). Expression of inducible Hsp70 enhances the proliferation of MCF-7 breast cancer cells and protects against the cytotoxic effects of hyperthermia. *Cell Stress & Chaperones*, **6**, 316–325. 36

REFERENCES

Basse, B. & Ubezio, P. (2007). A generalised age- and phase-structured model of human tumour cell populations both unperturbed and exposed to a range of cancer therapies. *Bulletin of Mathematical Biology*, **69**, 1673 – 1690. 10, 16, 29, 86

Basse, B., Baguley, B.C., Marshall, E.S., Joseph, W.R., Van Brunt, B., Wake, G.C. & Wall, D.J.N. (2003). A mathematical model for analysis of the cell cycle in cell lines derived from human tumors. *Journal of Mathematical Biology*, **47**, 295 – 312. 10, 36, 41, 86

Basse, B., Baguley, B.C., Marshall, E.S., Joseph, W.R., van Brunt, B., Wake, G.C. & Wall, D.J.N. (2004a). Modelling cell death in human tumour cell lines exposed to the anticancer drug paclitaxel. *Journal of Mathematical Biology*, **49**, 329 – 357. 10, 36, 39

Basse, B., Baguley, B.C., Marshall, E.S., Wake, G.C. & Wall, D.J.N. (2004b). Modelling cell population growth with application to cancer therapy in human tumour cell lines. *Progress in Biophysics and Molecular Biology*, **85**, 353 – 368. 10, 36, 41

Basse, B., Baguley, B.C., Marshall, E.S., Wake, G.C. & Wall, D.J.N. (2005). Modelling the flow cytometric data obtained from unperturbed human tumour cell lines: Parameter fitting and comparison. *Bulletin of Mathematical Biology*, **67**, 815 – 830. 10, 29, 86, 94

Basse, B., Marshall, E.S., Baguley, B.C. & Joseph, W.R. (2010). Analysis of radiation-induced changes to human melanoma cultures using a mathematical model. *Cell Proliferation*, **43**, 139 – 146. 55, 56, 57, 66, 74, 82, 83, 84

Begg, R.E. (2007). *Cell-population growth modelling and nonlocal differential equations*. Ph.D. thesis, University of Canterbury. 86

Begg, R.E., Wall, D.J.N. & Wake, G.C. (2010). On a multicompartment age-distribution model of cell growth. *IMA Journal of Applied Mathematics*, 1 – 27. 16

Bell, G.I. (1968). Cell growth and division. III. Conditions for balanced exponential growth in a mathematical model. *Biophysical Journal*, **8**, 431 – 444. 3, 9, 56

Bertuzzi, A., Faretta, M., Gandolfi, A., Sinisgalli, C., Starace, G., Valoti, G. & Ubezio, P. (2002). Kinetic heterogeneity of an experimental tumour revealed by BrdUrd incorporation and mathematical modelling. *Bulletin of Mathematical Biology*, **64**, 355–384. 51, 52

Bronk, B.V., Dienes, G.J. & Paskin, A. (1968). The stochastic theory of cell proliferation. *Biophysical Journal*, **8**, 1353 – 1398. 30

Byrne, H.M. (2010). Dissecting cancer through mathematics: from the cell to the animal model. *Nature Reviews Cancer*, **10**, 221– 230. 9

Caswell, H. (2001). *Matrix Population Models. Construction, Analysis, and Interpretation*. Sinauer Associates, Inc. Publishers, 2nd edn. 17, 110

Chiorino, G., Metz, J.A.J., Tomasoni, D. & Ubezio, P. (2001). Desynchronisation rate in cell populations: Mathematical modelling and experimental data. *J. Theor. Bio.*, **208**, 185–199. 29, 30

Daukste, L., Basse, B., Baguley, B.C. & Wall, D.J.N. (2009). Using a stem cell and progeny model to illustrate the relationship between cell cycle times of in vivo human tumour cell tissue populations, in vitro primary cultures and the cell lines derived from them. *Journal of Theoretical Biology*, **260**, 563 – 571. vii, 7, 53

Daukste, L., Basse, B., Baguley, B.C. & Wall, D.J.N. (2012). Mathematical determination of cell population doubling times for multiple cell lines. *The Bulletin of Mathematical Biology*, **74**, 2510 – 2534. vii, 6, 74

Deisboeck, T.S., Wang, Z., Macklin, P. & Cristini, V. (2011). Multiscale cancer modeling. *Annu. Rev. Biomed. Eng.*, **13**, 127 – 155. 9

Dittmat, T. & Zanker, K., eds. (2009). *Stem cell biology in health and disease*. Springer. 3, 85

Enderling, H., Anderson, A., Chaplain, M., Munro, A. & Vaidya, A. (2006). Mathematical modelling of radiotherapy strategies for early breast cancer. *Journal of Theoretical Biology*, **241**, 158 – 171. 55

Fried, J. (1973). A mathematical model of proliferating cell populations: further development and consideration of the resting state. *Mathematical Biosciences*, **18**, 397 – 408. 30

Furneaux, C.E., Marshall, E.S., Yeoh, K., Monteith, S.J., Mews, P.J. & Sansur, C.A. (2008). Cell cycle times of short-term cultures of brain cancers as predictors of survival. *British Journal of Cancer*, **99**, 1678 – 1683. 3, 41, 44, 86, 88, 97

Ganguly, R. & Puri, I.K. (2006). Mathematical model for the cancer stem cell hypothesis. *Cell Proliferation*, **39**, 3 – 14. 10

Guiotto, P. & Ubezio, P. (2000). The asymptotic behaviour of a proliferent - quiescent cells system. *Communications in Applied Analysis*, **4**, 345 – 361. 56

Holdaway, K.M., Finlay, G.J. & Baguley, B.C. (1992). Relationship of cell cycle parameters to in vitro and in vivo chemosensitivity for a series of Lewis lung carcinoma lines. *European Journal of Cancer*, **28A**, 1427 – 1431. 88

Illidge, T.M. (1998). Radiation-induced apoptosis. *Clinical Oncology*, **10**, 3 – 13. 55

Johnson, L.A., Byrne, H.M., Willis, A.E. & Laughton, C.A. (2011). An integrative biological approach to the analysis of tissue culture data: application to the antitumour agent rhps4. *Integrative Biology*, **3**, 843 – 849. 10

Johnston, M.D., Edwards, C.M., Bodmer, W.F., Maini, P.K. & Chapman, S.J. (2006). Mathematical modeling of cell population dynamics in the colon crypt and in colorectal cancer. *Proc. Nat. Acad. Sci. U.S.A*, **104**, 4008 – 4013. 86

Kantorovich, L.V. & Akilov, G.P. (1982). *Functional analysis*. Pergamon Press, 2nd edn. 93

Kerr, J.F., Winterford, C.M. & Harmon, B.V. (1994). Apoptosis. Its significance in cancer and cancer therapy. *Cancer*, **73**, 2013 – 2026. 55

Keyfitz, B.L. & Keyfitz, N. (1997). The McKendrick partial differential equation and its uses in epidemiology and population study. *Mathematical Comput. Modelling*, **26**, 1 –9. 16

Kim, J.J. & Tannock, I.F. (2005). Repopulation of cancer cells during therapy: an important cause of treatment failure. *Nature Reviews Cancer*, **5**, 516 – 525. 56

Kozusko, F. & Bourdeau, M. (2007). A unified model of sigmoid tumour growth based on cell proliferation and quiescence. *Cell Proliferation*, **40**, 824 – 834. 101

REFERENCES

Larsson, S., Ryden, T., Holst, U., Oredsson, S. & Johansson, M. (2007). Estimating the distribution of the G2 phase duration from flow cytometric histograms. *Mathematical Biosciences*, **211**, 1–17. 30

Lindeman, G.J. & Visvader, J.E. (1999). 11th Lorne Cancer Conference, Lorne, Victoria, Australia, 11-14th february 1999. *Biochem. Biophys. Acta*, **1424**, R57 – R62. 85

Linz, P. (1985). *Analytical and Numerical Methods for Volterra Equations*. SIAM. xi, 16, 109

Lotka, A. (1922). On the stability of the normal age distribution. *Proc. Nat. Acad. Sciences*, **8**, 339 – 345. 12

Marshall, E.S., Holdaway, K.M., Shaw, J.H., Finlay, G.J., Matthews, J.H. & Baguley, B.C. (1993). Anticancer drug sensitivity profiles of new and established melanoma cell lines. *Oncol Res*, **5**, 301 – 309. 88

Meisenberg, G. & Simmons, W.H. (1998). *Principles of medical biochemistry*. Mosby, Inc. 2

Metz, J. & Diekmann, O., eds. (1986). *The dynamics of physiologically structured populations*. Springer-Verlag. 9

Meyn, R.E. (1997). Apoptosis and response to radiation: implications for radiation therapy. *Oncology*, **11**, 349 – 356. 55

Moore, K.A. & Lemischka, I.R. (2006). Stem cells and their niches. *Science*, **311**, 1880 – 1885. 85

Nagl, S., ed. (2006). *Cancer Bioinformatics: From therapy design to treatment*. John Wiley & Sons. 2

Olofsson, P. & McDonald, T.O. (2009). A stochastic model of cell cycle desynchronization. *Digital Commons @ Trinity*, **0**, 1 – 23. 30

Pagano, M. (1995). *Cell Cycle: Materials and Methods*. Springer. 33

Parmar, J., Marshall, E.S., Charters, G.A., Holdaway, K.M., Shelling, A.N. & Baguley, B.C. (2000). Radiation-induced cell cycle delays and p53 status of early passage melanoma cell lines. *Oncol Res*, **12**, 149 – 155. 88

Pawlik, T.M. & Keyormarsi, K. (2004). Role of cell cycle in mediating sensitivity to radiotherapy. *Int. J. Radiat. Oncol. Biol. Phys.*, **59**, 928 – 942. 57

Prescott, D.M. (1987). Cell reproduction. *Int. Rev. CytoL*, **100**, 93 – 128. 41

Quintana, E., Shackleton, M., Sabel, M.S., Fullen, D.R., Johnson, T.M., Morrison, S.J.A. & et al. (2008). Efficient tumour formation by single human melanoma cells. *Nature*, **456**, 593 – 598. 104

Rew, D.A. & Wilson, G.D. (2000). Cell production rates in human tissues and tumours and their significance part 1: an introduction to the techniques of measurement and their limitations. *European Journal of Surgical Oncology*, **26**, 227 – 238. 41, 51, 52

Rockne, R., Alvord Jr., E., Rockhill, J. & Swanson, K. (2009). A mathematical model for brain tumor response to radiation therapy. *Journal of Mathematical Biology*, **58**, 561 – 578. 55

Schatton, T. & Frank, M. (2007). Cancer stem cells and human malignant melanoma. *Pigment Cell Melanoma Res.*, **21**, 39 – 55. 3, 85

Simms, K., Bean, N. & Koerber, A. (2012). A mathematical model of cell cycle progression applied to the MCF-7 breast cancer cell line. *Bulletin of Mathematical Biology*, **74**, 736 – 767. 10, 29, 33

Sole, R., Rodriguez-Caso, C., Deisboeck, T. & Saldana, J. (2008). Cancer stem cells as the engine of unstable tumour progression. *Journal of Theoretical Biology*, **253**, 629 – 637. 3, 85

Steel, G.G. (1977). *Growth kinetics of tumours*. Clarendon Press: Oxford. 3, 30, 51, 52

Taylor, I., Hodson, P., Green, M. & Sutherland, R. (1983). Effects of tamoxifen on cell cycle progression of synchronous MCF-7 human mammary carcinoma cells. *Cancer Research*, **43**, 4007–4010. 36

Terry, N.H.A. & White, R.A. (2006). Flow cytometry after bromodeoxyuridine labeling to measure s and g_2+m phase durations plus doubling times *in vitro* and *in vivo*. *Nature Protocols*, **1**, 859–869. 30, 51, 52

Tindalla, M.J. & Please, C.P. (2007). Modelling the cell cycle and cell movement in multicellular tumour spheroids. *Bull*, **69**, 1147 – 1165. 10

Watson, J.V. (1991). Tumour growth dynamics. *Br. Med. Bull.*, **47**, 47 – 63. 97

Watt, F.M. & Hogan, B.L. (2000). Out of Eden: stem cells and their niches. *Science*, **287**, 1427 – 1430. 85

White, R.A. & Terry, N.H.A. (2000). Cell kinetics: Mathematical models and experimental bases. *Mathematical and Co*, **32**, 113 – 124. 30

Wilson, G.D., McNally, N.J., Dische, S., Saunders, M.I., Des Rochers, C., Lewis, A.A. & Bennett, M.H. (1988). Measurement of cell kinetics in human tumours *in vivo* using bromodeoxyuridine in corporation and flow cytometry. *British Journal of Cancer*, **58**, 423 – 431. 85